

SUPERCONDUCTING PROXIMITY EFFECT CURRENTS
IN INDIUM ABOVE ITS TRANSITION TEMPERATURE

Thesis by
John B. Trenholme

In Partial Fulfillment of the Requirements
For the Degree of
Doctor of Philosophy

California Institute of Technology
Pasadena, California

1970

(Submitted July 18, 1969)

ACKNOWLEDGEMENTS

I am deeply indebted to Dr. Peter V. Mason, whose guiding inspiration and friendship made this work possible despite numerous difficulties. His constant assistance and interest have encouraged my efforts; his knowledge of superconductivity, both theoretical and experimental, has been of inestimable aid.

Dr. Jon Mathews has been a constant source of help with the many mathematical questions raised in this work, and my numerous discussions with him on the subject of superconductivity have greatly helped my understanding of the subject.

I am grateful to the California Institute of Technology for permitting me to spend a year at the Indian Institute of Technology in Kanpur, India. This sojourn did little to advance the present work, but was of incalculable educational value.

A number of suggestions of Dr. Floyd Humphrey have been incorporated in this work.

The cheerful assistance of Ruth Stratton has greatly aided in the preparation of the manuscript.

Most importantly, the love and inspiration of my wife, Maude (the Wartootinating Wart), have guided me at many difficult points, and insured the success of this venture.

ABSTRACT

The superconducting proximity effect, in which superconductivity diffuses from a superconductor into an adjacent non-superconductor, was investigated using the SNS sandwich method in order to test the predictions of the de Gennes-Werthamer theory of temperature dependence of the Ginzburg-Landau equation. Sandwiches were made in which Pb injected superconductivity into a central layer of In, so that the maximum lossless current through the In could be found as a function of temperature down to the In transition temperature (3.4K). Techniques were used to insure uniform current flow, and to avoid annealing. The log of the critical current density of the sandwiches decreased linearly with temperature above the In transition; the current became much larger below the transition. The de Gennes-Werthamer theory was extended by the addition of the nonlinear term in the Ginzburg-Landau equation; exact solutions of the one-dimensional Ginzburg-Landau equation in the presence of current (but with $\underline{A} = 0$) were used to find the theoretical temperature variation of the critical current density. The experimental and theoretical curves showed the same linear behavior (although there were slope and value variations), thus verifying the de Gennes-Werthamer theory near the transition temperature of a material.

TABLE OF CONTENTS

I.	INTRODUCTION	1
	A. The Superconducting State	1
	B. The Proximity Effect	3
	C. Previous Measurements of the Proximity Effect	4
	D. The SNS Sandwich Method	6
	E. Purpose of the Present Work	6
II.	PREPARATION OF THE SAMPLES	10
	A. Preliminary Discussion	10
	B. Details of the Preparation	12
	C. Effects of Annealing on the Samples	16
III.	MEASUREMENT OF THE SAMPLES	18
	A. The Cryostat	18
	B. N Material Mean Free Path and Transition Temperature	18
	C. Apparatus for Sandwich Measurements	21
	D. Samples with Al Center Layers	24
	E. Effects of an External Magnetic Field	26
IV.	RESULTS OF THE SANDWICH MEASUREMENTS	30
	A. V-I Characteristics	30
	B. Critical Current versus Temperature	32
V.	THEORETICAL MODEL AND PREDICTIONS	41
	A. Ginzburg-Landau Equation	41
	B. Temperature Dependence of k^2 and r_B^2	44

C. S Region	51
D. N Region; Critical Current	53
E. Boundary Conditions	57
F. Magnetic Effects	59
VI. COMPARISON OF THEORY AND EXPERIMENT	66
A. Reduction of Sandwich Currents to Current Densities	66
B. Numerical Computations from the Theory	67
C. Comparison of Theory and Experiment	79
D. Suggestions for Further Work	86
E. Summary	87
APPENDIX A. THE QUANTUM INTERFERENCE VOLTMETER	90
A. Introduction	90
B. Two-Junction Quantum Interference	90
C. The Principle of the Voltmeter	94
D. Fabrication of the Two-Junction Ring--The SLUG	97
E. Characteristics of the SLUG	100
F. The SLUG Voltmeter	100
G. Use of the Voltmeter to Measure the Sandwich Characteristics	106
APPENDIX B. EXACT CALCULATION OF THE CRITICAL CURRENT DENSITY	108
A. Introductory Discussion	108
B. Simultaneous Solution of Eq. (24) and Eq. (28)	108
C. The Search for the Critical Current Density	112
D. Improvements to the Method of Search	113

I. INTRODUCTION

A. The Superconducting State

The superconducting state [1] appears when many metals and alloys [2] are cooled to low temperatures (less than 25K for presently known materials). Below a temperature which is characteristic of the specific material (called the transition temperature or critical temperature) a number of unusual and interesting properties are seen. These superconducting properties include the flow of electrical currents without any associated voltage drop (lossless currents), the expulsion of magnetic fields from the interior of the material (Meissner effect), the quantization of the magnetic flux through a hole in the material, and the appearance of an energy gap in the excitation spectrum of the electrons. The Bardeen-Cooper-Schrieffer (BCS) theory [3] has shown that these remarkable properties are the result of the formation of electron pairs (the so-called Cooper pairs) and a subsequent condensation of these quasi-Boson pairs into a single cooperative state. The pairs form because of some attractive interaction between the electrons (in many cases due to the electron-lattice interaction). The superconducting properties arise from the fact that the cooperative condensed state acts in many ways as a single macroscopic quantum state, or "wave

[1] E. Lynton, Superconductivity, John Wiley & Sons, New York, 1962; this is a good general reference on superconductivity.

[2] R. Weast (Ed.), Handbook of Chemistry and Physics (49th Edition), Chemical Rubber Co., Cleveland, 1968, p. E-81.

[3] J. Bardeen, L. Cooper, and J. Schrieffer, Phys. Rev. 108, 1175 (1957).

function of the superelectrons". Ginzburg and Landau [4] independently developed a very successful phenomenological theory of superconductivity based on this idea of a superelectron wave function; Gor'kov [5] showed that the Ginzburg-Landau theory in fact followed from the BCS theory, if the wave function was interpreted as the (spatially varying) energy gap. In the Ginzburg-Landau theory, a partial differential equation describes the spatial behavior of the energy gap in a material (see Section V). The coefficients in the differential equation depend on the pairing interaction in the material, and on the temperature. The temperature dependence of these Ginzburg-Landau coefficients has been derived on the basis of a semi-classical approximation by de Gennes [6] and Werthamer [7]. Their derivation depended on the use of a diffusion kernel in the integral equations on which the results were based, and so the de Gennes-Werthamer temperature dependence of the Ginzburg-Landau coefficients is valid only in the "dirty limit" in which the electron mean free path is much shorter than the pure bulk coherence length of the superconductor (see Section V).

[4] V. Ginzburg and L. Landau, Zh. Eksp. Teor. Fiz. 20, 1064 (1950); Trans., D. ter Haar, Men of Physics: L. D. Landau I, Pergamon Press, New York, 1965.

[5] L. Gor'kov, Zh. Eksp. Teor. Fiz. 36, 1918 (1959); Trans., Sov. Phys. JETP 36, 1364 (1959).

[6] P. de Gennes, Rev. Mod. Phys. 36, 225 (1964).

[7] N. Werthamer, Phys. Rev. 132, 2440 (1963).

Once the superconducting state is understood to be a condensed state of electrons, it is not hard to see that superconductivity might "leak" into a normal metal in contact with a superconductor, because the electrons can easily travel from one metal to the other. Such a leakage of superconductivity is known as the proximity effect.

B. The Proximity Effect

When a material below its transition temperature (henceforth referred to as an S material) is in contact with a nonconductor, the electron wave functions in the S material must terminate at the boundary because of the Coulomb barrier. The pair condensate (which is made up of electrons) therefore also terminates at the boundary. However, when the S material is in good electrical contact with a material above its transition temperature (henceforth called an N material), there is no strong Coulomb barrier. Instead, the Cooper pairs may travel across the SN interface, and the uncondensed or normal electrons may travel from the N material into the S material. Once the pairs have entered the N side, they will eventually depair. Likewise, the normal electrons will pair up once they are inside the S material. The result of these diffusions of pairs and normal electrons is that the amount of superconductivity is decreased in the S material near the SN boundary, and that induced superconductive properties extend some distance into the N material from the boundary. This induction of superconductivity in an N material in contact with a superconductor (and the concomitant reduction of superconductivity in an S material adjacent to an N material) is called the proximity effect.

The de Gennes-Werthamer theory of the temperature dependence of the coefficients in the Ginzburg-Landau equation predicts the temperature dependence of the behavior of superconductivity in a material. Comparison of the predictions with experiment is relatively easy below the transition temperature, but it is quite difficult above this temperature; an isolated specimen of N material has no measurable superconducting properties (even close to its transition temperature) because the pair state is not present. However, an S material in contact with the N material injects pairs into it, as discussed above, and the way in which the amount of pair state decays with distance in the N material gives us information about the pairing interaction in that material. We thus have in the proximity effect a powerful tool for the measurement of the pairing properties of materials above their transition temperatures, and thus for a test of the de Gennes-Werthamer theory in that region.

C. Previous Measurements of the Proximity Effect

The proximity effect was first investigated by finding the transition temperature of superimposed thin films of two different materials [8]. Such double films have transition temperatures intermediate between the transition temperatures that the two components would have in isolation. The results of these experiments are explained well by the de Gennes-Werthamer theory. (At this point it is desirable to modify the definition of S and N materials, since the proximity

[8] P. Hilsch, Z. Phys. 167, 511 (1962).

effect is seen to modify the transition temperature of different materials in contact. An S material will therefore be defined as one below the transition temperature it would have in isolation, and an N material as one above that temperature.)

The double film experiment originally yielded information only at one temperature. A modification [9] of this experiment, in which the critical current parallel to the plane of the interface was measured as a function of temperature, depended largely on the properties of the S material. This modification is thus not suitable for measurements of the pairing tendency in the N material.

The energy gap on the outside of the N material in a double film was measured [10] in another experiment. The energy gap is proportional to the pair density, so this type of experiment is potentially capable of measuring the pair decay as a function of temperature. Unfortunately, thermal effects smear the gap measurement near the transition temperature, and so the technique is precise only at low temperatures.

The penetration depth for a magnetic field in a material depends inversely on the amount of superconductivity in the material, so measurements of the penetration depth [11] supply information on the

[9] P. Smith, et al., Phys. Rev. Letters 6, 686 (1961).

[10] E. Guyon, et al., Phys. Cond. Mat. 5, 123 (1966).

[11] P. de Gennes and J. Matricon, Solid State Com. 3, 151 (1965).

amount of induced superconductivity in the N material of an SN double film. However, the penetration depth depends on a spatial average of the amount of pair state and so is not sensitive to the details of the spatial distribution of superconductivity.

D. The SNS Sandwich Method

The SNS sandwich method is a method of investigating the decay of superconducting electron pairs in N material which avoids many of the difficulties of previous methods. This method was devised by Meissner [12],[13] and improved by Clarke [14]. Their experiment consisted of finding the maximum lossless current which could be carried across a three-layer sandwich consisting of an N layer between two S layers. Currents of many amperes per square centimeter can be carried across micron-thick N layers in such structures. This method is ideally suited to the measurement of the pairing tendency in the N material, because (as will be seen in Section V) the maximum lossless current depends only weakly on the properties of the S regions, and quite strongly on the N region properties.

E. Purpose of the Present Work

The present work was undertaken to make a direct test of the de Gennes-Werthamer prediction of the temperature dependence of the pairing properties of materials above their transition temperatures. The proximity effect, especially as exploited in the SNS sandwich

[12] H. Meissner, Phys. Rev. 109, 686 (1958).

[13] H. Meissner, Phys. Rev. 117, 672 (1960).

[14] J. Clarke, Proc. Roy. Soc. (London) A308, 447 (1969).

method, is an ideal measuring tool in this type of investigation for the reasons discussed above.

The choice of material is as important as the choice of method if we are to make a definitive test of the theory. The transition temperature of the material is the base point for calculations of the temperature dependences, and so any test of the theory should use a material of known transition temperature. In addition, comparison right down to the transition temperature is necessary for complete comparison, and so the use of a material with a transition temperature which is experimentally accessible is desirable. In the work of Meissner, the N region was of materials such as Cu, Ag, Au, Pt, and Fe, which have never been observed to superconduct. Clarke used Cu, which has a transition temperature of less than .001K (if it superconducts at all). Their results are thus not an effective test of the theory. The material chosen for this work was In (some Al samples were also made), which has a convenient transition temperature of about 3.4K. This choice makes a direct test of the theory possible.

The S material of the sandwiches must have a transition temperature well above that of the N material if it is to serve as a strong source of pair state, because the strength of superconductivity decreases near the transition temperature of a superconductor. Most superconductors with transition temperatures well above the 3.4K transition of In are difficult to deposit as thin films; a notable exception is Pb, which has a 7.2K transition temperature and is easily evaporated from heated boats. It was therefore decided to make the S regions of Pb.

Because Pb and In are quite soluble in each other [15], some method of stabilizing the sandwich structures was necessary. Stabilization was accomplished by depositing the sandwiches on substrates cooled to about 100K, thus reducing the amount of thermal energy available for diffusion and other annealing effects. An added advantage of such low temperature deposition is that it produces short electron mean free paths in the materials. Theoretical interpretation is presently possible only in the case of short mean free paths, and so low temperature deposition allows us to avoid the addition of impurities resorted to by Clarke to insure short mean free paths. In addition, the choice of materials for an SNS sandwich is severely limited at room temperature (as Clarke has pointed out) by the effects of interdiffusion, chemical combination, electrochemical effects, and other destructive forces; the presently used method of low temperature deposition sharply reduces these effects and thus greatly broadens the choice of materials for experimentation.

The pattern of flow of the currents in the sandwiches of both Meissner and Clarke was non-uniform, making reduction of currents to current densities inexact. The results of the theory are in terms of current densities, and so comparison between theory and experiment was rendered difficult. Meissner produced his sandwiches by plating S wires with N layers, and then pressing the wires together. The area and thickness of the sandwiches was thus poorly controlled. Clarke

[15] M. Hansen, Constitution of Binary Alloys, 2nd Ed., McGraw-Hill Book Company, New York, 1958, p. 854.

produced his sandwiches by vacuum deposition through masks, and so he had good control of their geometry. However, he did not use a superconducting ground plane to insure uniform current flow in the sandwiches and so it can be expected that the currents in his sandwiches tended to bunch at the edges of the thin films [16] when the currents were large. Thus Clarke's results for large critical currents were subject to unknown but appreciable errors. The sandwiches in this work (which were also produced by vacuum deposition through masks) were therefore supplied with superconducting ground planes to insure uniform current flow. The resulting absence of nonlinearity allowed precise comparison with theory.

In summary, SNS sandwiches with In as the center layer were measured to determine the correctness of the de Gennes-Werthamer theory of the temperature dependence of the pairing properties of materials above their transition temperatures. The sandwiches were deposited at low temperature to prevent diffusion of the materials (and to provide short electron mean free paths). They had superconducting ground planes to insure uniform current flow.

[16] V. Newhouse, Applied Superconductivity, John Wiley & Sons, New York, 1964, p.122.

II. PREPARATION OF THE SAMPLES

A. Preliminary Discussion

The sandwich samples (see Fig. 1) were made of an upper strip of Pb about 300μ wide and 7300\AA thick, a center dot of In about 5 mm wide and varying in thickness from 1μ to 8.3μ , and a lower Pb strip similar to the upper strip and at right angles to it. The fabrication in the form of an X made the geometry of the actual crossover of the Pb strips insensitive to the exact positions of the masks used, and also made possible four-terminal measurements of the V-I characteristics of the sandwiches (such four-terminal measurement avoids any problem of non-superconducting connections to the sample). Although the In spot was considerably larger than the actual crossover area of the Pb strips, the current flow was confined to the area of crossover because the thickness of the In spot was much smaller than its other dimensions. Any currents which did not travel directly from one Pb strip to the other thus would have had to travel much greater distances through the In than direct currents, and so would have been correspondingly smaller.

A thin plastic insulating layer separated the sandwich structure from a Pb ground plane, which was needed to assure uniformity of the current flow. A superconductor thicker than a few penetration depths expels all flux from inside it, and so the ground plane and Pb strips capture between them the flux due to currents in the Pb strips. When the ground plane is close to the Pb strips and parallel to them, the trapped flux is uniform, and so the current flow in the strips is also uniform (by Ampere's law).

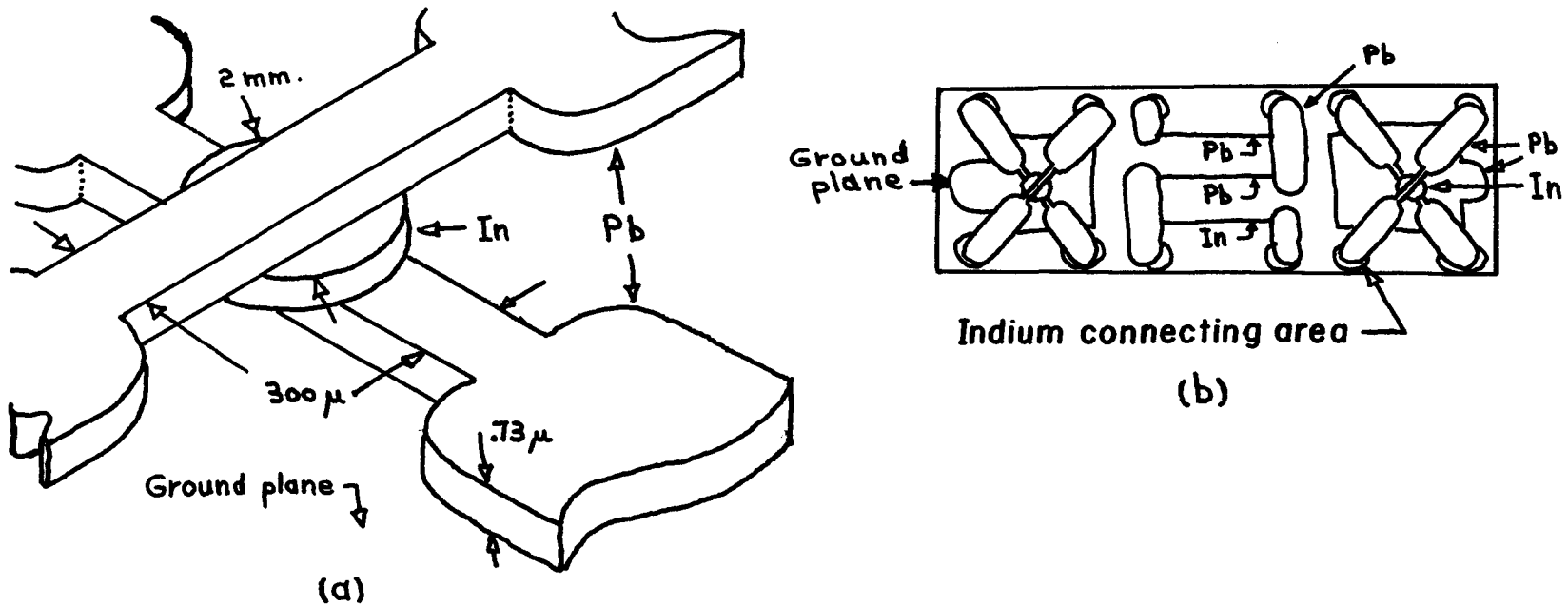


Fig. 1. (a) Enlarged view (thickness exaggerated) of the sandwich structure. (b) Top view (actual size) showing two sandwiches deposited on their glass substrate; also shown are the resistivity test strips deposited at the same time as the various layers of the sandwich.

Long, narrow strips of the materials used in the sandwich layers were deposited simultaneously with the layers, so that their electron mean free paths and material transition temperatures could be determined.

B. Details of the Preparation

The substrates on which the samples were prepared were 1" by 3" soft glass microscope slides. The slides were manually scrubbed with water and detergent. They were then ultrasonically agitated in detergent solution, immersed in acetone for several minutes, washed with methanol, and degreased in hot trichloroethene vapor. They were then clamped to a Cu block at room temperature and placed in the vacuum chamber.

The Pb ground planes were deposited by vacuum evaporation (from a resistance heated Ta boat about 20 cm below the substrate) in a liquid-nitrogen-trapped vacuum system at a pressure of about 10^{-6} Torr. The ground plane thickness was about 7300\AA ; it was measured (to 5%) by a quartz crystal deposition monitor calibrated (for Pb, In, and Al) against measurements of film thickness made with an interferometer. To assure current uniformity, the ground plane had to be several penetration depths thick; the penetration depth for Pb is about 400\AA , so the thickness used was quite sufficient. After deposition of the ground planes, the sample was removed from the vacuum, and the ground planes were checked visually for uniformity.

Indium connecting areas for the attachment of external connecting leads were then soldered onto the substrate with a low wattage

soldering iron; they were positioned so as to fall under the future positions of the connecting strips from the sandwich structures and test strips. The purpose of such areas was to act as thermal ballast during the soldering of the external connections, so that the thin Pb strips would not be destroyed in the process of lead attachment.

An insulating layer was then applied to isolate the ground planes electrically from the sandwiches. Such a layer had to be thin compared to the width of the Pb strips to assure uniform current flow, and pinhole free to maintain electrical isolation. Experiments with thin layers of polystyrene, methyl methacrylate, photoresist [17], and Formvar[®] [18] revealed that no single layer would simultaneously be pinhole free and of suitable thickness. It was therefore decided to use a double layer, so that pinholes in one layer would be covered by the other. If such a double layer is to be formed, the formation of the second layer must not disturb the first, and so the solvent for the second layer material must not dissolve the first layer. Therefore, the solubilities in various solvents of the substances mentioned above were determined; the solvents tried were acetic acid, trichloroethene, p-dioxane, toluol, xylol, benzene, ethylene dichloride, and a mixture of .6 toluol and .4 ethanol (by volume). The best combination of layers and solvents was found to be an initial layer of photoresist diluted in

[17] Kodak thin film resist.

[18] Grade 15/95E; supplied through the courtesy of the Monsanto Company.

xylool, followed by a layer of Formvar dissolved in p-dioxane. The concentration of the photoresist in the xylool was adjusted until coatings made from the solution displayed several interference fringes in white light, implying a thickness of several wavelengths of visible light ($.5\mu$). The substrate, with its attached ground plane and connecting areas, was dipped into the solution, allowed to drain, and dried in an inverted position to avoid dust adhesion. It was then dipped into the solution of Formvar in p-dioxane (whose concentration was also adjusted to give several-optical-fringe thickness coatings) and dried as before. Once the second layer had dried, the connecting areas were remelted with the low wattage soldering iron to remove the insulating layers on them, so that good contact with the Pb strips would be made.

The fabrication of the sandwiches was then undertaken. The substrate was clamped to a Cu block; small amounts of silicone vacuum grease between the block and the substrate just below the future positions of the cross-overs insured good thermal contact to the block. The block and substrate were then placed into the vacuum chamber, pumped down, and cooled to around 100K by placing liquid nitrogen in a pot attached to the Cu block. The vacuum was maintained in the 10^{-7} Torr range with the aid of a liquid nitrogen large-area trap in the vacuum chamber. The connecting strips and sandwich structure were then evaporated (again from resistance heated Ta boats 20 cm below the substrate) through masks. The boats were heated to outgas the materials, while the substrate was protected by a solid mask. The Pb strip next to the insulating layer was deposited first, the mask was changed without breaking the vacuum (mask changes took about 30 seconds) and

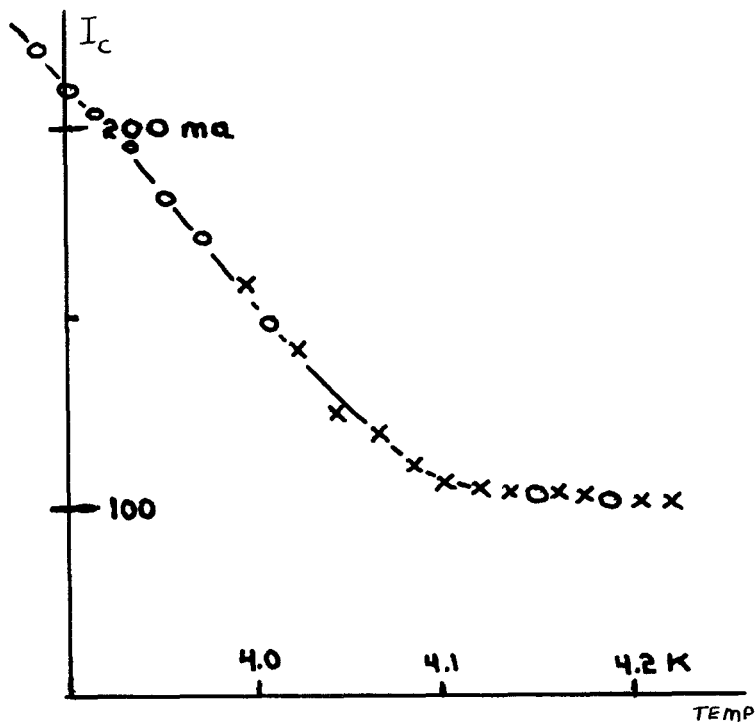
the In layer deposited. Again the mask was changed, and the top Pb layer deposited. During the depositions, the indicated pressure rose into the 10^{-6} Torr range. The time to evaporate the layers varied, but was usually several hundred seconds per layer. Two sandwiches were deposited simultaneously to increase the chances of producing a working sample (see Fig. 1). The thicknesses of the layers were measured by the crystal monitor. The Pb strips had 7300\AA thickness; the In spots varied from 1μ to 8.3μ in thickness.

Once they had been deposited, the sandwiches were removed from the vacuum chamber and placed quickly in liquid nitrogen (the time of exposure to room temperature air was less than a minute). They were then tested for shorts between the ground plane and the sandwich; such shorts, if detected, were vaporized by discharging a $.1\mu\text{f}$ capacitor charged to 30 volts between the layers. About half of the samples displayed such shorts; no correlation with the preparation procedure was noted. If a short was seen in the actual crossover area of the sandwich, the sample was rejected (the vaporization produced a visible flash which allowed the position of any shorts to be determined). Electrical leads were then soldered to the sample. It was attached to the test fixture and transferred to the liquid helium dewar for testing. The samples were kept under liquid nitrogen at all times from their removal from the vacuum chamber until their placement into the helium dewar; the various operations on them were all carried out under liquid nitrogen. This maintenance of low sample temperature avoided any stresses due to thermal cycling, and also reduced any possible annealing effects.

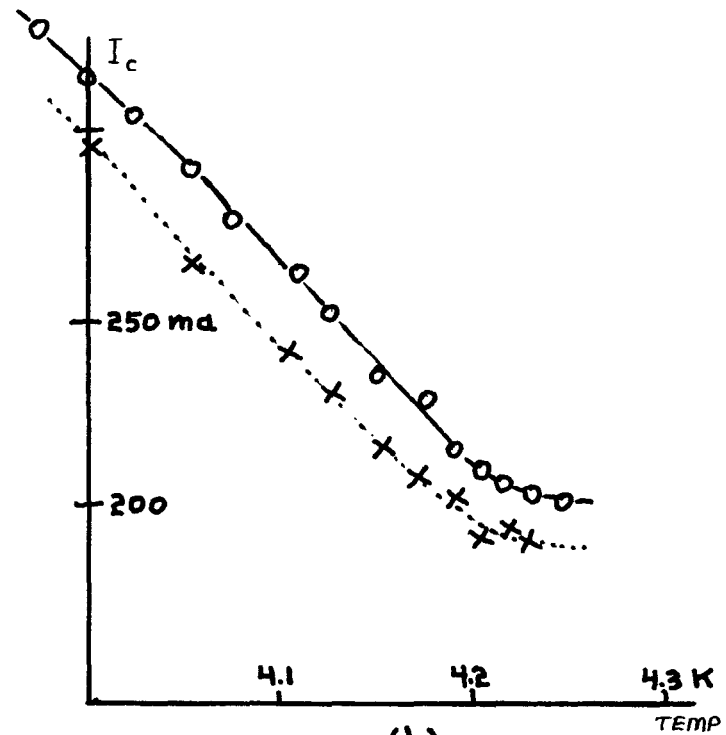
C. Effects of Annealing on the Samples

To find out if any annealing of the samples was taking place at liquid nitrogen temperatures, one of the samples (which had been measured within an hour of preparation) was remeasured after a day's storage in liquid nitrogen. There was essentially no change in the critical current versus temperature curve, as shown in Fig. 2a (the critical current versus temperature is the most important property of the sandwiches). Practically all the samples were measured within a day of preparation, so the storage did not introduce any measurable annealing effects.

The possibility of annealing at higher temperatures (for instance during the removal from the vacuum system) was investigated by allowing another sandwich to warm to temperatures near room temperature (but below the ice point) for several hours. When remeasured after this treatment, the sandwich critical current curve was decreased by about 5% (see Fig. 2b). We deduce that the 60 second exposure during removal from the vacuum chamber probably had little effect.



(a)



(b)

Fig. 2 (a) Effect of 24 hour storage at 80K on sandwich characteristics. Circles - before storage. Crosses - after storage.
 (b) Effect of raising to near 300K for several hours. Circles - before heating. Crosses - after heating.

III. MEASUREMENT OF THE SAMPLES

A. The Cryostat

The cryostat was a standard liquid nitrogen jacketed glass double dewar. A pump and manostat allowed regulation of the temperature of the liquid helium bath from 4.2 K to below 2 K. The temperature of the bath was determined to .001 K from its pressure as measured by mercury and oil manometers (using the 1958 He⁴ pressure-temperature relationship), and by a carbon resistance thermometer calibrated against the manometers. The observed fluctuations in the readings of the resistance thermometer suggest that the manostat held the temperature to well within .001 K at any given setting. Measurements were normally taken with the temperature decreasing, to avoid temperature stratification in the liquid helium [19].

B. N Material Mean Free Path and Transition Temperature

The N material mean free path and transition temperature were found by displaying the V-I curve of the test strip of N material on an oscilloscope. A 60 Hz sinusoidal current was applied to the strip from leads attached to its ends, and the resulting voltage was brought out on separate shielded leads attached at the same points (a test with Pb strips showed that the common resistance of the leads was negligible). The resistance of the strip at 4.2 K was thus determined, and the mean free path was then calculated from the relationship $\rho l = 2 \times 10^{-11} \Omega \text{cm}^2$,

[19] A. Rose-Innes, Low Temperature Techniques, Van Nostrand, Princeton, 1964; p. 93.

where ρ is the resistivity and ℓ is the mean free path [20]. The resistivity was found from the resistance using the length and width of the strip (determined by the use of a calibrated microscope after the samples had warmed up) and its thickness (as measured by the crystal deposition monitor). Once the 4.2 K resistance had been found, the sample temperature was lowered until a zero-resistance region was seen on the V-I plot at low currents. The critical current at which voltage appeared was then measured for several temperatures at and below the first appearance of superconductivity. The appearance of voltage was gradual rather than abrupt, so the critical currents thus measured were accurate only to 10%. The transition temperature of the test strip was found from a plot of critical temperature versus temperature such as Fig. 3. Plots for the test strips always had gradual rather than abrupt increases of critical current as the temperature was lowered; such a broad transition is indicative of inhomogeneities in the test strip. The width of the transition was typically .05 K (the transition of Fig. 3 was broader than average).

The resistance (and thus mean free path) of the Pb strips was also measured, by lifting the sample above the surface of the liquid helium in the dewar until its temperature rose above the transition temperature of the Pb. Such observations were made to check that the mean free paths in the Pb were of the same order as the In mean free paths; the order-of-magnitude accuracy obtained is sufficient because

[20] A. Toxen and M. Burns, Phys. Rev. 130, 1808 (1963).

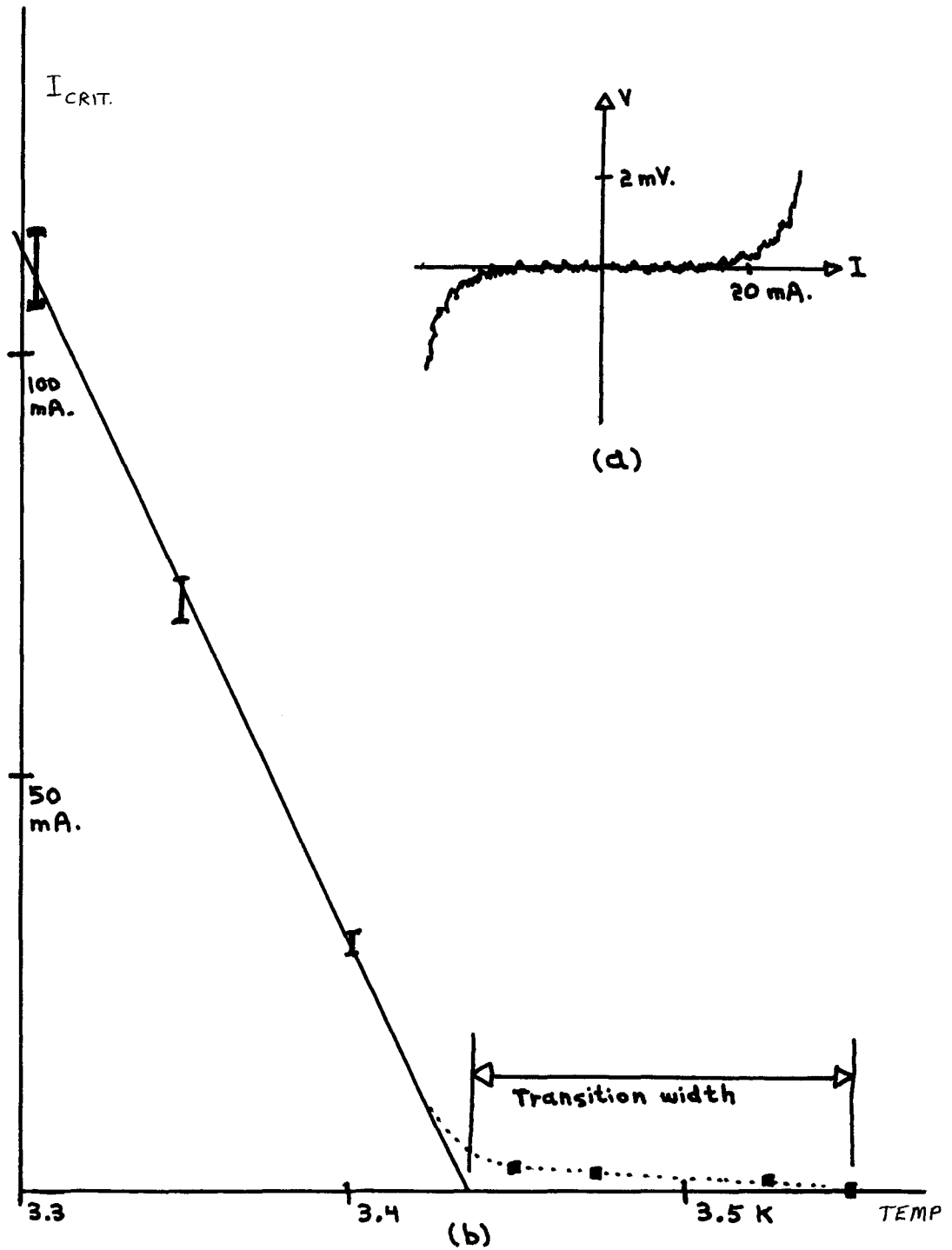


Fig. 3. (a) V-I characteristic of a typical test strip during determination of the critical current. Critical current ~ 16 mA. (b) Critical current versus temperature of a test strip. The transition width is the temperature range between the zero current extrapolated from the low-temperature behavior and the actual current zero.

the sandwich properties depend only weakly on the properties of the S regions (see Section VI).

C. Apparatus for Sandwich Measurements

The electrical equipment used in the measurements of the sandwich V-I characteristics and critical currents is indicated in Fig. 4 . Current was introduced into two arms of the sandwich from a floating source; the current leads were run through low-pass filters to bypass high frequency interference from outside the dewar. The sandwich voltage resulting from this current was measured across the other two arms by a voltmeter of nanovolt resolution based on the use of a quantum interference device called a SLUG (the voltmeter is discussed in detail in Appendix A). The output of a SLUG voltmeter depends on the input voltage in an oscillatory manner, so it was considerably easier to observe the first appearance of voltage across the device than to plot the full V-I curve. (Production of a complete V-I curve involved manual nulling of the total input voltage to the voltmeter by means of an external offset voltage--see Appendix A). Thus most of the data is in the form of critical current versus temperature curves. The critical current was found by plotting the output of the voltmeter versus the sandwich current on an X-Y plotter; when there was a non-zero critical current a flat region appeared in the normally oscillatory output of the voltmeter, as Fig. 5 shows. The transition was always quite abrupt, and the critical current could be determined to within 10 μ a.

The critical current versus temperature characteristics of the samples are discussed in Section IV.

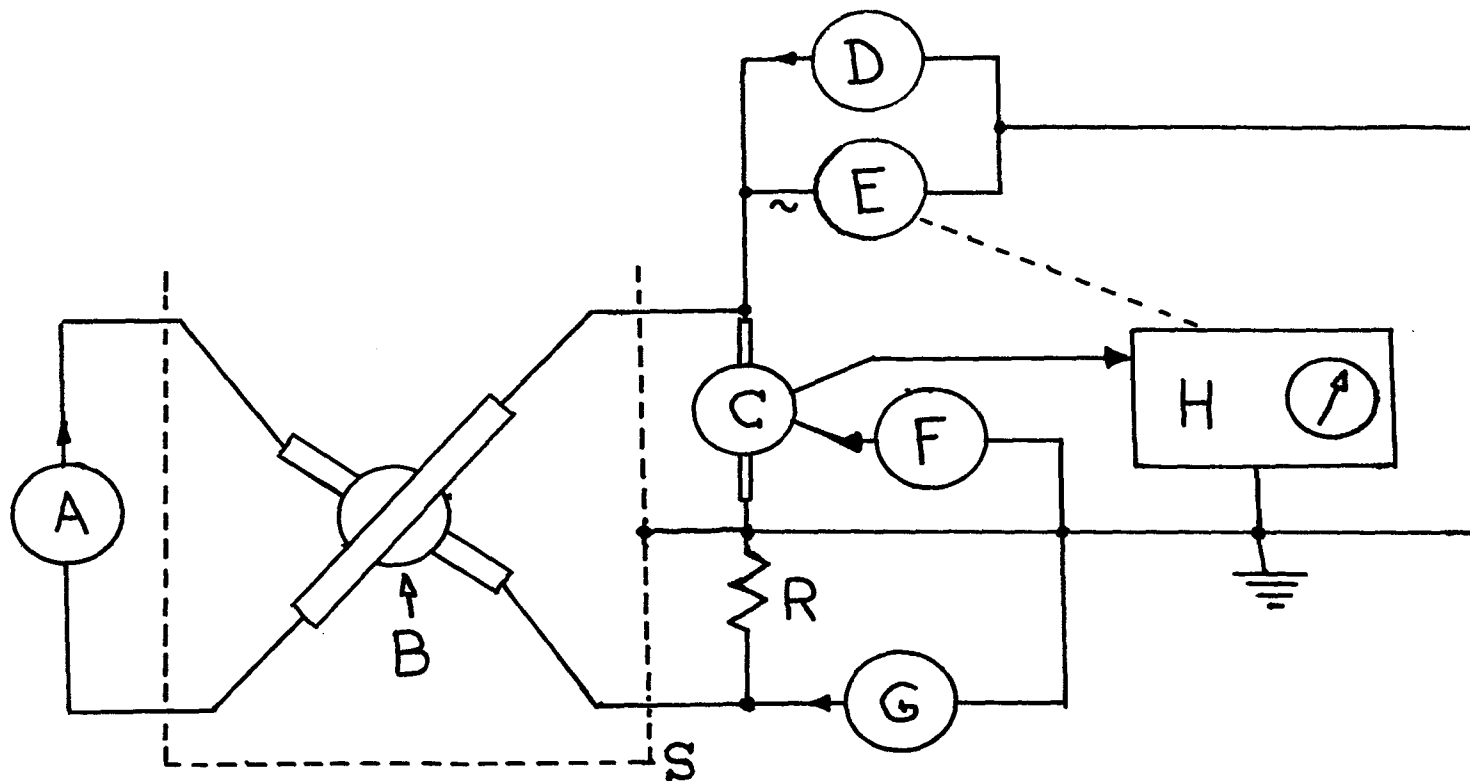


Fig. 4. Diagram of the electrical setup during measurements on the samples. A - sandwich current supply. B - sandwich. C - SLUG. D - Nb wire current supply. E - supply of small ac current. F - SLUG current supply. G - current supply for nulling device voltage. H - Amplifier and synchronous detector (phase locked to ac current). R - small resistor (approx. $1\mu\Omega$). S - superconducting shield. See Appendix A for details.

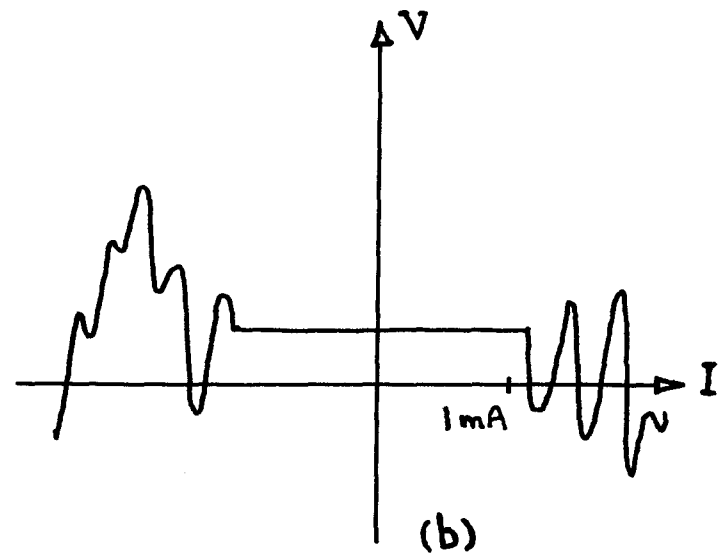
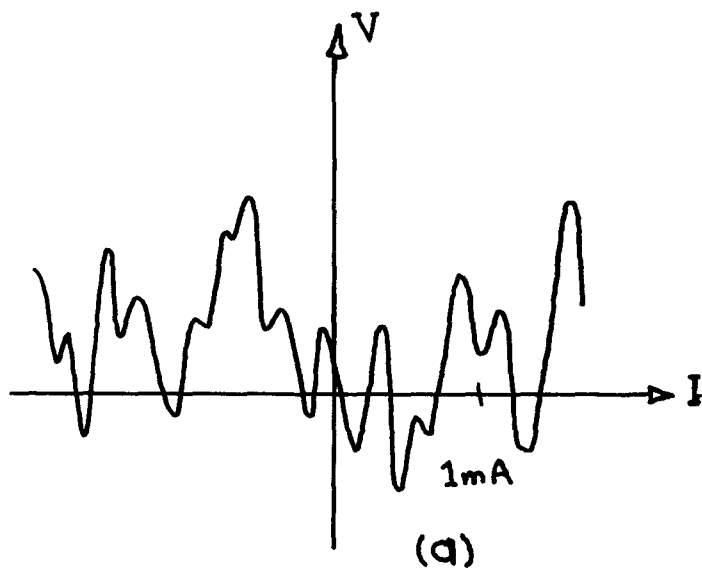


Fig. 5. (a) SLUG output voltage versus sandwich input current when the sandwich is resistive (i.e., when its critical current is zero). (b) The same when the sandwich critical current is non-zero.

D. Samples with Al Center Layers

An attempt to measure the critical current for temperatures all the way from the transition of the central N layer to the transition of the outer S layers was made by preparing sandwiches with Al center layers and In outer layers. This choice of materials put both the center layer transition temperature (1.19 K for bulk Al) and the outer layer transition temperature (3.40 K for bulk In) in the range of convenient experimentation. Unfortunately, the Al films invariably had very short electron mean free paths of 3 to 12 \AA . The de Gennes-Werthamer theory predicts that such short electron mean free paths will lead to a very rapid decrease of critical current with temperature above the transition temperature of the N layer (see Section VI). The theory therefore predicts that the region of currents due to induced superconductivity will be indistinguishable from the region of rapid decrease of critical current caused by the rapid decrease with temperature of the strength of ordinary superconductivity just below the critical temperature. Indeed, any theory in which the superconducting state is made up of paired combinations of normal-state electron wave functions ought to show such behavior for short mean free paths, because the many collisions with the lattice which the electrons must undergo to get across the N region when the mean free path is short will give the pairs numerous opportunities to relax to the unpaired equilibrium state of the N region.

A rapid decrease of current with temperature is just what was observed with the In-Al-In sandwiches, as we see in Fig. 6. For

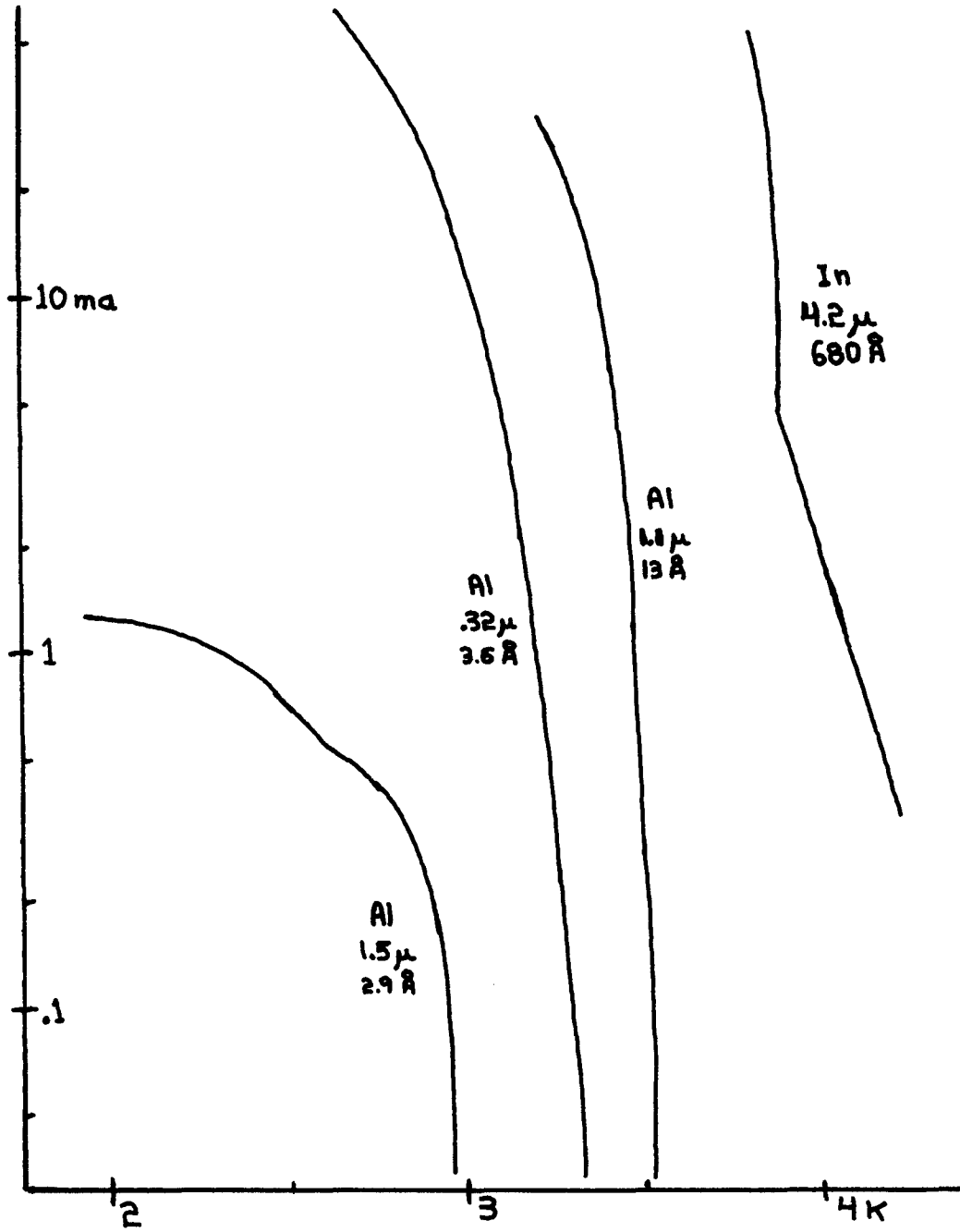


Fig. 6. Log critical current versus temperature for In-Al-In sandwiches of short mean free path. A Pb-In-Pb sandwich is shown for reference. Upper figure - N thickness. Lower figure - N mean free path.

comparison, the curve for a Pb-In-Pb sandwich is also shown; at higher temperatures it shows a characteristic region of lesser slope due to induced superconductivity (see Section IV). The In-Al-In sandwich measurements thus support the de Gennes-Werthamer theory (or any pairing theory) by verifying that proximity effect currents are not observed in the region of short mean free paths (where they are not expected).

The rise above the bulk value of the Al transition temperature (as defined by the temperature where the critical current goes to zero) in the sandwiches was even more marked in the case of the Al films than in that of the In films.

E. Effects of an External Magnetic Field

An external magnetic field could be applied along the long axis of the substrate by means of a coil in the nitrogen dewar surrounding the helium dewar. A weak-link superconducting bridge like the sandwiches of the present work is sensitive to fields of a few Gauss [21], but filamentary bridges of a strongly superconducting material such as Pb are affected only by kilogauss fields. Magnetic field dependence of the critical current thus is a test of the quality of a sandwich. This test was not applied to the Pb-In-Pb sandwiches, but was used with the In-Al-In sandwiches. The critical current versus external field curves for one of the Al samples are shown in Fig. 7 for two different

[21] J. Rowell, Phys. Rev. Letters 11, 200 (1963).

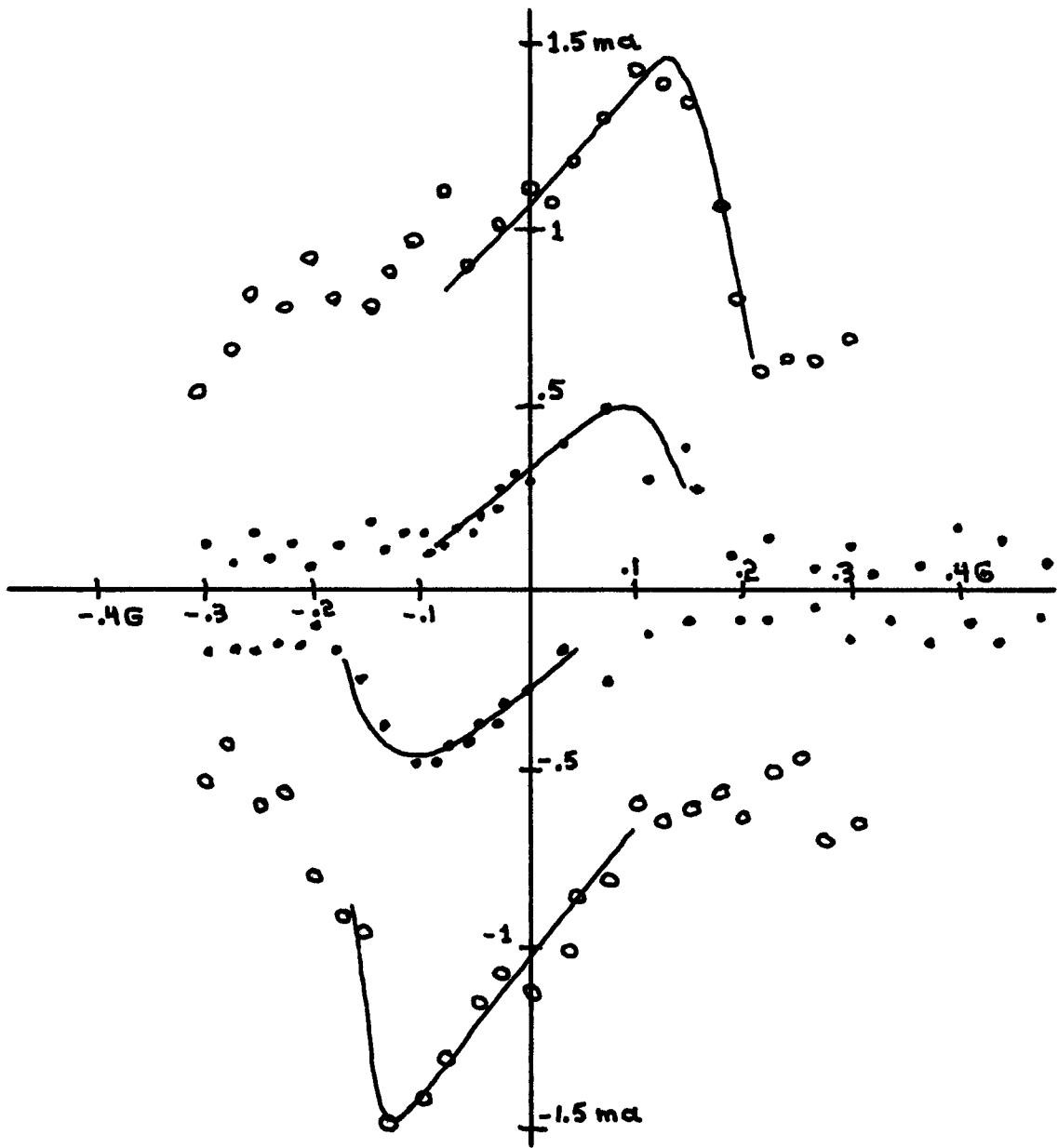


Fig. 7. Critical current (in both directions) versus external magnetic field at two different temperatures. Circles - 3.21K. Dots - 3.28K. The curves are for an In-Al-In sandwich.

temperatures, and thus for two different zero-field critical currents. This sandwich was strongly self-field limited (see Section V) at both temperatures, which causes the maxima to be displaced from zero field; curves of the type expected from self-field limiting have been drawn through the points.

Because the critical currents of the sandwiches were so sensitive to external magnetic fields, the experimental dewar was surrounded during all measurements by a magnetic shield which reduced the field at the sample to less than 5 mG.

Even with the external field reduced to negligible levels, flux trapped in the ground plane, the Pb strips, or in the junction itself can bias the sandwich away from the zero-field condition and introduce an asymmetry in the critical currents. Such asymmetric behavior is shown in Fig. 8 for one of the In samples. When the asymmetry was less than 15%, the average of the two critical currents was used as the actual critical current; samples with larger asymmetry were rejected.

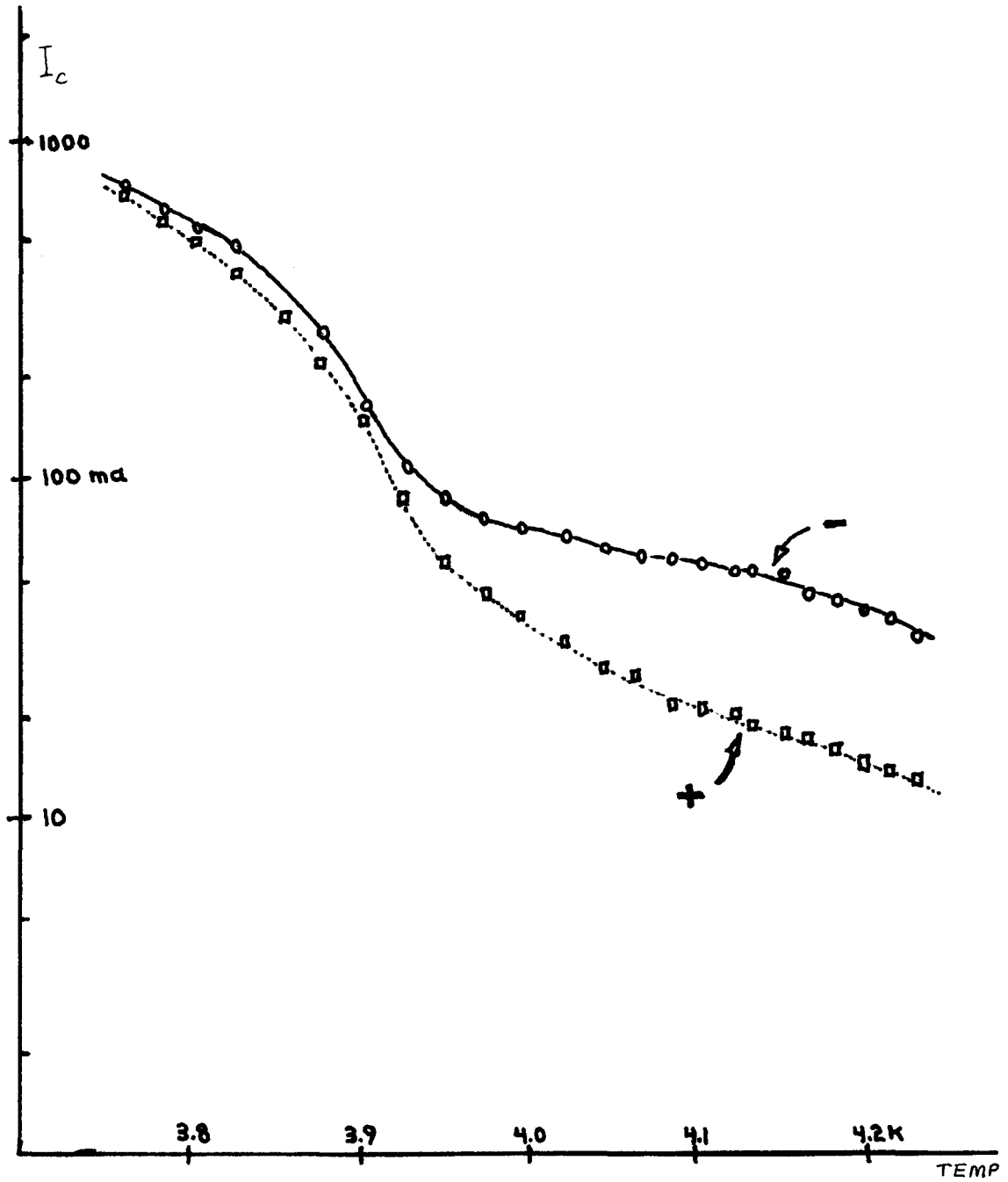


Fig. 8. Difference in critical current in (arbitrarily defined) + and - directions, due to flux trapped in junction.

IV. RESULTS OF THE SANDWICH MEASUREMENTS

A. V-I Characteristics

The V-I curves for one of the samples (as taken on a chart recorder--see Appendix A) are shown in Fig. 9 for various temperatures. As the current is increased from zero, a region with no measurable voltage drop is first seen; such current without any associated voltage drop indicates superconductive transport of current. At some current the superconductive transport ceases, and voltage abruptly appears. The current at which the voltage appears is the critical current of the sandwich; the critical current determination is quite precise, because the transition is so sharp. The V-I characteristic approaches a straight line through the origin when the current is well above the critical current; more of this line is traced out near the origin when the critical current is smaller, so we conclude that all of it would be traced out for zero critical current (that is, for no superconductivity) and identify the slope of the line with the normal resistance of the sandwich N layer. Therefore the V-I plot at any given temperature consists of a zero-voltage region at low currents, an abrupt appearance of voltage at the critical current of the sandwich, and a fairly rapid approach to the normal-state behavior of the N layer as the current is raised above the critical current. (It should be noted that absolute values of voltages are uncertain by a factor of two, but that relative values are accurate to 5% --see Appendix A).

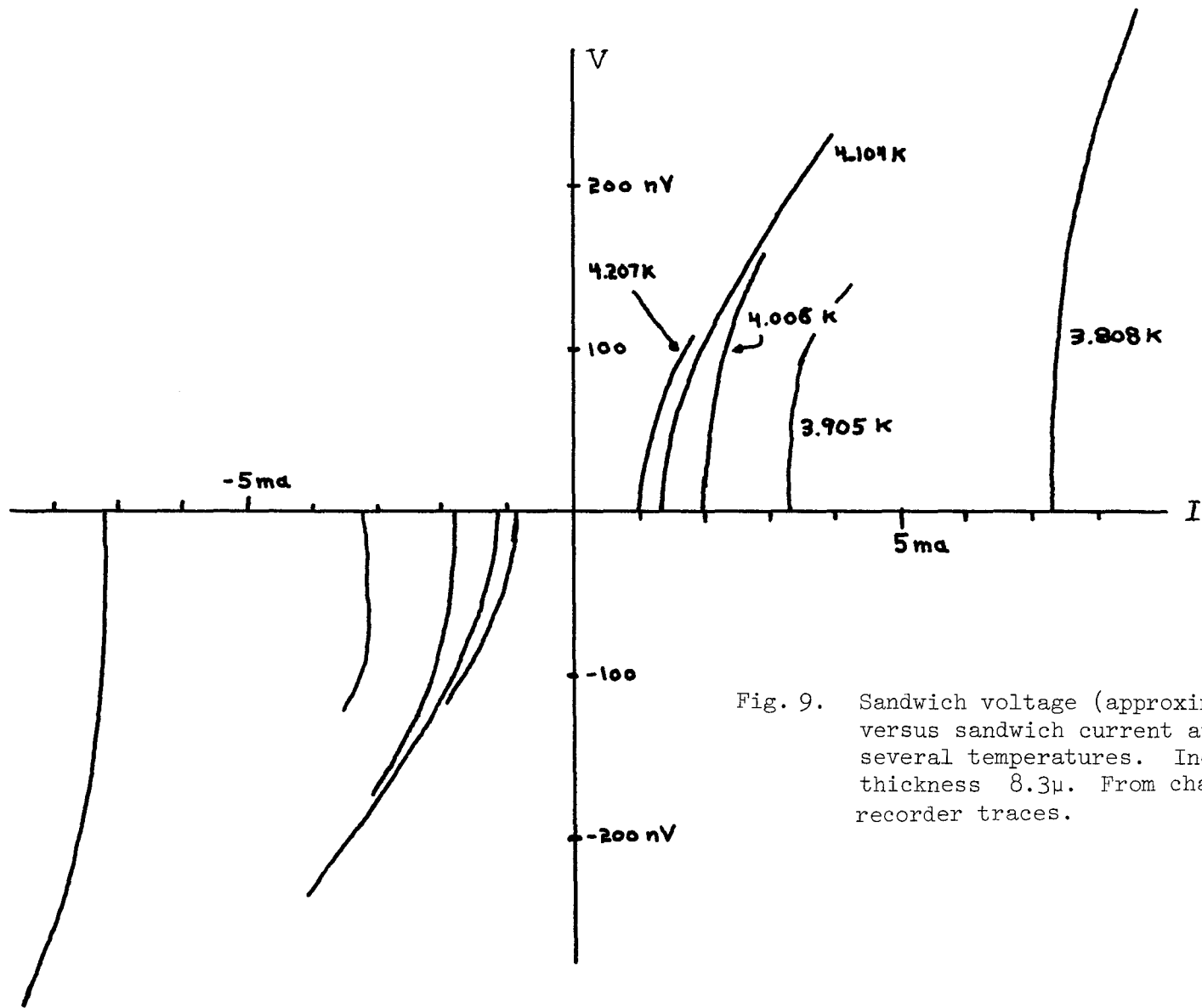


Fig. 9. Sandwich voltage (approximate) versus sandwich current at several temperatures. Indium thickness 8.3μ . From chart recorder traces.

B. Critical Current versus Temperature

The critical current increases as the temperature is lowered, as Fig. 9 shows. The critical current versus temperature curve for a sample can be plotted as in Fig. 10 ; the plot consists of discrete points because the temperature was lowered in discrete increments. This figure shows the effect of using a material with an experimentally accessible transition temperature for the N layer; there are clearly two different regions, with a sharp corner or knee between them. Such a knee was not seen in the experiments of Meissner and Clarke, who used materials which did not have transition temperatures in the measured temperature range. We thus conclude that the knee represents the transition of the In layer from the normal state to the superconducting state. To check this conclusion, we test to see if the region below the knee in temperature has a critical current which varies parabolically with temperature. This would be expected from an intrinsic superconductor because Silsbee's rule [22] predicts that the critical current of a material which is superconducting in its own right is proportional to the critical magnetic field of the material, and because the critical field varies parabolically with temperature. Figure 11 shows a plot of the critical current of the sample of Fig. 10 versus T^2 for temperatures below the knee, along with a straight line representing Silsbee's rule. The agreement is good except for a tail near, but below, the knee temperature. Recalling

[22] E. Lyton, Superconductivity, John Wiley & Sons, New York, 1962; p. 5.

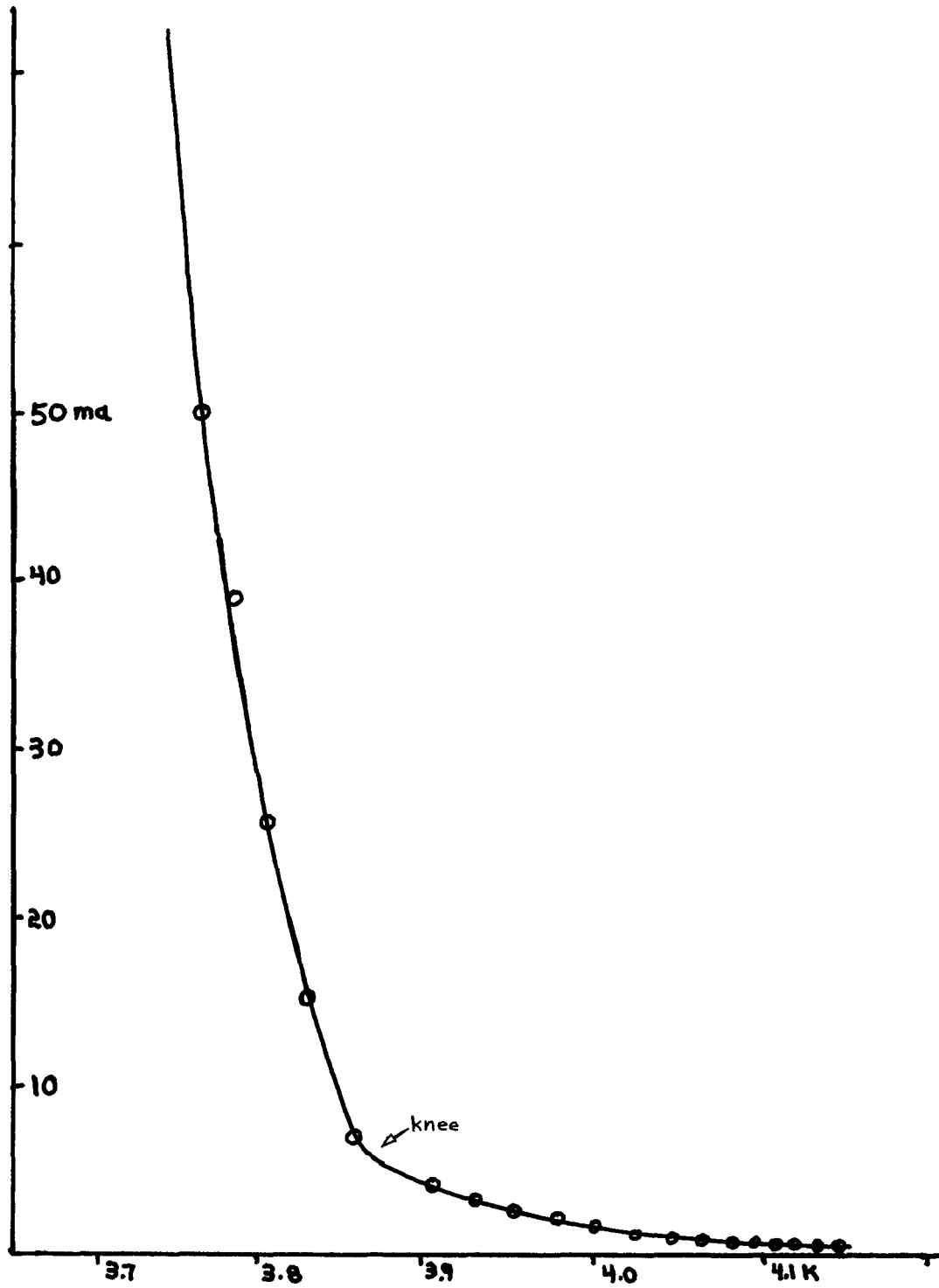


Fig. 10. Critical current versus temperature for Pb-In-Pb sandwich. Indium thickness, 4.2 μ .

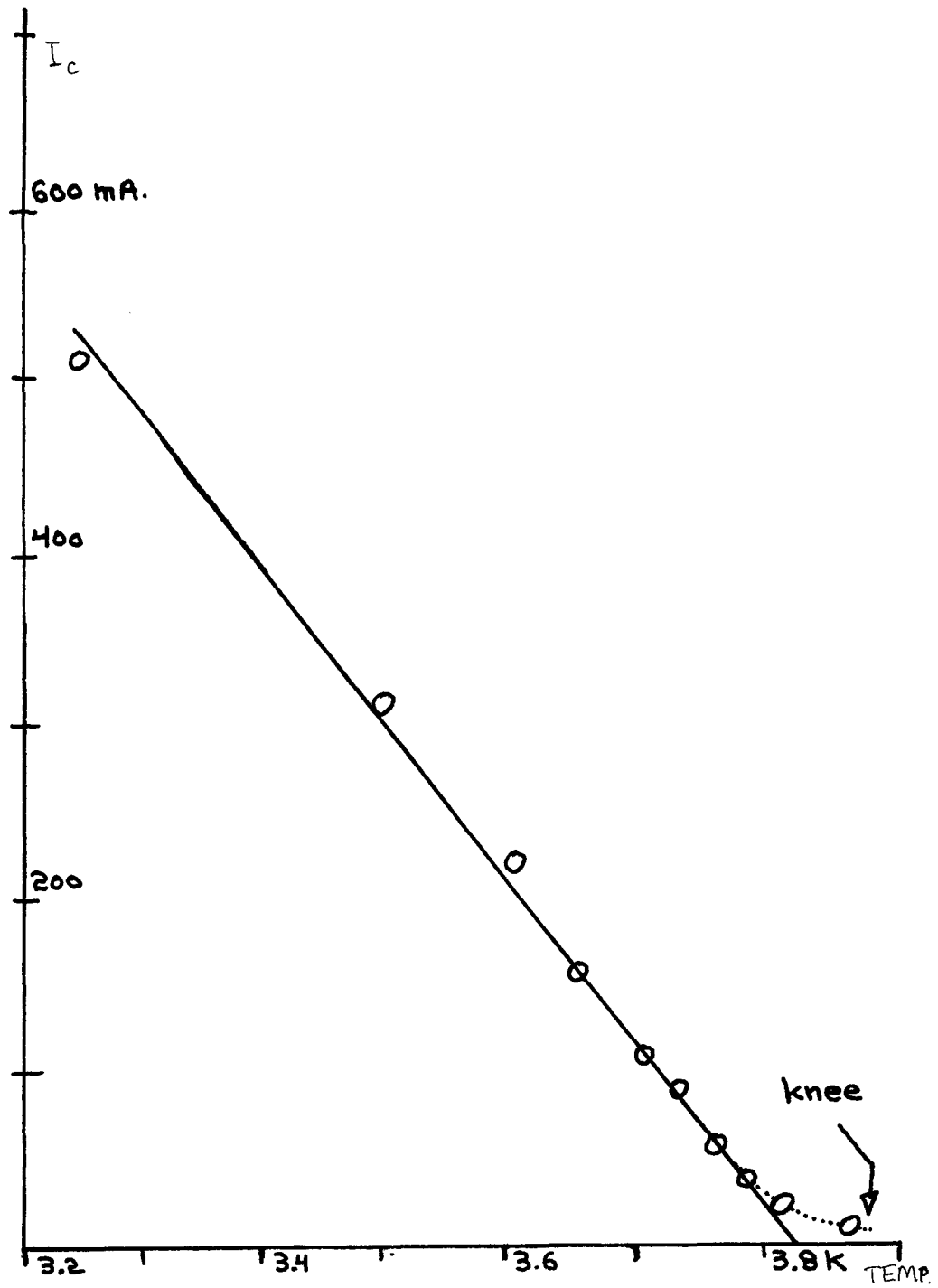


Fig. 11. The temperature region below the knee of the sample of Fig. 10 (points), showing the fit to the behavior expected from Silsbee's rule (line).

the broad transition of the test strips (Section III.B), we ascribe this effect to inhomogeneities in the In layer. The identification of the temperature region below the knee as the region of ordinary superconductivity is thus verified. The knee is therefore the transition temperature of the In layer above which the In has no intrinsic superconductive properties. This means that the region above the knee is the experimentally interesting region of induced superconductivity.

The temperature region above the knee due to the In transition is best presented on a plot of log critical current versus temperature, because of the large range of critical currents in this region. Such a plot is shown in Fig. 12. This figure shows the curves for two sandwiches on the same substrate when both happened to work, and gives some idea of the reproducibility of the results (the rise at high temperatures of one of the curves is atypical and the curve was not used.) Lines of best fit have been drawn by eye through the data points. Figure 13 shows such best fit lines for all reliable samples. For comparison, the curves for a sandwich made with Cu as the center layer (and with no ground plane) and for a thin In sample with no ground plane are also shown. The curves are marked with the thickness of the In layer and with the electron mean free path in the In layer (the mean free path is important to the theory). The fact that the curves in the region of induced superconductivity above the knee are fairly good straight lines indicates that the current varies essentially exponentially with temperature in this region (the peculiar behavior of the 4.14μ sample, which seems to show no proximity effect current, is unexplained). The general trend of these curves is

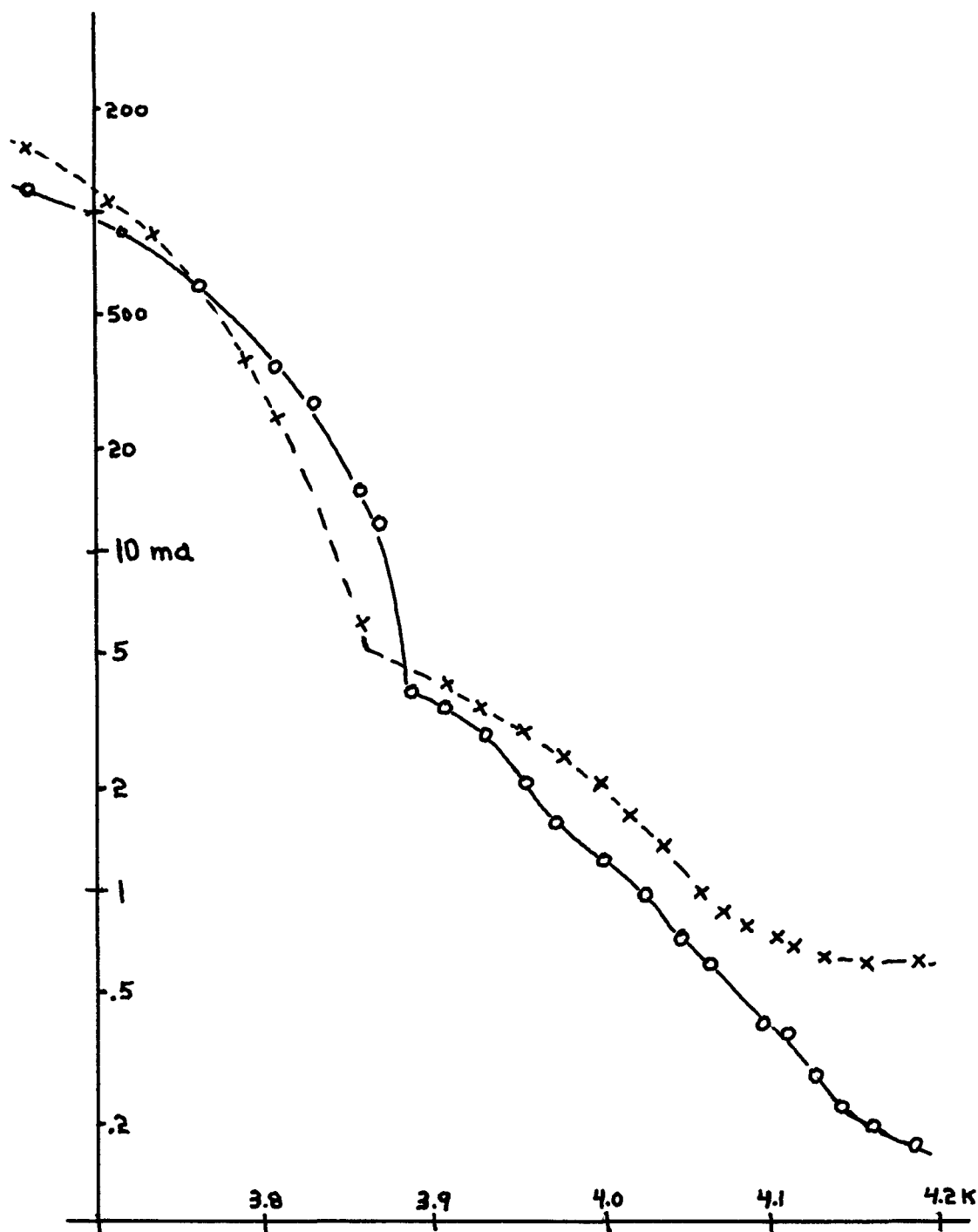


Fig.12 Log critical current versus temperature, showing approximate exponential region above knee temperature. The agreement of two samples on one substrate is also shown. Indium thickness 4.2μ .

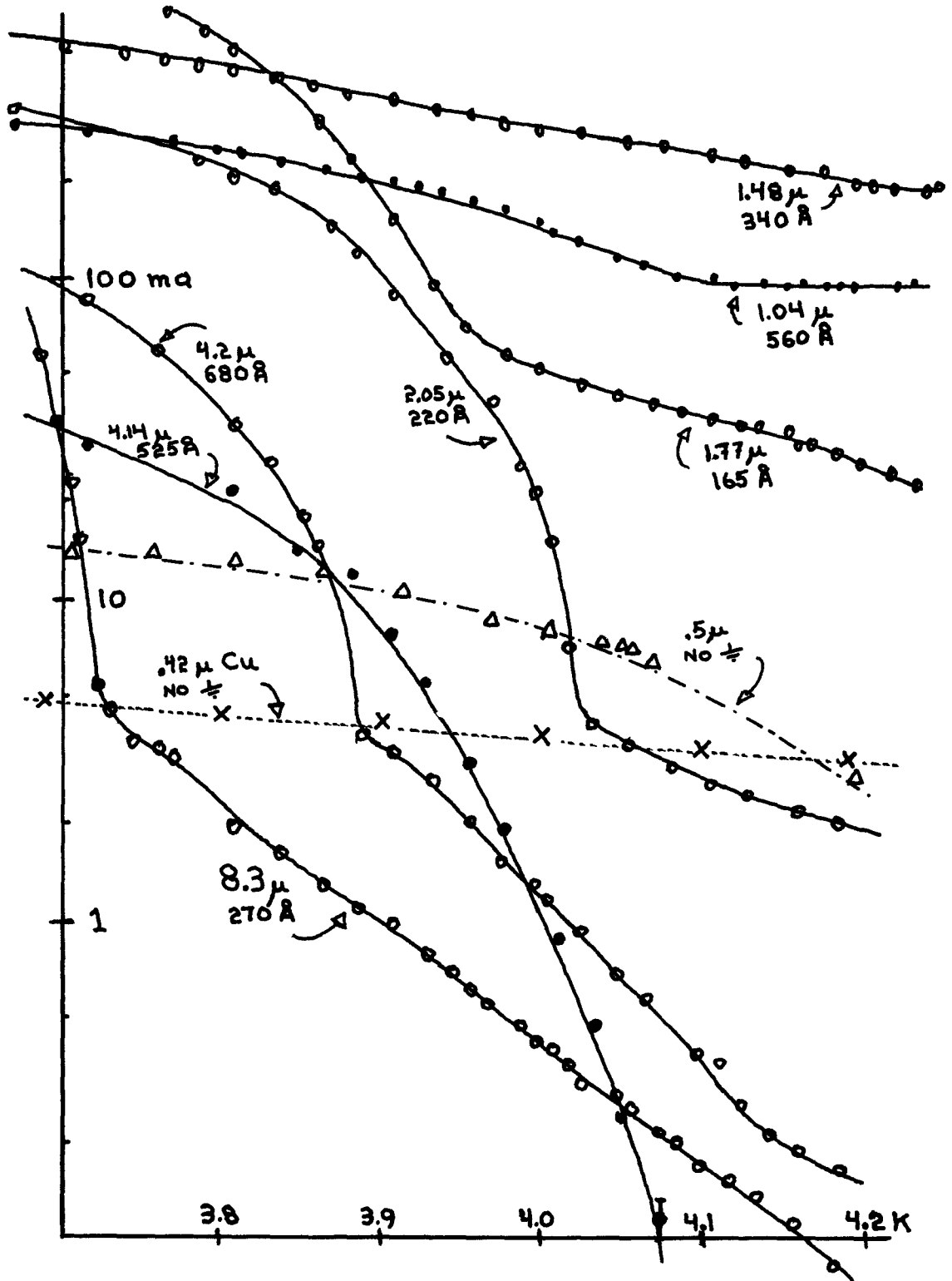


Fig. 13. Log critical current versus temperature for all good samples. Upper figure - In thickness. Lower figure - electron mean free path in In.

evident. As the thickness of the In increases, the current at any given temperature decreases, and the slope of the exponential region of the curves increases. This is just what we might expect from our picture of the diffusion of superconducting Cooper pairs into the N region. At any given temperature the reduction of current with thickness is due to the smaller density of pairs at the center of the thicker regions, while the increase of slope with thickness is expected from a model in which the current decreases by a given fraction in length L , and thus depends on $\exp(-2W_N/L)$, where $2W_N$ is the thickness of the N region and L is a temperature-dependent length characteristic of the pair diffusion process.

Another interesting feature is apparent from Fig. 13. As the In becomes thinner, its transition temperature becomes higher. Even for films many microns thick, it is above the transition temperature of pure In in bulk, which is 3.40 K. The transition temperatures of the mean free path test strips were also above the bulk value, although not as much as the sandwich In. Figure 14 shows the transition temperatures of the sandwiches and test strips for the various samples as a function of thickness. It is clear that there is a tendency for the thinner films to have a larger increase (at least in the sandwiches). The most likely cause of the rise is strain in the films, which is known to increase the transition temperature [23]. Deposition at low temperatures produces a built-in strain in thin films [24], and additional strain

[23] A. Toxen, Phys. Rev. 123, 442 (1961)

[24] R. Hoffman, in Physics of Thin Films Vol. 3, Academic Press, New York; p. 219.

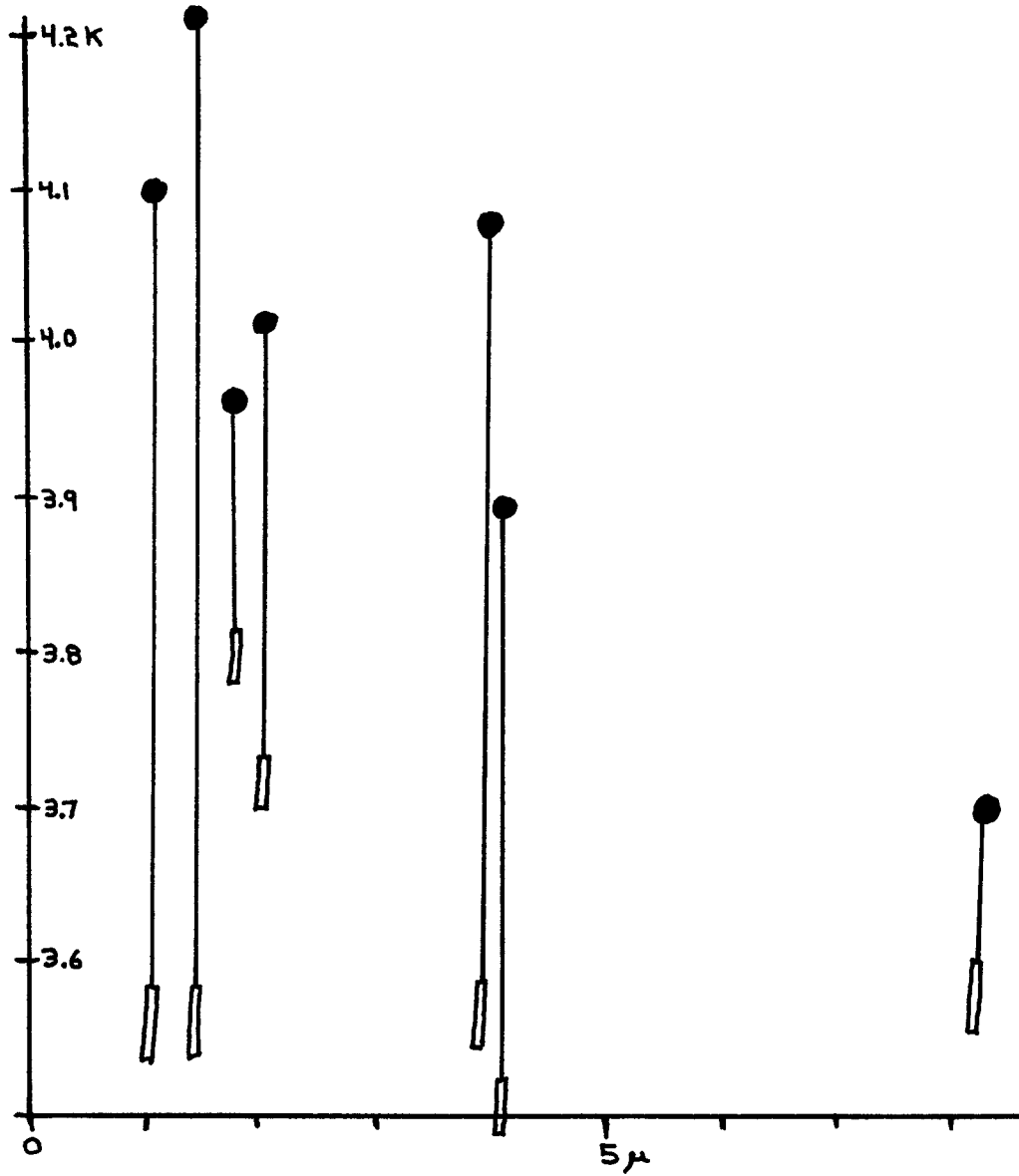


Fig. 14. Transition temperatures of sandwich and test strip versus thickness. Black dot - sandwich knee temperature. Open rectangle - test strip transition.

is undoubtedly caused by differential contraction of the layers upon cooling to liquid helium temperatures. The greater effect in the sandwich layers is explained by the increased strain due to the Pb layers on either side of the In.

V. THEORETICAL MODEL AND PREDICTIONS

A. Ginzburg-Landau Equation

Gor'kov [25] has shown that the superconductivity in a metal near its superconducting transition temperature T_c can be described in terms of a spatially varying energy gap $D(r)$. This gap obeys a Ginzburg-Landau [26] type equation

$$\left(\nabla - i \frac{e}{\hbar} \underline{A}\right)^2 D = -k^2 \left(1 - \frac{D^* D}{r_B^2}\right) D \quad (1)$$

where e is the charge of a Cooper pair of electrons (twice the electronic charge), \underline{A} is the vector potential, k is the (temperature dependent) characteristic inverse length for variations of D , and r_B is the (temperature dependent) equilibrium amplitude of D in the interior of a bulk superconductor. Gor'kov also showed that the current density is given by

$$\underline{j} = C \operatorname{Im}[D^*(\nabla - i \frac{e}{\hbar} \underline{A}) D] \quad (2)$$

where C is a constant; we see that $D^* D$ can be thought of as a "density of superelectrons". De Gennes [27] has shown that in a dirty metal (one in which the electron mean free path ℓ is much less than

[25] L. Gor'kov, Zh. Eksp. Teor. Fiz. 36, 1918 (1959); [Trans.--Sov. Phys. JETP 36, 1364 (1959)].

[26] V. Ginzburg and L. Landau, Zh. Eksp. Teor. Fiz. 20, 1064 (1950); Trans.--D. ter Haar, Men of Physics: L. D. Landau I, Pergamon Press, New York, 1965)].

[27] P. de Gennes, Superconductivity of Metals and Alloys, Benjamin, New York, 1966; Section 8-3.

the pure bulk coherence length ξ_0 (which in the BCS [28] theory is given by $\xi_0 = e^{\gamma} \hbar v_f / \pi^2 k_B T_c$, where v_f is the Fermi velocity of the metal, and $e^{\gamma} = 1.7810724\dots$) an equation like Eq. (1) holds at all temperatures. We shall thus use Eq. (1) as a model for the superconductivity in our sandwiches; in this formalism the difference between the S and N regions arises from the fact that k and r_B differ in the two regions. (k_B is Boltzmann's constant.)

We shall make two simplifying assumptions in order to make solution of Eq. (1) possible. Firstly, we assume that magnetic field effects due to external fields, and due to currents in the sample, are negligible; we thus set $\underline{A} = 0$. Secondly, we suppose that the two superconductors on both sides of the center metal impose uniform boundary conditions in the plane of the sandwich, so that the gap in the N region will vary only across the sandwich, and not in its plane. Taking a coordinate system with its x axis across the sandwich (see Fig. 15) we can then simplify Eq. (1) to

$$D'' = -k^2 \left(1 - \frac{D^* D'}{r_B^2}\right) D \quad (3)$$

(Hereafter we denote differentiation with respect to x by a prime.)

The current density becomes

$$j = C \operatorname{Im}(D^* D') \quad (4)$$

[28] J. Bardeen, L. Cooper, and J. Schrieffer, Phys. Rev. 108, 1175 (1957).

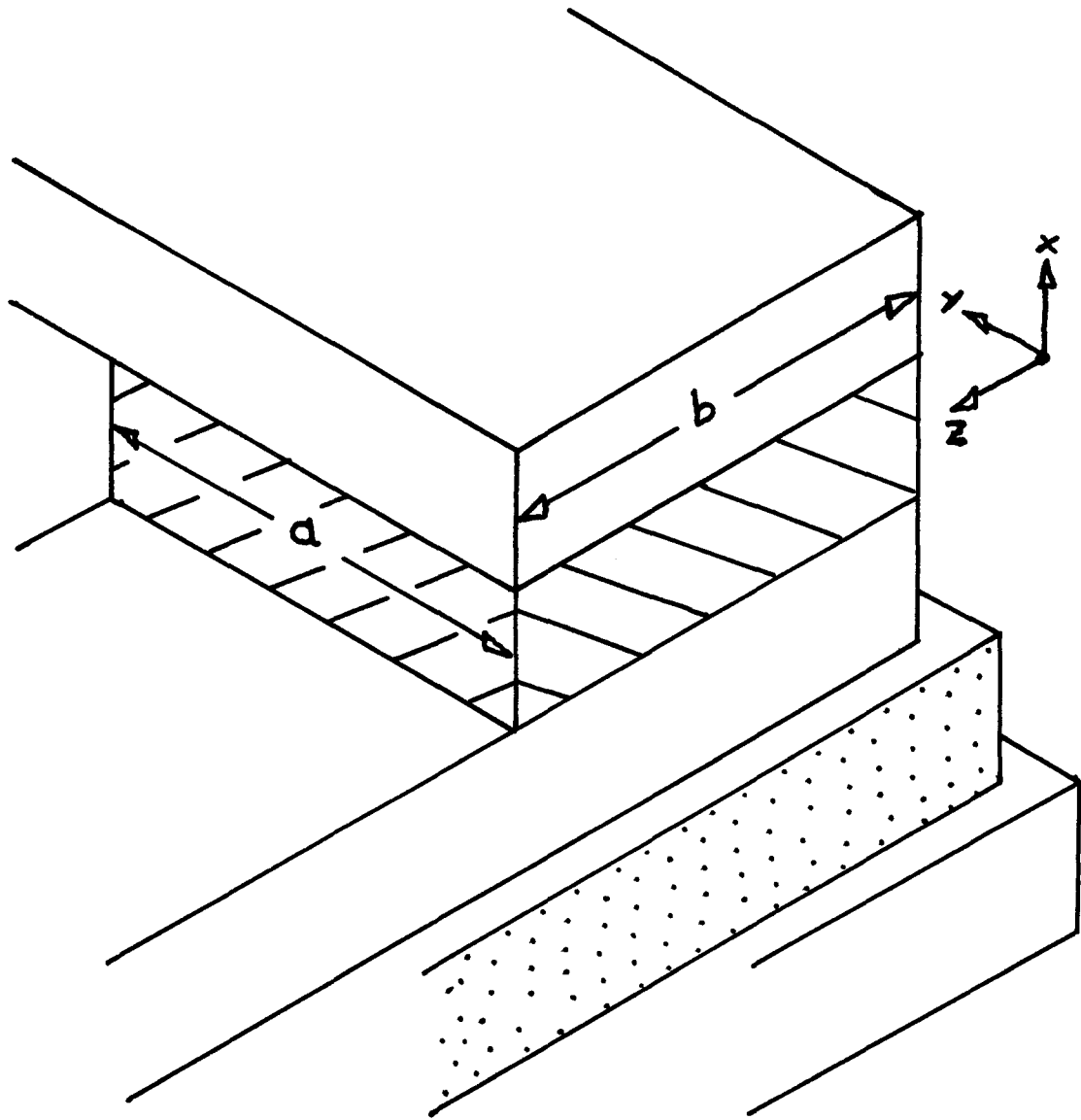


Fig. 15. Schematic illustration of sandwich structure, showing (from top to bottom) the upper Pb strip, In layer, lower Pb strip, insulating layer, and Pb ground plane. The origin of coordinates is at the center of the junction.

Writing D in terms of its amplitude and phase $D = re^{i\phi}$, we find that the real part of Eq. (3) becomes

$$r'' = r(\phi')^2 - k^2 \left(1 - \frac{r^2}{r_B^2}\right) r \quad (5)$$

and the imaginary part can be written in the form

$$\frac{1}{r} (r^2 \phi')' = 0 \quad (6)$$

Equation (4) becomes

$$j = Cr^2 \phi' \quad (7)$$

from which we see that Eq. (6) implies conservation of current, as long as $r \neq 0$. We can use Eq. (7) to eliminate ϕ' from Eq. (5) which then becomes

$$r'' = \frac{j^2}{C^2 r^3} - k^2 \left(1 - \frac{r^2}{r_B^2}\right) r \quad (8)$$

B. Temperature Dependence of k^2 and r_B^2

The constants k^2 and r_B^2 in Eq. (8) both vary with temperature; as we shall see, both are positive below the transition temperature T_c and negative above it.

According to the de Gennes-Werthamer dirty limit theory [29], the temperature dependence of k^2 is found from the implicit equation

[29] A. Jacobs, Phys. Rev. 162, 375 (1967).

$$\chi\left(\frac{k^2 L^2 T_c}{T}\right) = \ln\left(\frac{T}{T_c}\right) \quad (9)$$

where $\chi(x) = \psi\left(\frac{x}{2} + \frac{1}{2}\right) - \psi\left(\frac{1}{2}\right)$, and ψ is the digamma function [30]. The quantity L^2 is given by $L^2 = \hbar v_f \ell / 6\pi k_B T_c = \frac{\pi}{6e\gamma} \xi_0 \ell$. We see from the form of Eq. (9) that $k^2 L^2$ depends only on the ratio T/T_c , or that k^2/T_c depends on T/T_c alone. Solutions of Eq. (9) are shown in Fig. 16 for various values of T_c ; the most interesting feature of these curves is the fact that k^2 approaches its limiting behavior at high temperatures only logarithmically, a situation which offers hope of detecting incipient superconductivity at temperatures above the transition temperature by measurement of k^2 . As T becomes much larger than T_c we have from Eq. (9)

$$k^2 L^2 \approx -\frac{T}{T_c} \left[1 - \frac{2}{\ln(T/T_c)}\right], \quad T \gg T_c$$

while near T_c we find

$$k^2 L^2 \approx \frac{4}{\pi^2} \left(1 - \frac{T}{T_c}\right), \quad T \approx T_c \quad (10)$$

At low temperatures k^2 approaches a constant value

$$k^2 L^2 \approx \frac{1}{2e\gamma}, \quad T \ll T_c$$

For numerical computations it is convenient to have an expression for

[30] M. Abramowitz and I. Stegun, Handbook of Mathematical Functions National Bureau of Standards, Washington, D.C. 1964; p. 258.

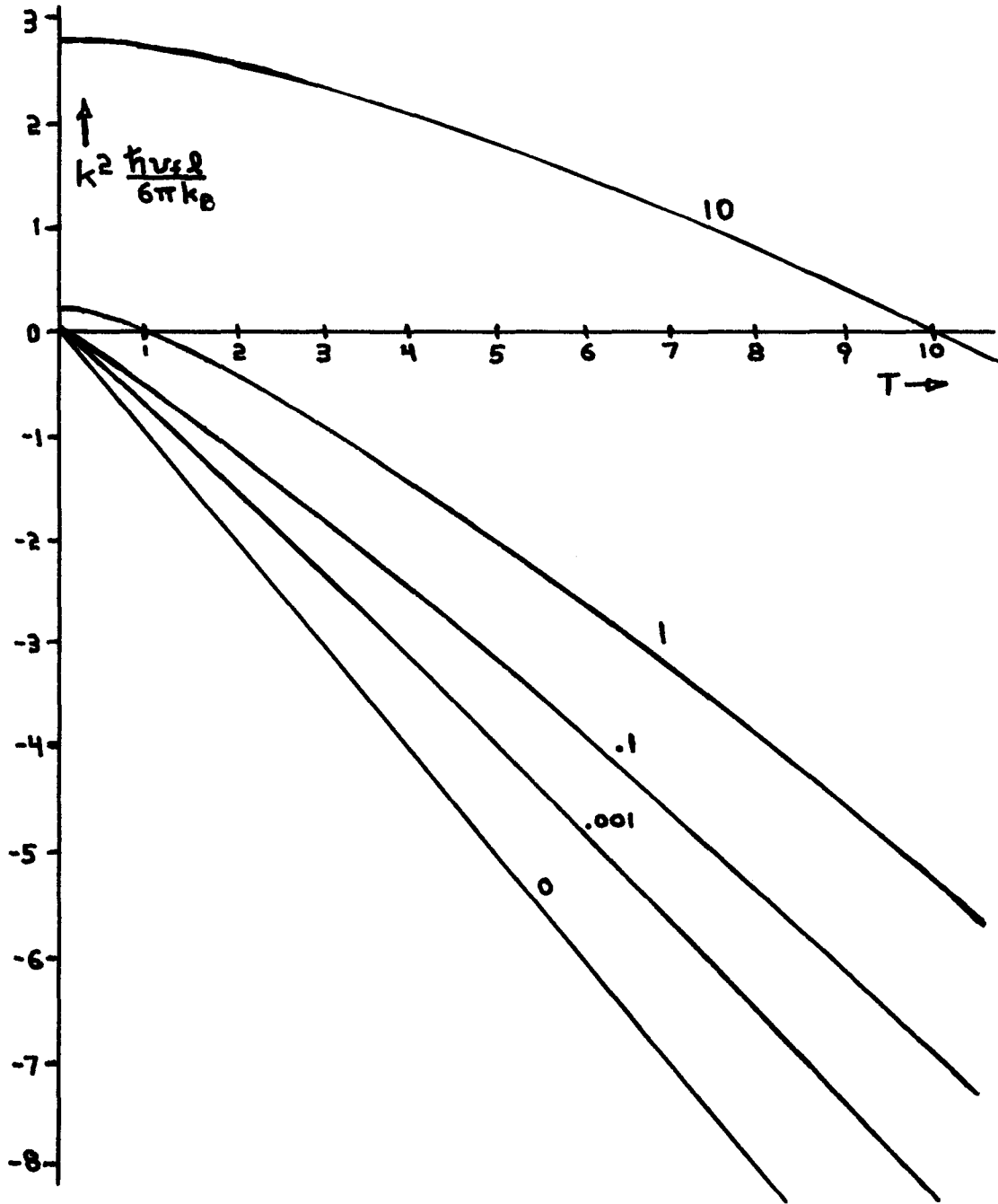


Fig. 16. Temperature dependence of the inverse length k in the Ginzburg-Landau equation for various critical temperatures, showing the slow approach to the asymptotic behavior for zero critical temperature.

k^2 which is simpler to use than Eq. (9). Above T_c very accurate results are achieved by approximating $\chi(x)$ by $\frac{-2}{1+x} + 2 + (\frac{\pi^2}{4} - 2)x$ for $x < 0$. (This reproduces the behavior as x approaches -1, and matches value and slope at the origin.) The result (accurate to better than 1%) of this approximation is

$$k^2 L^2 = -\frac{T}{T_c} \frac{(\frac{\pi^2}{4} + \ln \frac{T}{T_c})}{2(\frac{\pi^2}{4} - 2)} \left[1 - \sqrt{1 - \frac{4(\frac{\pi^2}{4} - 2) \ln \frac{T}{T_c}}{(\frac{\pi^2}{4} + \ln \frac{T}{T_c})^2}} \right], T > T_c$$

Below T_c the solution of Eq. (9) can be fitted with a polynomial in $(1 - \frac{T}{T_c})$ to give the result (again, good to 1%)

$$k^2 L^2 = \frac{4}{\pi^2} (1 - \frac{T}{T_c}) - .08 (1 - \frac{T}{T_c})^2 - .045 (1 - \frac{T}{T_c})^6, T < T_c$$

The de Gennes-Werthamer theory is based on the assumption that D is infinitesimal, and thus does not treat the nonlinear term (in r_B^2) of Eq. (1). However, de Gennes has discussed this term in the dirty limit [31]; he finds that r_B^2 is the same as the BCS value, which is found from the implicit integral equation

$$\frac{1}{NV} = \int_0^{\hbar\omega_c} \frac{\tanh\left(\frac{\sqrt{\epsilon^2 + r_B^2}}{2k_B T}\right)}{\sqrt{\epsilon^2 + r_B^2}} d\epsilon \quad (11)$$

[31] P. de Gennes, op. cit., Section 7-2.

where N is the energy density of the states per unit volume at the Fermi surface, and V is the BCS interaction parameter (ω_c is the cutoff frequency for the interaction). Equation (11) has been numerically integrated in the limit $\hbar\omega_c \gg k_B T_c$ by Muhlschlegel [32]; we can reproduce his results to 1% accuracy with the polynomial

$$r_B^2 = \left(\frac{\pi}{e\gamma} k_B T_c\right)^2 \left[1 + .00533 \frac{T}{T_c} - 2.00533 \left(\frac{T}{T_c}\right)^4 + \left(\frac{T}{T_c}\right)^5\right],$$

$$T < T_c$$

in which we have used the results of BCS that at $T = 0$, $r_B = \frac{\pi}{e\gamma} k_B T_c$, and that when T is near T_c

$$r_B^2 = 3.016 \left(\frac{\pi}{e\gamma} k_B T_c\right)^2 \left(1 - \frac{T}{T_c}\right).$$

The term of Eq. (8) in r_B^2 is dominant only if r_B^2 is small compared to r^2 , and so we are not interested in the behavior of r_B^2 far above T_c , as long as it is large. Thus we approximate the behavior above T_c by a linear extension of the behavior near T_c

$$r_B^2 = -3.016 \left(\frac{\pi}{e\gamma} k_B T_c\right)^2 \left(\frac{T}{T_c} - 1\right), \quad T > T_c \quad (12)$$

If needed, a more accurate result could be derived by integrating Eq. (11) for temperatures above T_c .

[32] B. Muhlschlegel, Z. Physik 155, 313 (1959).

A physical understanding of k^2 and r_B^2 can be gained from examining Eq. (8) (with $j=0$ for simplicity) for various temperatures. When T is below T_c , r'' initially decreases from zero linearly with r (see Fig. 17). Such negative curvature for positive r indicates stable solutions of the sin or cos type to Eq. (8), and thus shows that superconductivity is initially favored. This is because the gain in energy due to the pairing interaction is greater than the loss of free energy due to the reduced entropy of the pair state. However, as the fraction of paired electrons increases (i.e., as r increases), the pairing gain per pair becomes less, and r'' increases through zero under the continued influence of the entropy reduction. At higher temperatures the entropy contribution is larger, and the initial decrease of r'' with r has smaller slope. Above T_c it is in fact disadvantageous for the electrons to pair, and the initial slope of r'' is positive; at larger r the same pair energy decrease as at lower temperatures causes upward curvature of the r'' curve (Fig. 17).

The initial slope of the r'' versus r curve is described by the coefficient k^2 , and so we see that this coefficient describes the balance of pairing and entropy effects. When pairing outweighs entropy (for small r) k^2 is positive, and when entropy outweighs pairing k^2 is negative. The upturning at larger r is due to the term $r^3 k^2 / r_B^2$ which describes the dropoff of pairing. (We see from Fig. 18 that this term varies slowly with temperature, and because the pairing interaction is essentially temperature independent while the entropy effects are strongly temperature dependent, we ascribe this second term to the pairing effects).

From the above argument, the extension of r_B^2 above T_c is seen as a reflection of the temperature independence of the pairing interaction.

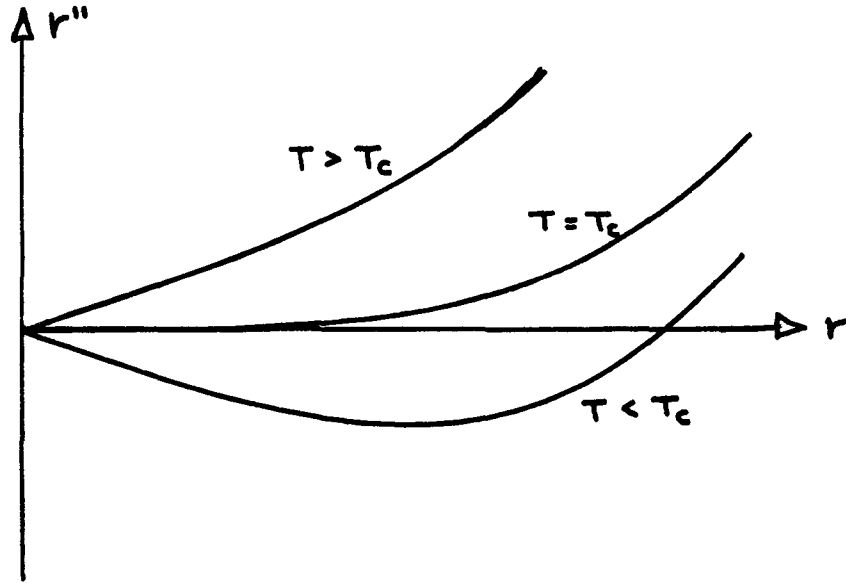


Fig. 17. r'' versus r (from Eq. (8) with $j = 0$) for temperatures below, at, and above the transition temperature T_c . Values of r'' less than zero indicate that superconductivity is energetically favored.

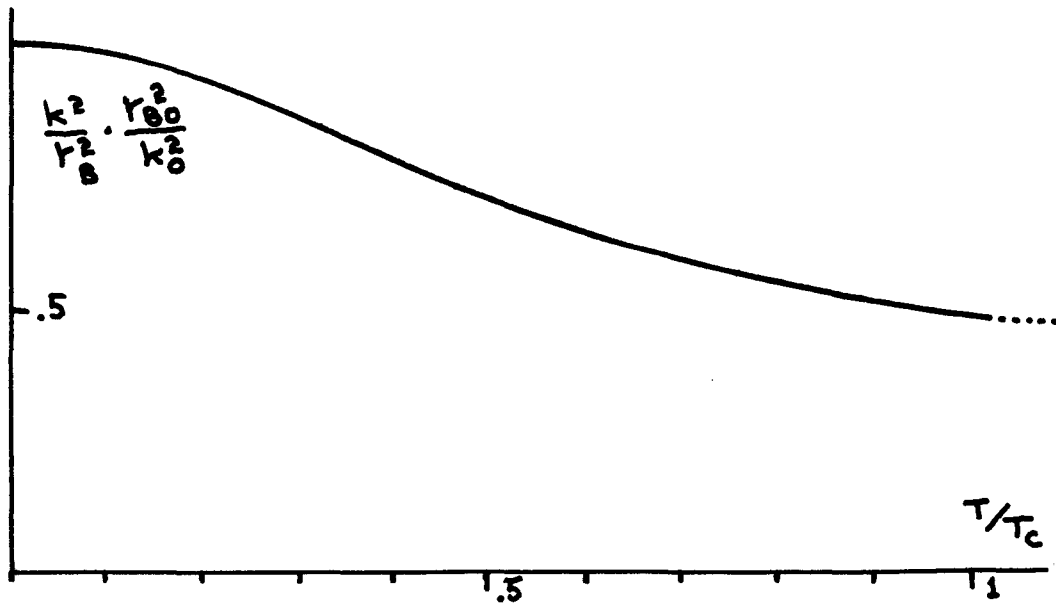


Fig. 18. The temperature variation of the term in k^2/r^2 of Eq. (8), showing the small variation compared to that of k^2 (Fig. 16).

The variation of r_B^2 with temperature is shown in Fig. 19 for various values of T_c , along with the presumed extension above T_c .

We note here that the BCS theory gives the relation

$$k_B T_c = \frac{2e\gamma}{\pi} \hbar\omega_c e^{-\left(\frac{1}{NV}\right)}$$

C. S Region

We will assume that the maximum current through the N region is small enough that in the S region (where r is much larger than in the N region) the current term $j^2/C^2 r^3$ in Eq. (8) can be ignored. We then have the equation

$$r'' = -k^2 \left(1 - \frac{r^2}{r_B^2}\right) r \quad (13)$$

which can be solved by the standard method of letting $p = r'$, so that $p \frac{dp}{dr} = r''$, resulting in the first integral

$$(r')^2 = B_1 - k^2 \left(1 - \frac{r^2}{r_B^2}\right) r^2 \quad (14)$$

where B_1 is the constant of integration. In general, the solution for r will be in terms of elliptic functions; however when the S region is thick compared to k^{-1} (a condition which holds unless T is near T_{cs}) r approaches r_B and r' approaches zero in the interior of the S region, and so $B_1 = k^2 r_B^2 / 2$. Equation (14) then becomes

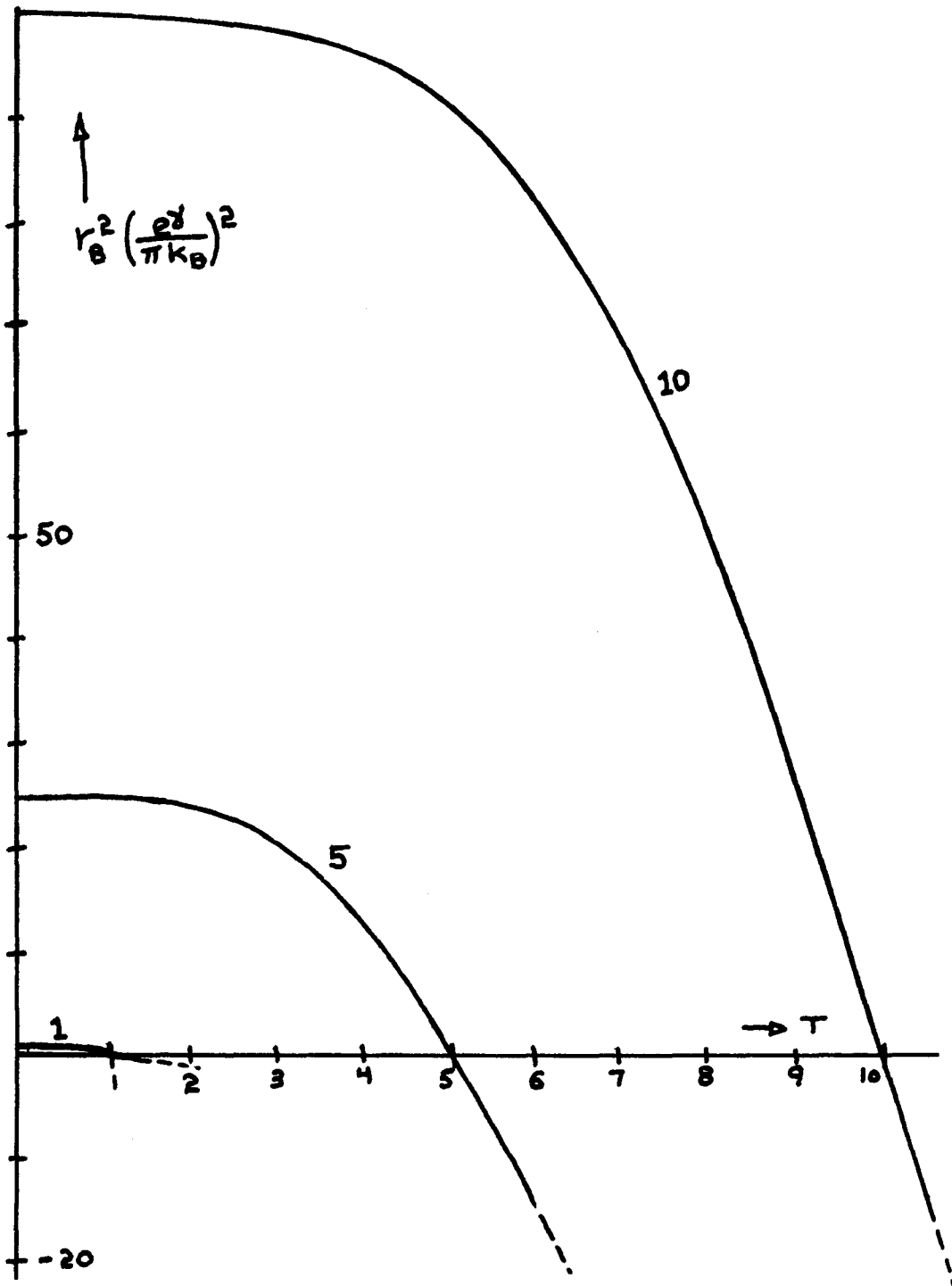


Fig. 19. Temperature dependence of the equilibrium gap in the Ginzburg-Landau equation for various critical temperatures, along with the assumed extension to temperatures above the critical temperature.

$$r' = \frac{k}{r_B \sqrt{2}} (r_B^2 - r^2) \quad (15)$$

which integrates to

$$r = r_B \tanh\left[\frac{k}{\sqrt{2}} (x - x_0)\right]$$

D. N Region; Critical Current

In the N region, where T is greater than T_c , both r_B^2 and k^2 are negative, and it is convenient to define the positive quantities

$$\alpha^2 = -k^2$$

and

$$r_m^2 = -r_B^2$$

From this point we will reserve k and r_B for reference to the properties of the S region, and use α and r_m to describe the N region.

We first consider the situation $r \ll r_m$. Equation (3) then becomes approximately linear

$$D'' = \alpha^2 D \quad (16)$$

This equation has the standard solution

$$D = E \cosh(\alpha x) + F \sinh(\alpha x)$$

where E and F are constants set by the boundary conditions. We presume that the two S regions on either side of the central N region are identical in their effect on the boundary conditions; D will then have the same amplitude (but, in general, different phase)

at the two interfaces. Let the boundaries of the N region be at $x = \pm W_N$, and take the total phase difference to be θ ; without loss of generality we write

$$D(\pm W_N) = r_N e^{\pm i\theta/2}$$

where r_N is the amplitude of D at the N side of the SN interface. We find

$$D = r_N \cos(\theta/2) \frac{\cosh(\alpha x)}{\cosh(\alpha W_N)} + i r_N \sin(\theta/2) \frac{\sinh(\alpha x)}{\sinh(\alpha W_N)} \quad (17)$$

from which, using Eq. (4), we derive the Josephson-type [33] relation between current and phase difference

$$j = \frac{C\alpha r_N^2}{\sinh(2\alpha W_N)} \sin \theta \quad (18)$$

If r_N does not depend on θ (this is true when $\alpha W_N \gg 1$), then the largest possible current density comes for $\sin(\theta) = 1$; this defines the critical current density j_c as

$$j_c \approx \frac{C\alpha r_N^2}{\sinh(2\alpha W_N)} \quad \begin{array}{l} r_N \ll r_m \\ \alpha W_N \gg 1 \end{array} \quad (19)$$

In the derivation of Eq. (19) we have assumed that $r \ll r_m$, and as the maximum value of r is r_N we must therefore have $r_N \ll r_m$.

When r_N is comparable to or larger than r_m , Eq. (8) is no longer approximately linear, and the calculation of the critical

[33] B. Josephson, Phys. Letters 1, 251 (1962).

current is more difficult. We must write down the solution to the equation for r and then try to match the boundary conditions. Above the critical current, such matching will not be possible, and so we can find the critical current as the maximum current for which we can find a boundary-matched solution to Eq. (8).

The fundamental equation for r is

$$r'' = \frac{j^2}{C^2 r^3} + \alpha^2 r + \frac{\alpha^2}{r_m^2} r^3 \quad (20)$$

For algebraic simplicity, we utilize the variables

$$\sigma = \alpha x \quad , \quad \rho = r/r_m$$

and Eq. (20) becomes

$$\frac{d^2 \rho}{d\sigma^2} = \frac{\Lambda}{\rho^3} + \rho + \rho^3 \quad (21a)$$

where

$$\Lambda = \left(\frac{j}{C \alpha r_m^2} \right)^2 \quad (21b)$$

We now assume a symmetric solution with $\rho = \rho_0$ and $\frac{d\rho}{d\sigma} = 0$ at the center of the N region, where $\sigma = 0$. The first integral of Eq. (21) is then found by the same method used in the S region, and is

$$\left(\frac{d\rho}{d\sigma} \right)^2 = \Lambda \left(\frac{1}{\rho_0^2} - \frac{1}{\rho^2} \right) + (\rho^2 - \rho_0^2) + \frac{1}{2}(\rho^4 - \rho_0^4) \quad (22)$$

The change of variable $\delta = \rho^2$ [34] allows the transformation of the second integral

$$\int_{\rho_0}^{\rho} \frac{\rho d\rho}{\sqrt{(\rho^2 - \rho_0^2)[\rho^4 + \rho_0^2(\rho_0^4 + 2\rho_0^2) + 2\Lambda]}} = \frac{\sigma}{\rho_0 \sqrt{2}}$$

into the standard elliptic integral form

$$\int_{\delta_0}^{\delta} \frac{d\delta}{\sqrt{(\delta - \delta_0)[\delta^2 + \delta(\delta_0 + 2) + 2\Lambda/\delta_0]}} = \sigma \sqrt{2} \quad (23)$$

The solution for r is then found by standard methods [35] in terms of elliptic functions. There are two types of solution, depending on the relative values of j and r_0 :

$$1) \quad j \leq \frac{C\alpha r_0}{2\sqrt{2} r_m} (r_0^2 + 2r_m^2)$$

$$\gamma_1 = -\left(\frac{1}{2} r_0^2 + r_m^2\right) + \sqrt{\left(\frac{1}{2} r_0^2 + r_m^2\right)^2 - 2\left(\frac{j r_m}{C\alpha r_0}\right)^2}$$

$$\gamma_2 = -\left(\frac{1}{2} r_0^2 + r_m^2\right) - \sqrt{\left(\frac{1}{2} r_0^2 + r_m^2\right)^2 - 2\left(\frac{j r_m}{C\alpha r_0}\right)^2}$$

$$r^2 = \gamma_1 + \frac{r_0^2 - \gamma_1}{\text{cn}^2 \left(\alpha x \sqrt{\frac{r_0^2 - \gamma_1}{2r_m^2}} \middle| \frac{\gamma_1 - \gamma_2}{r_0^2 - \gamma_2} \right)} \quad (24a)$$

[34] J. Mathews (private communication).

[35] M. Abramowitz and I. Stegun, op. cit. ; p. 597.

$$\begin{aligned}
 2) \quad j &\cong \frac{C\alpha r_o}{2\sqrt{2} r_m} (r_o^2 + 2r_m^2) \\
 \zeta &= \sqrt{2r_o^2(r_o^2 + r_m^2) + 2\left(\frac{jr_m}{C\alpha r_o}\right)^2} \\
 r^2 &= r_o^2 - \zeta + \frac{2\zeta}{1 + \operatorname{cn}\left(\alpha x \sqrt{\frac{2\zeta}{r_m^2}} \left| \frac{1}{2} - \frac{3r_o^2 + 2r_m^2}{4\zeta} \right. \right)} \quad (24b)
 \end{aligned}$$

These solutions must be fitted to the boundary conditions at the SN interface.

E. Boundary Conditions

De Gennes, on the basis of the dirty approximation ($\ell \ll \xi_o$) has derived [36] the boundary conditions

$$\frac{r_N}{N_N V_N} = \frac{r_s}{N_s V_s} \quad (25a)$$

$$\frac{v_{fN} \ell_N}{V_N} r'_N = \frac{v_{fs} \ell_s}{V_s} r'_s \quad (25b)$$

where the subscripts s and N indicate the values at the edges of the respective regions.

Equation (15) relates r_s and r'_s by

$$r'_s = \frac{k}{r_B \sqrt{2}} (r_B^2 - r_s^2) \quad (26)$$

[36] P. de Gennes, Rev. Mod. Phys. 36, 225 (1964).

and r_N and r'_N can be related by Eq. (22);

$$(r'_N)^2 = \frac{j^2}{c^2} \left(\frac{1}{r_o^2} - \frac{1}{r_N^2} \right) + \alpha^2 (r_N^2 - r_o^2) + \frac{\alpha^2}{2r_m^2} (r_N^4 - r_o^4) \quad (27)$$

We may now eliminate r_s , r'_s , and r'_N from Eq. (25), Eq. (26), and Eq. (27) to yield a relation between r_o and r_N at the boundary:

$$\frac{j^2}{c^2} \left(\frac{1}{r_o^2} - \frac{1}{r_N^2} \right) + \alpha^2 (r_N^2 - r_o^2) + \frac{\alpha^2}{2r_m^2} (r_N^4 - r_o^4) = B \left[r_B^2 - \left(\frac{N_s V_s}{N_N V_N} \right)^2 r_N^2 \right]^2 \quad (28a)$$

where
$$B = \left(\frac{v_{fs} \ell_s V_N k}{v_{fN} \ell_N V_s r_B \sqrt{2}} \right)^2 \quad (28b)$$

Equations (24) and (28) must be solved simultaneously (putting $x = W_N$ into Eq. (24) so that $r = r_N$) to find r_o , and thus determine the complete solution. (If $j > j_c$, no solution exists.)

In the case where $r_N \ll r_m$, the situation is considerably simplified. Equation (17) then applies, and (once more assuming $\alpha W_N \gg 1$) we have

$$r'_N \approx \alpha r_N \quad (29)$$

Elimination of r_s , r'_s , and r'_N from Eq. (25), Eq. (26), and Eq. (29) then yields

$$r_N = r_B \frac{N_N V_N}{N_s V_s} G \left(\sqrt{1 + G^{-2}} - 1 \right) \quad (30a)$$

where

$$G = \frac{\alpha v_{fN} \ell_N N_N}{\sqrt{2} k v_{fs} \ell_s N_s} \quad \begin{array}{l} r_N \ll r_m \\ \alpha W_N \gg 1 \end{array} \quad (30b)$$

The critical current is then found by substituting this value of r_N into Eq. (19).

F. Magnetic Effects

When no external field is present, a superconducting ground plane forces currents to flow uniformly on the side of a strip which is toward the ground plane, and not on the other side. When an external field is present, a surface current flows on the outside surface; this current is just sufficient to cancel the external field so that $\underline{H} = 0$ inside the strip.

Applying these principles to our sandwich, and recalling that the S strip next to the ground plane will act in turn as a ground plane for the strip away from the ground plane, we find that (see Fig. 20) the current in the sandwich flows in uniformly on the bottom of the upper strip, across the N region, and then back to the edge of the lower strip below where it came in (If it did not flow back this way we could not have $\underline{H} = 0$ in the lower strip). From this edge it then goes beneath the lower strip, turns through a right angle, and flows away on the lower surface of the lower strip. This right angle turn introduces the only nonuniformity in the current flow, as the current concentrates at the inside of the corner (see Fig. 21). We will ignore this nonuniformity.

Let us first consider the case when the effect of the magnetic fields is small. Uniformity of boundary conditions then leads to uniformity of current in the junction. From the form of Eq. (2), we see that to maintain the form of Eq. (13) we must choose a gauge with $A_y = A_z = 0$, and Eq. (18) will take the form

$$j = j_c \sin(\theta - \frac{ed}{\hbar} A_x)$$

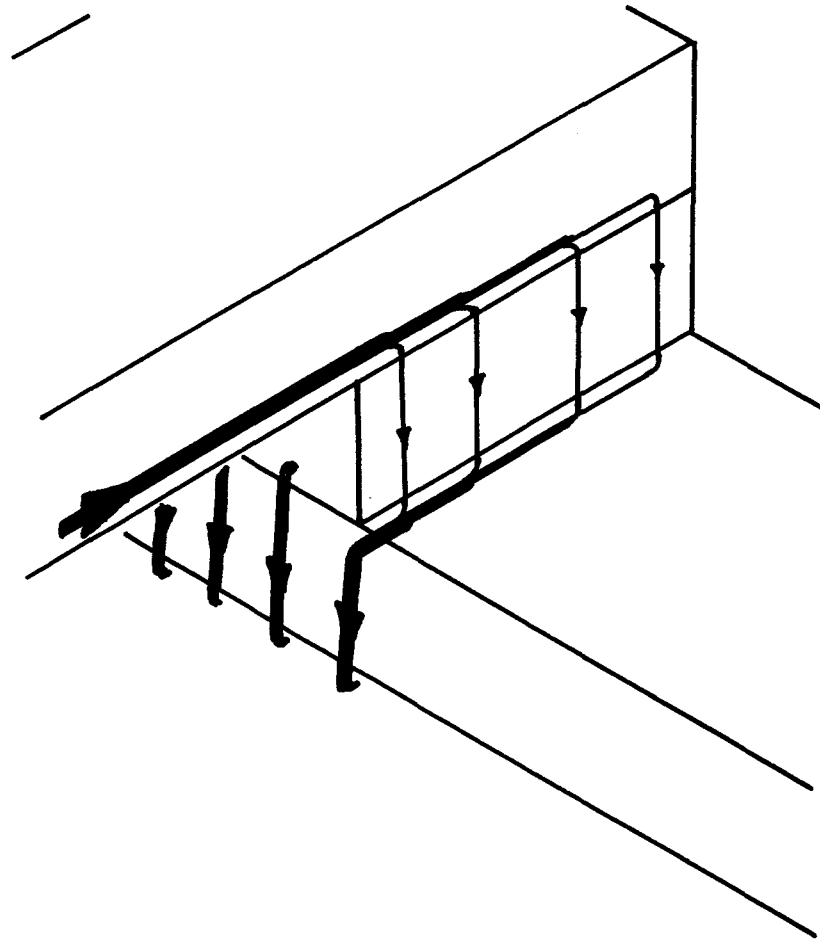


Fig. 20 Top view of sandwich, showing current flow when magnetic effects are negligible (except for the shielding effects of the superconductors).

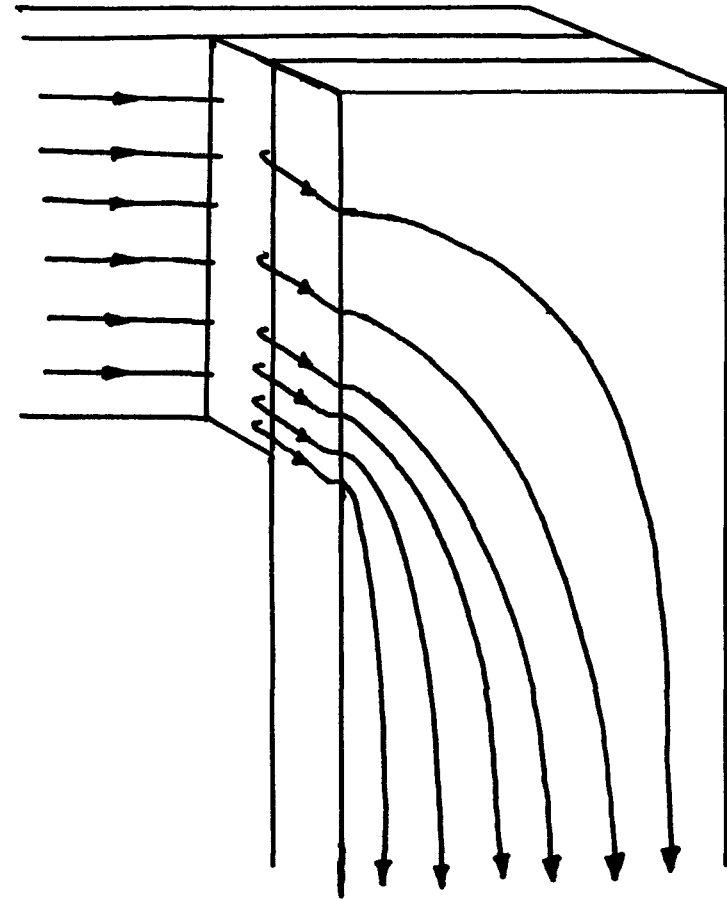


Fig. 21 Bottom view of sandwich, showing current crowding at the inside corner. The effects of this crowding are neglected.

where $d = 2(W_N + \lambda)$ and λ is the penetration depth in the S region. The self field due to the current I flowing through the junction is

$$\underline{H}_s = -e_z \frac{I}{b} \left(\frac{1}{2} + \frac{y}{a} \right)$$

where a and b are the dimensions of the junction (see Fig. 15). In the presence of an external field

$$\underline{H}_o = H_o \hat{e}_z$$

we have (choosing $A_x = 0$ at $y = 0$)

$$A_x = \mu_o \left[-H_o y + \frac{I}{2b} y \left(1 + \frac{y}{a} \right) \right]$$

We can no longer have $\sin(\theta) = 1$ all over the junction; to maximize the total junction current we must minimize the spread in A_x across the junction, which we can do by setting

$$\frac{1}{\mu_o} \frac{\partial A_x}{\partial y} \Big|_{y=0} = \frac{I}{2b} - H_o = 0$$

Thus the external field which maximizes total current is

$$H_m = \frac{I}{2b}$$

which is just half the self field I/b . The magnetic diffraction pattern [37] is thus shifted as shown in Fig. 22, and with no

[37] J. Rowell, Phys. Rev. Letters 11, 200 (1963).

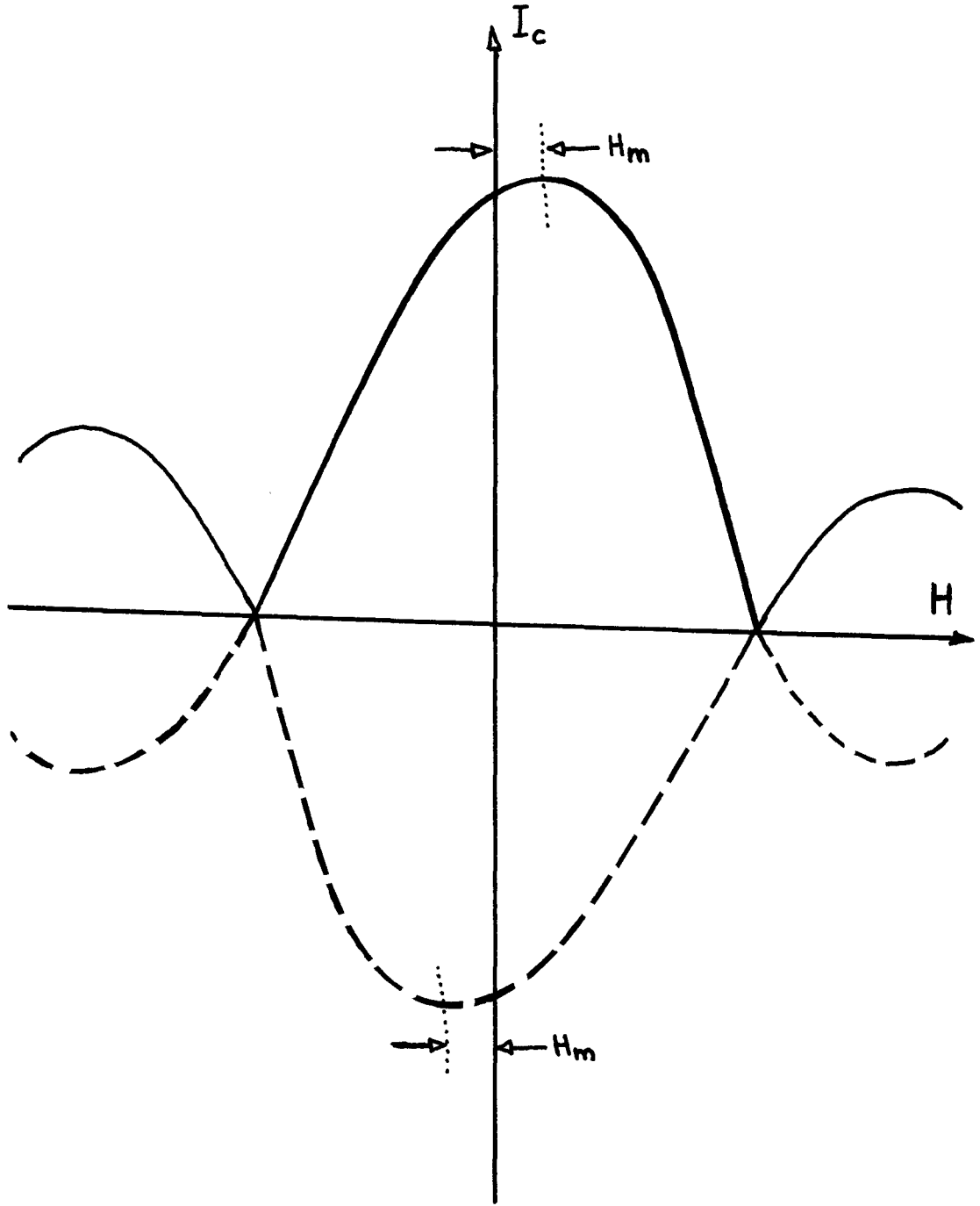


Fig. 22 The shift in the magnetic diffraction pattern due to self-field limiting when the effect is small. See text.

external field the total junction current is decreased below $j_c ab$.

We find this decrease by defining $\theta = \frac{\pi}{2} + \delta$, and approximating $\cos(x) \cong 1 - \frac{x^2}{2}$. Then the current becomes

$$I = j_c b \int_{-a/2}^{a/2} [1 - \frac{1}{2}(\delta - \frac{ed}{\hbar} A_x)^2] dy$$

Integrating over the junction, we find

$$I = j_c ab [1 - \frac{\delta^2}{2} + \delta \frac{\mu_o eda}{24\hbar b} I - \frac{23}{480} (\frac{\mu_o edaI}{2\hbar b})^2]$$

which is maximized for $\delta = \frac{eda\mu_o}{24\hbar b} I$, which gives

$$I_m = j_c ab [1 - \frac{1}{90} (\frac{\mu_o eda}{\hbar b} I_m)^2]$$

We have assumed that the junction current is uniform; this is true if the junction is much smaller than the Josephson penetration length [38] which is given by

$$\lambda_J = \sqrt{\frac{\hbar}{\mu_o ed j_c}}$$

In the opposite extreme, when the junction is much larger than λ_J , the current all flows in a strip of effective width $2\lambda_J$ along the current input side of the junction. The maximum current of the junction is then

$$I_m = 2b \sqrt{\frac{\hbar j_c}{\mu_o ed}} \tag{31}$$

[38] R. Ferrell and R. Prange, Phys. Rev. Letters 10, 479 (1963).

An external field along z causes current $H_0 b$ to flow around the device as shown in Fig. 23, adding to (or subtracting from) the flow on the current-flow side of the junction, and also flowing on the other side (which is also capable of carrying current I_m). The result is that the critical current limits of the junction are shifted from $\pm I_m$ to $\pm I_m + H_0 b$, up to the limit $H_0 b = I_m$ at which the critical current is exceeded by the current due to the external field alone. At this point one or more flux quanta enter the junction, and more cycles of change in the current limits take place, but at lower current levels [39]. This leads to a graph of I_m versus H_0 as shown in Fig. 24 .

[39] C. Owen and D. Scalapino, Phys. Rev. 164, 538 (1967).

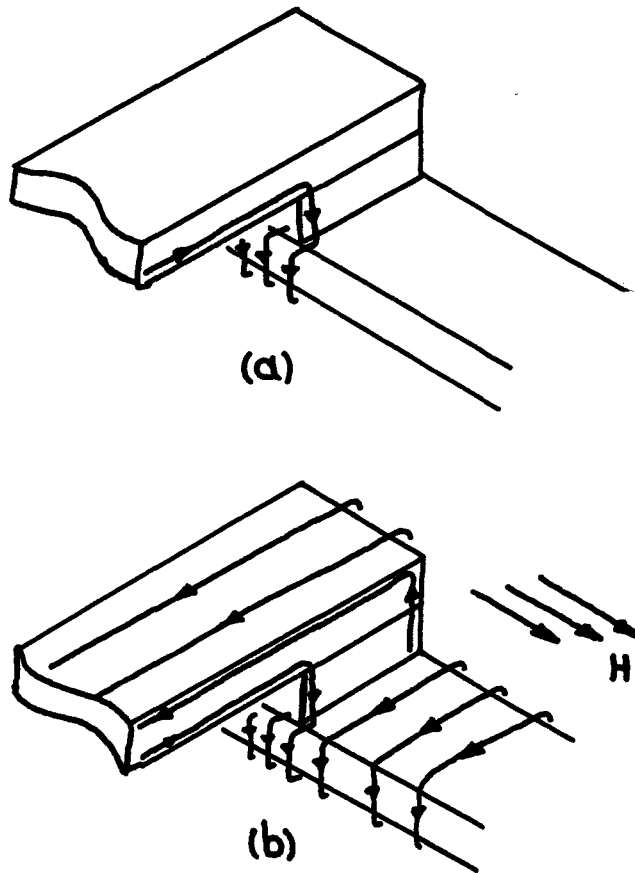


Fig. 23 (a) Current flow due to input current alone when the junction is strongly self-field limited. (b) Current flow due to external field alone when the junction is strongly self-field limited.

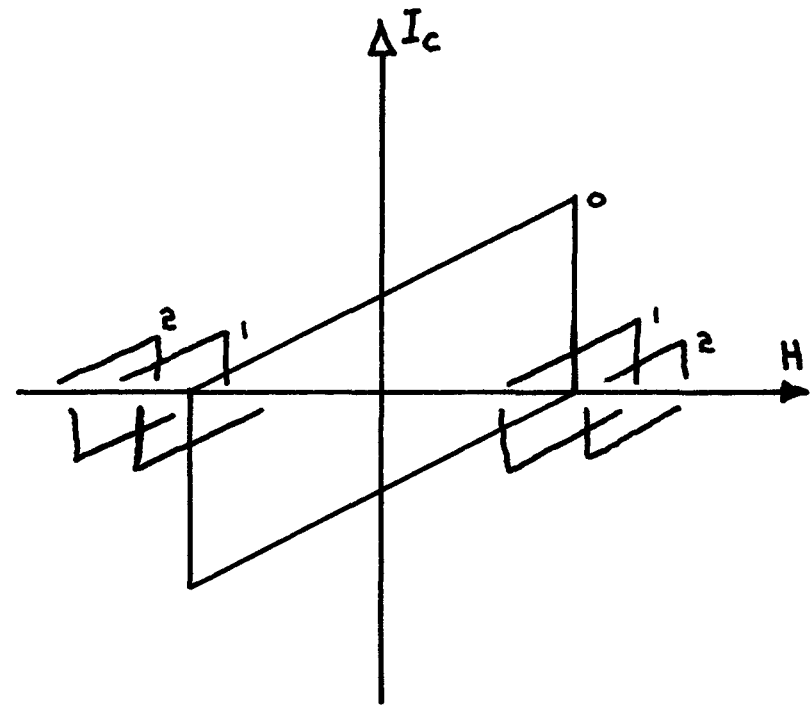


Fig. 24 The magnetic diffraction pattern when the junction is strongly self-field limited. See text. The number of flux quanta in the junction is shown on the curves.

VI. COMPARISON OF THEORY AND EXPERIMENT

A. Reduction of Sandwich Currents to Current Densities

The theoretical results of Section V are in terms of current densities, but the sandwich property experimentally measured is the critical current. To facilitate comparison between theory and experiment, the sandwich currents were therefore reduced to current densities. Such reduction requires that the spatial distribution of the currents be known; the reduction is particularly straightforward if the current distribution is uniform. Current uniformity across the Pb strips (Fig. 1) was insured by the use of a ground plane; the efficacy of this method may be judged from Fig. 13, where the $.5\mu$ sandwich without a ground plane is seen to have critical currents two orders of magnitude less than samples of greater thickness which do have ground planes, although its relative thinness ought to lead to larger critical current densities. With lateral current uniformity guaranteed by the ground plane, there is still the problem of self-field limiting (Section V.F.). When the sandwich dimension along the upper Pb strip is smaller than the Josephson penetration length, the current is uniform in the sandwich and the current density is found as $j_c = I_m/ab$, where I_m is the sandwich critical current and a and b (see Fig. 15) are the length and width of the crossover area. (The N material outside the crossover area makes a negligible contribution to the current because of the much longer distances which the current would have to travel to get from one S strip to the other.) On the other hand, when a is larger than

the Josephson penetration length, the current all flows along one edge due to the self-field limiting and the critical current density is found from Eq. (31) as $j_c = \mu_o ed(I_m/2b)^2/\hbar$. The crossover between the uniform region and the self-field limited region comes when the current densities calculated from the two formulas are equal, or when I_m has the transition value I_t , where

$$I_t = \frac{4\hbar b}{\mu_o eda}$$

Calculation of I_t for the measured sandwiches shows that the critical currents of the sandwiches were all at or above I_t , so the sandwiches were always self-field limited. The critical current densities were therefore calculated from Eq. (31) to correct for the self-field limiting; the resulting current densities are shown in Fig. 25.

B. Numerical Computations from the Theory

In order to gain a greater understanding of the predictions of the theory outlined in Part V, numerical computations of the critical current density as a function of temperature were made for various values of the material parameters of the S and N layers. To roughly represent the actual samples, the basic values adopted were

$$\begin{array}{ll} T_{cN} = 3.7 \text{ K} & T_{cS} = 8.7 \text{ K} \\ \xi_{oN} = .5\mu & \xi_{oS} = .1\mu \\ \lambda_N = .03\mu & \lambda_S = .03\mu \end{array}$$

$$V_N/V_S = .6 \quad N_N/N_S = 1$$

The N region half-width W_N was set at $W_N = 2\mu$, and the S regions

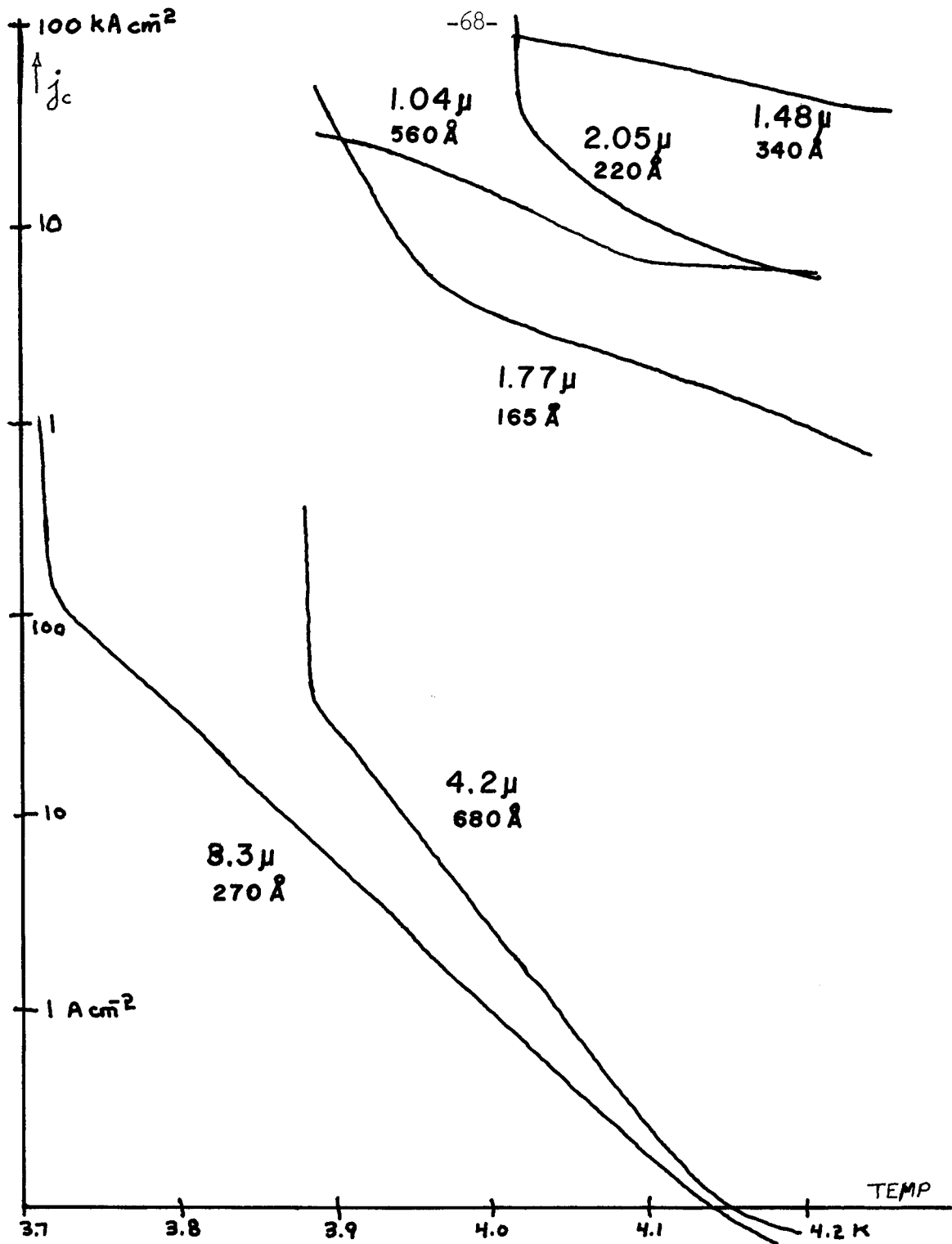


Fig. 25. The experimental data of Fig. 13 corrected for self-field limiting, and reduced to current densities.

were assumed to be much thicker than k^{-1} so that Eq. (15) would hold (This assumption will be seen to be justified). The exact value of T_{cs} has little effect as long as it is well above T_{cN} ; the value given above was chosen for numerical convenience.

Each of the parameters above (except for T_{cs}) was then varied about its basic value, while the other parameters were held constant. The resulting curves of critical current versus temperature then show the effect of the variation of each parameter in turn.

The calculation of the critical current densities was done in two different ways. At a temperature well above T_{cN} (above about 4.7 K for the basic parameters above) the interface value r_N drops below r_m and the linear approximation of Eq. (19) and Eq. (30) holds. The calculation of the critical current at any given temperature between this temperature and T_{cs} is then straightforward; the Ginzburg-Landau equation constants α , r_m , k , and r_B are found for the given temperature from the de Gennes-Werthamer theory (with the addition of r_B) via Eq. (9) and Eq. (11) (using the appropriate approximations to these equations given in Section V.B.). The critical current density is then found from Eq. (19) and Eq. (30).

Near the critical temperature of the N material, the linear approximation is not valid and the exact solutions of Eq. (24) must be used. In this temperature region the critical current density was found as the maximum current density for which a solution to Eq. (24) and Eq. (28) could be found (details of this process are given in Appendix B).

A comparison of the results of these two different methods of calculation of the critical current density is shown in Fig. 26 (for

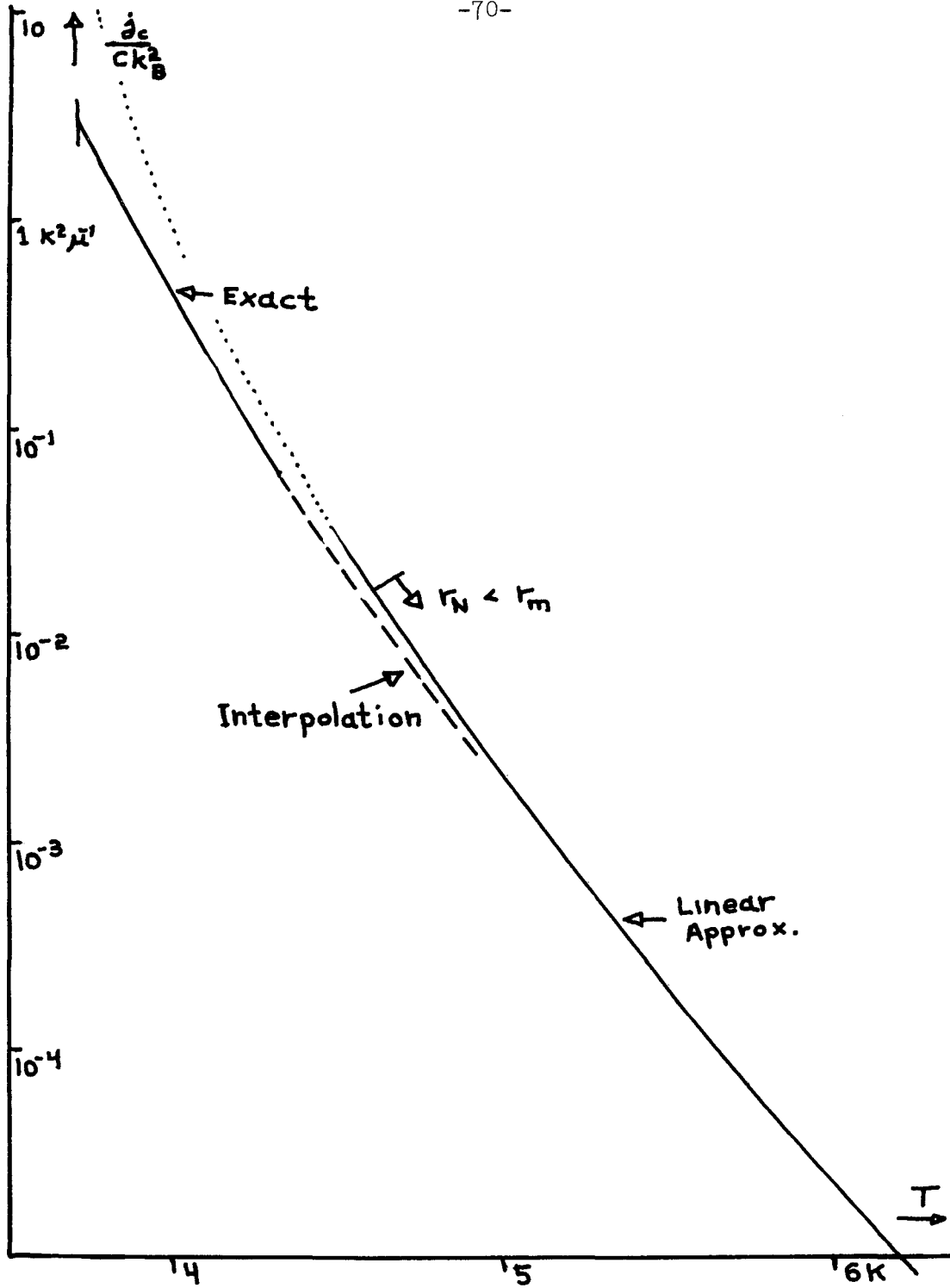


Fig. 26. Comparison of exact critical current density and the results of the linear approximation (which is valid for $r_N \ll r_m$). Interpolation between the two curves is shown.

which W_N was 1). The exact solution is shown only near T_{cN} because it becomes difficult to compute at higher temperatures. The linear approximation is self-consistent and therefore accurate once r_m is much less than the value of r_N found from Eq. (30); the point where this occurs is indicated. An interpolation between the exact solution and the region where the linear approximation is accurate is indicated in Fig. 26. The theoretical curves in the remainder of this section were produced by exact calculations near T_{cN} and by the use of the linear approximation in the region of its validity; interpolation was made between the two solutions.

The temperature variation of the Ginzburg-Landau equation constants in the S and N regions is shown in Fig. 27. The S region constants k and r_B are only slowly varying in the temperature range used in this work; they therefore have little effect on the temperature variation of the critical current density. The effect of a different T_{cs} can be estimated from the fact that k and r_B drop to zero at T_{cs} ; unless T_{cs} is close to the experimental region the S region constants will not vary strongly in that region and the exact value of T_{cs} will be irrelevant. The N region constants α and r_m vary rapidly near T_{cN} and less rapidly at higher temperatures; from Eq. (10) and Eq. (12) we find that α and r_m vary as $\sqrt{T - T_{cN}}$. Also shown in Fig. 27 are the interface value r_N and center value r_0 of the energy gap amplitude; r_N decreases slowly, while r_0 drops off abruptly.

The behavior of the $\ln(j_c)$ versus T curve well above T_{cN} can be derived from the linear approximation result of Eq. (19) that

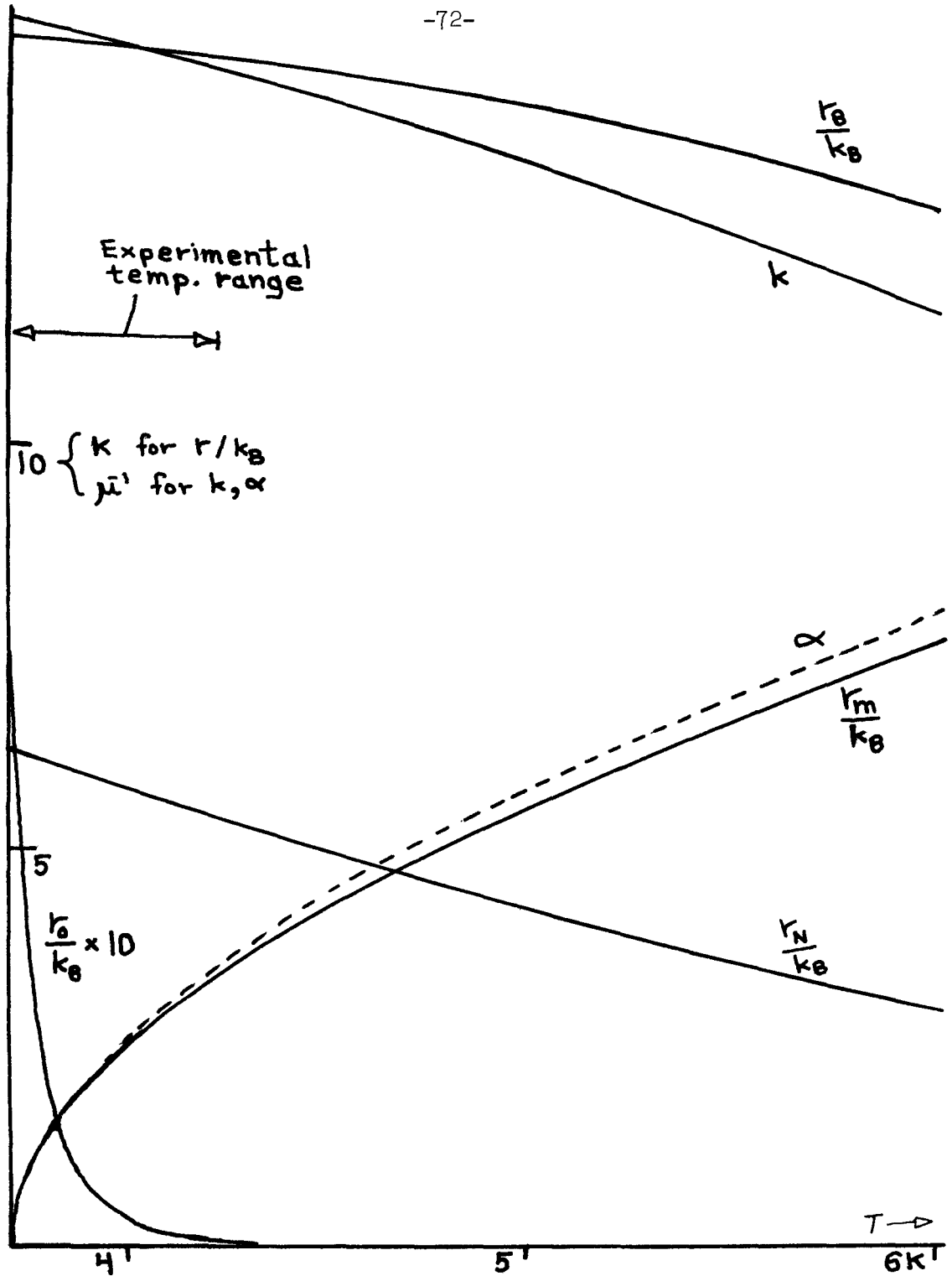


Fig. 27. Temperature variation of the S and N region material constants, and of the edge and center values of r in the N region, for the basic sample. See text.

$j_c \approx \text{Cor}_N^2 / \sinh(2\alpha W_N)$. Assuming that $\alpha W_N \gg 1$ in the linear temperature region (an assumption which is true for all the experimental samples) we have

$$\ln(j_c) \approx \text{Const.} + \ln(\text{Cor}_N^2) - 2\alpha W_N$$

We ignore the temperature variation of $\ln(\text{Cor}_N^2)$ with respect to that of $2\alpha W_N$ and find the temperature variation of α from Eq. (10) (recall $\alpha^2 = -k^2$). This yields

$$\ln(j_c) \approx \text{Const.} - 1.17 \frac{W_N \sqrt{T - T_{cN}}}{\sqrt{\xi_{oN} \ell_N T_{cN}}} \quad (32)$$

which suggests that in the temperature region where the equation is linear the slope of the $\ln(j_c)$ versus T curves should depend strongly on the N region properties W_N , ξ_{oN} , and ℓ_N , and only weakly on the S region properties ξ_{oS} and ℓ_S (which indirectly affect r_N). To check this expectation, the results of the critical current density calculations will now be examined.

The effect of varying W_N , ξ_{oN} , and ℓ_N on the critical current density is shown in Fig. 28, Fig. 29 and Fig. 30. The effects are large and depend on $W_N / \sqrt{\xi_{oN} \ell_N}$ as expected from Eq. 32; in fact, if the three quantities are varied while $W_N / \sqrt{\xi_{oN} \ell_N}$ is kept constant, the resulting curves are indistinguishable on the scale of the figures.

The much smaller effects of the S region properties ξ_{oS} and ℓ_S are shown in Fig. 31 and Fig. 32. We see from these curves that the S region properties have a small effect not only on the slope but also on the absolute value of the critical current density versus temperature

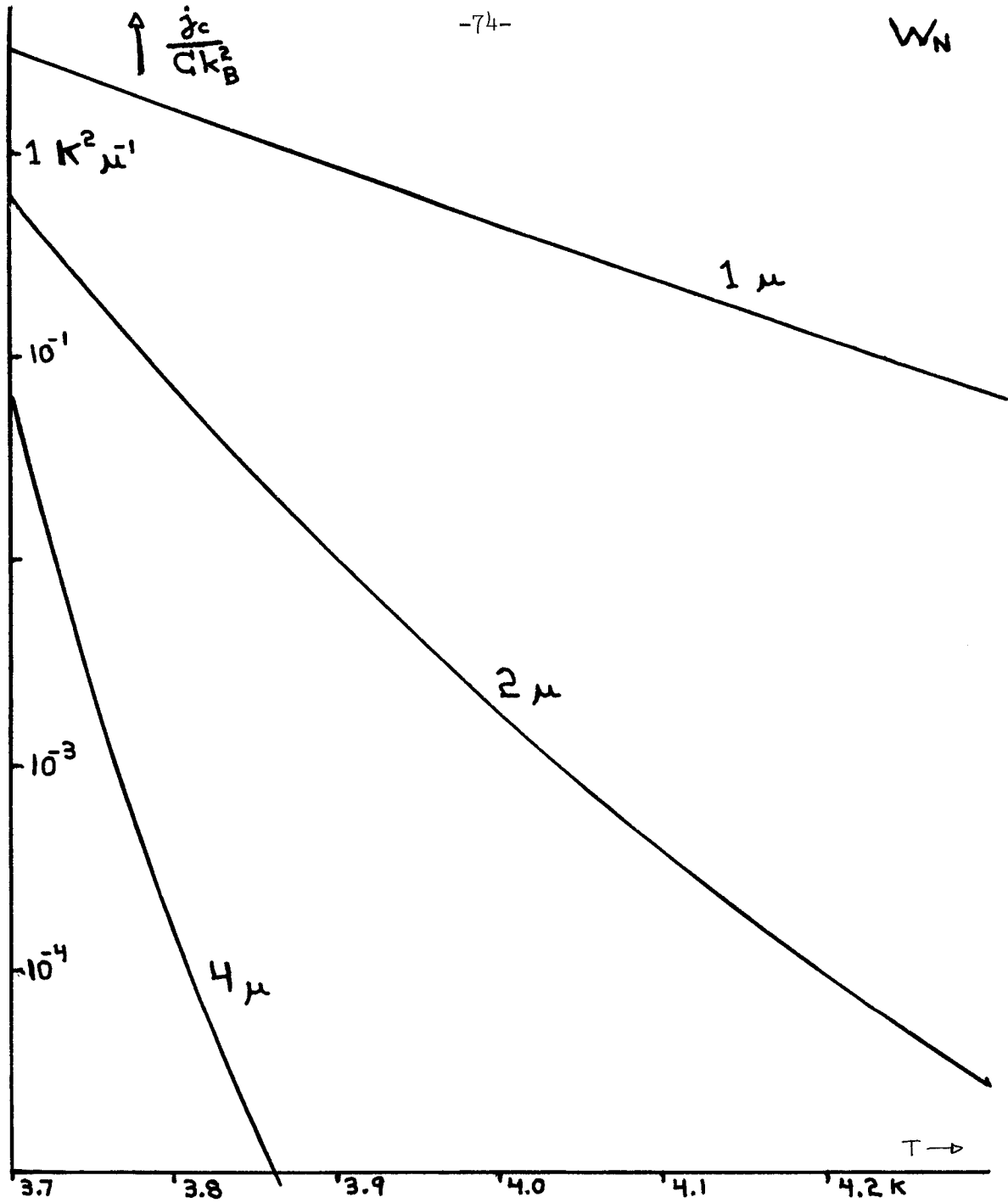


Fig. 28. The large variation in the critical current density due to changes in the N region half-width W_N .

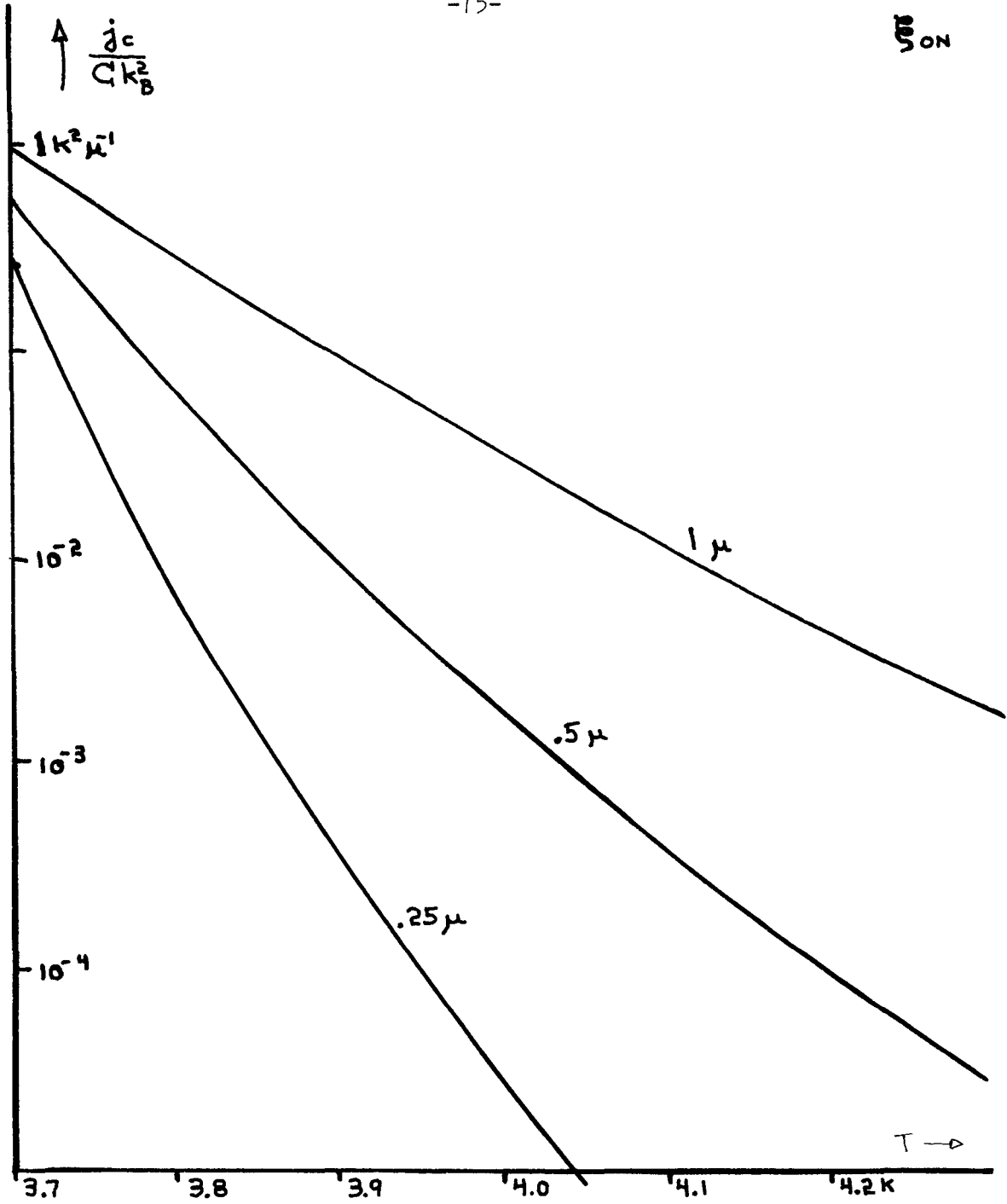


Fig. 29. The large variation in the critical current density due to changes in the N region pure bulk coherence length ξ_{ON} .

λ_N

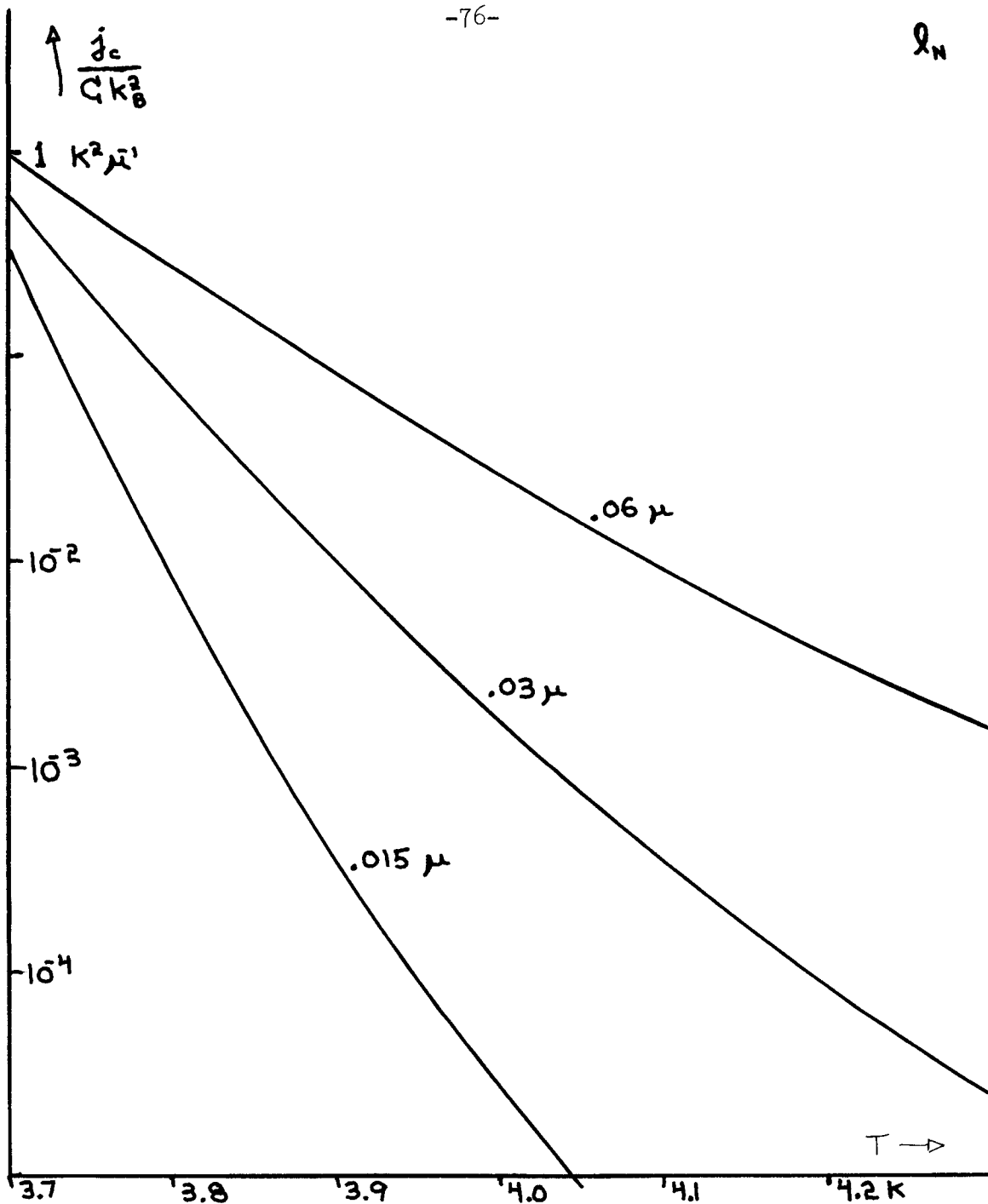


Fig. 30. The large variation in the critical current density due to changes in the N region electron mean free path λ_N .

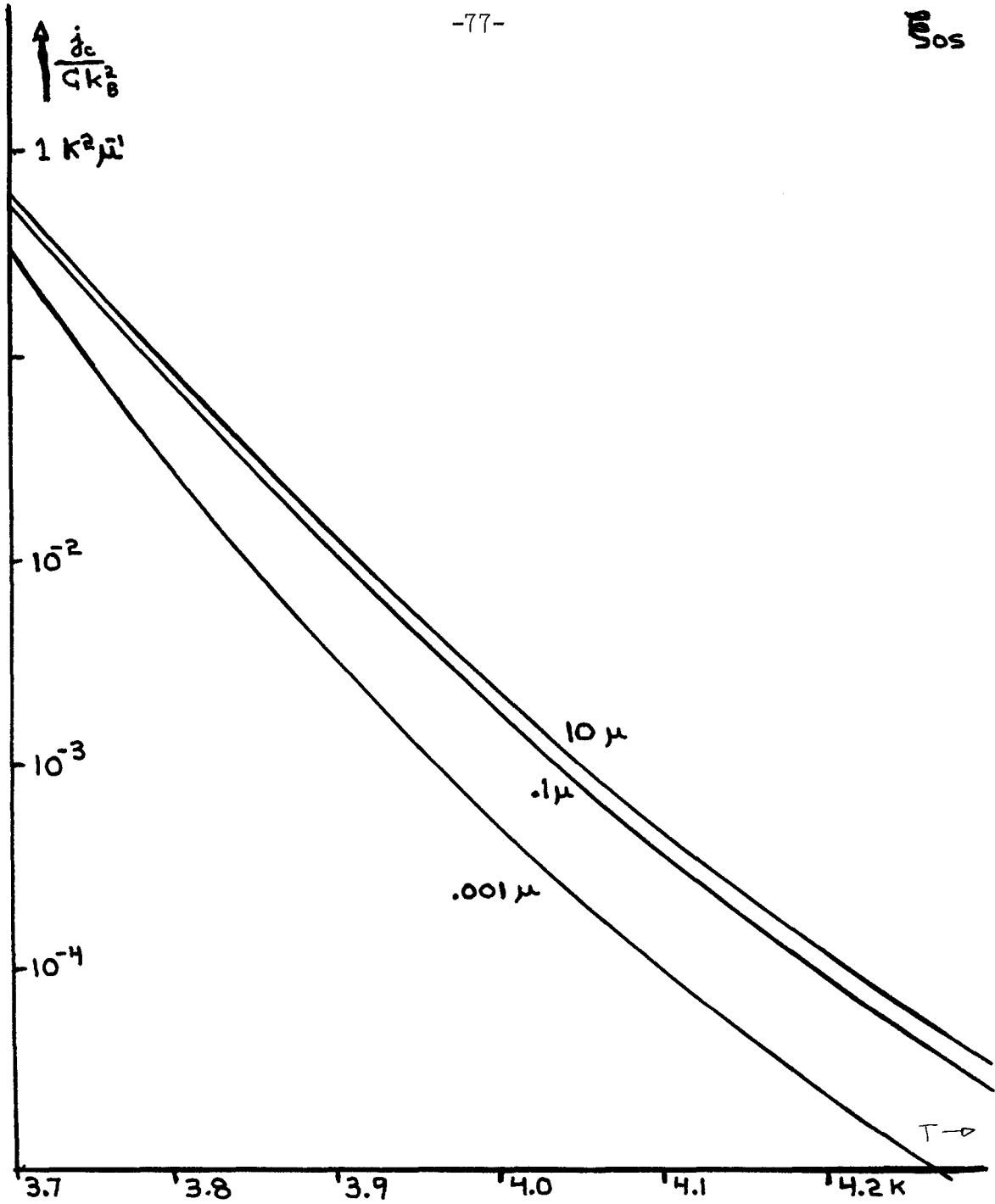


Fig. 31. The small variation in the critical current density due to changes in the S region pure bulk coherence length ξ_{0S} . Note the large change in ξ_{0S} between curves.

λ_s

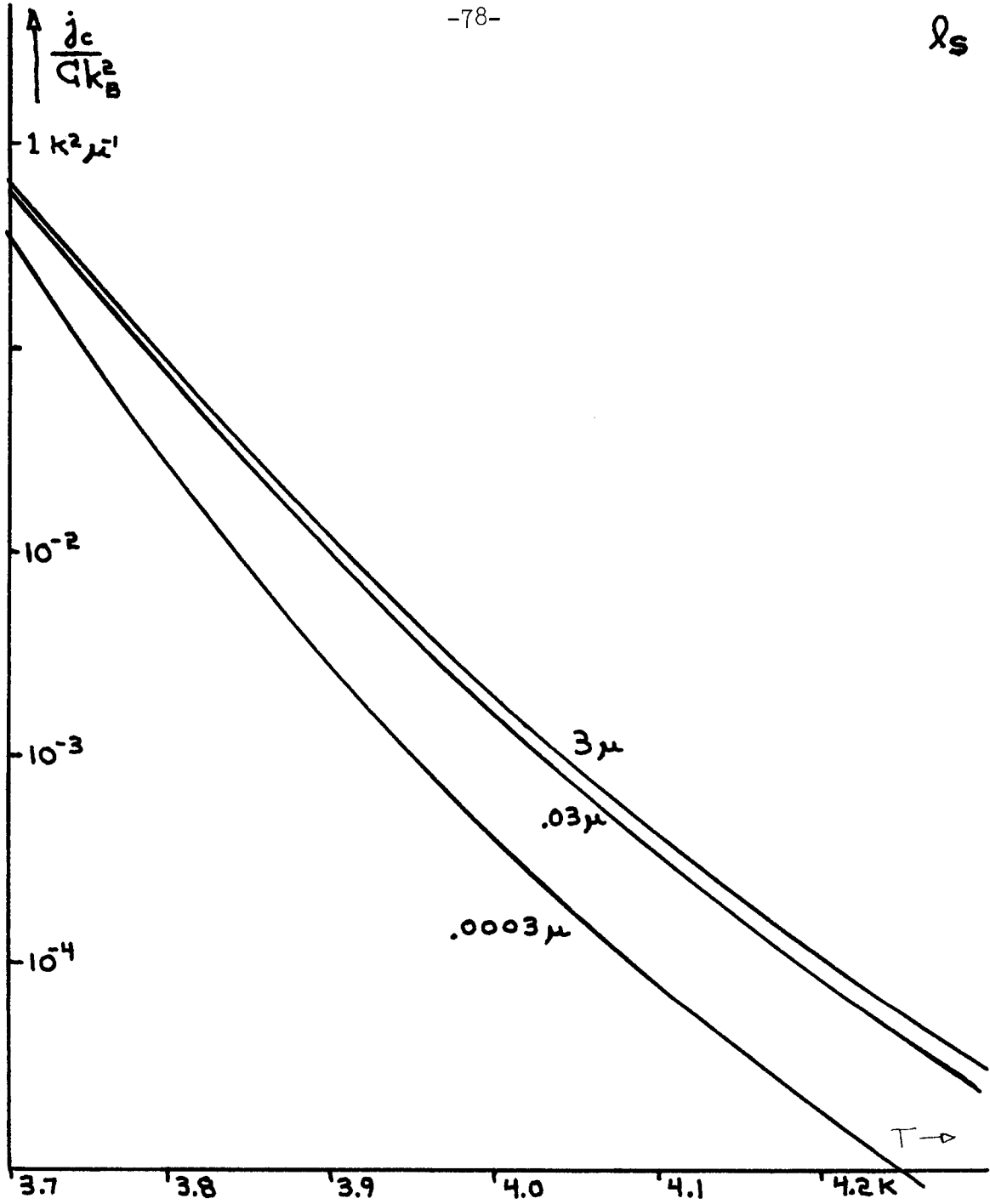


Fig. 32. The small variation in the critical current density due to changes in the S region electron mean free path λ_s . Note the large change in λ_s between curves.

curves (note that the S region parameters change by a factor of 100 between curves in these figures). We conclude that any superconductor with a transition temperature well above the experimental temperature range is suitable as an injector of superconductivity in an SNS sandwich experiment; the coherence length and electron mean free path of the superconductor have little effect.

The effect of the variation of N_N/N_S is shown in Fig. 33; it is seen to be small. The larger effect of varying V_N/V_S is shown in Fig. 34, where we see that the absolute value of the curves is affected but not their slope. Finally, Fig. 35 shows the result of the simultaneous variation of T_{cN} and of ξ_{oN} (which we recall depends inversely on T_{cN}). The curves are shifted in temperature, but the critical current density at the N material transition temperature is fairly constant.

C. Comparison of Theory and Experiment

The theory is best checked by comparison of the predictions of the theory for the sandwiches with the actual results of the sandwich measurements. Current densities were derived from the sandwich measurements by the method described in Section VI.A. Theoretical curves of current density versus temperature were calculated by the method of Section VI.B. The S region material constants used in the calculations were the same for each sample, because of the insensitivity of the theory to the S region properties; the values used were $T_{cS} = 7.2$ K, $\xi_{oS} = .083\mu$ [40], and $\ell_s = .03\mu$. N_N and N_S were taken to be equal,

[40] J. Bardeen and J. Schrieffer in Progress in Low Temperature Physics III, North-Holland, Amsterdam, 1961; p. 243.

$$\frac{N_N}{N_S}$$

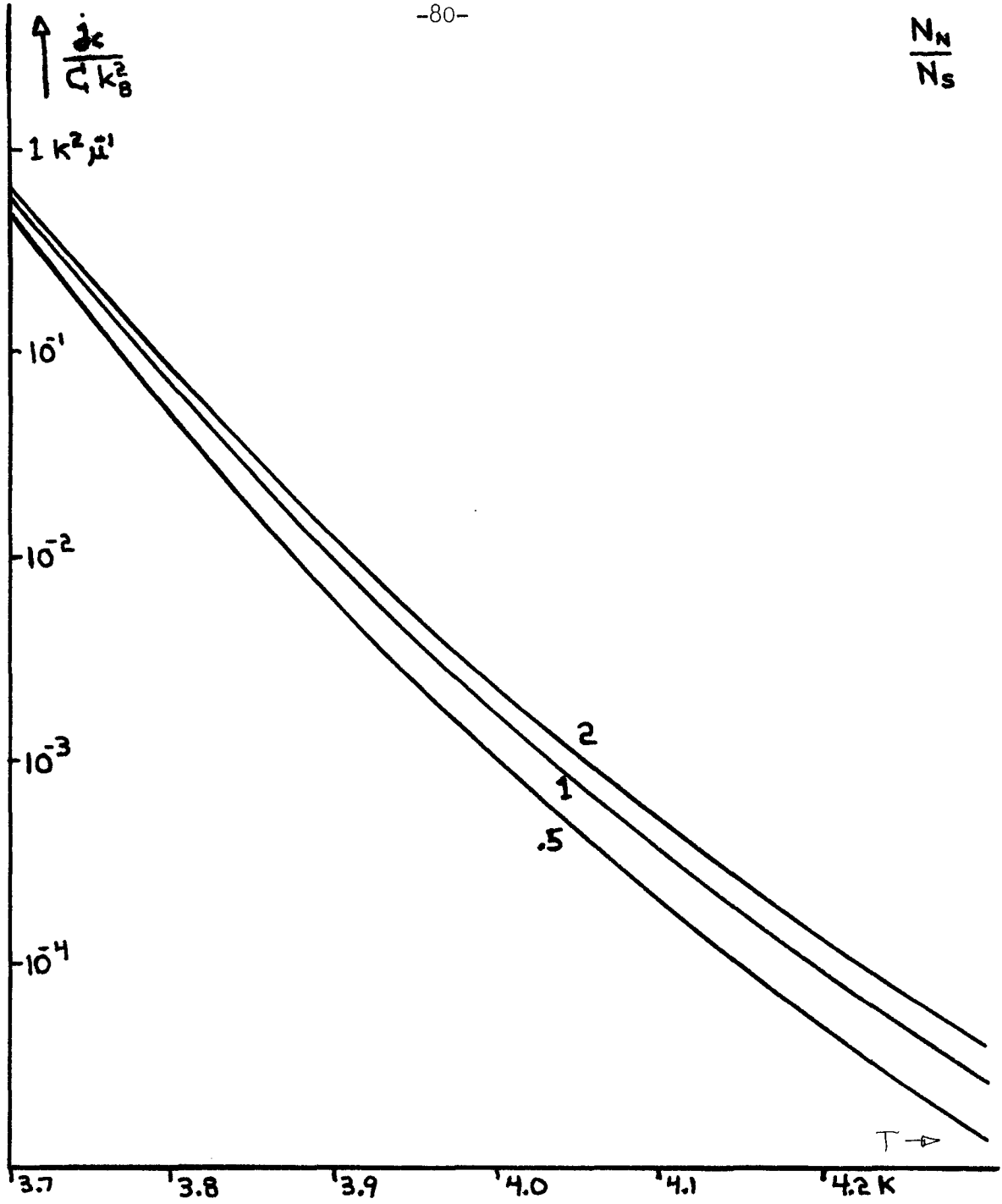


Fig. 33. The variation in the critical current density due to changes in the ratio of the energy density of states per unit volume at the Fermi surface N_N/N_S .

$$\frac{V_N}{V_S}$$

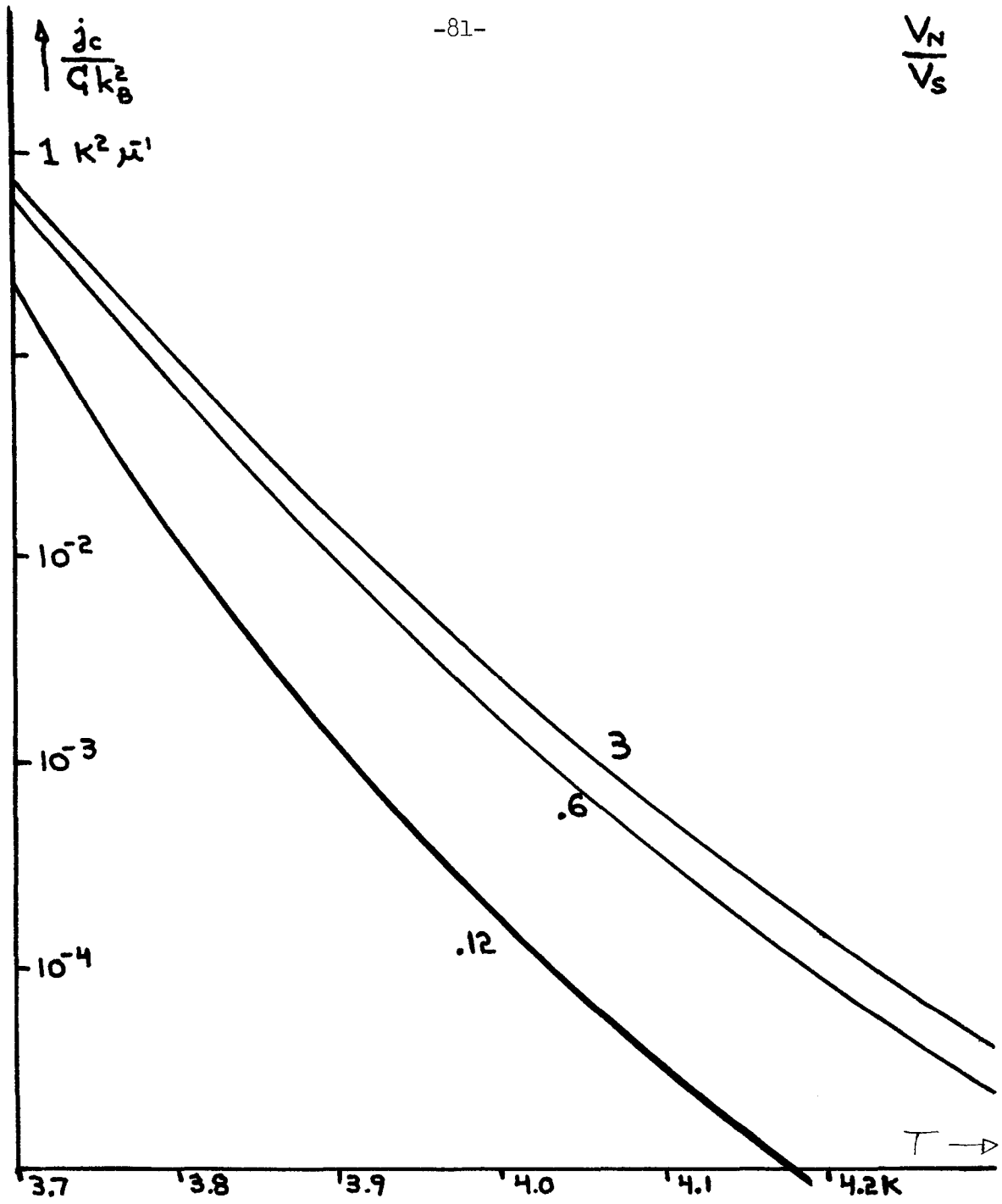


Fig. 34. The variation in the critical current density due to changes in the ratio of the BCS interaction parameters V_N/V_S .

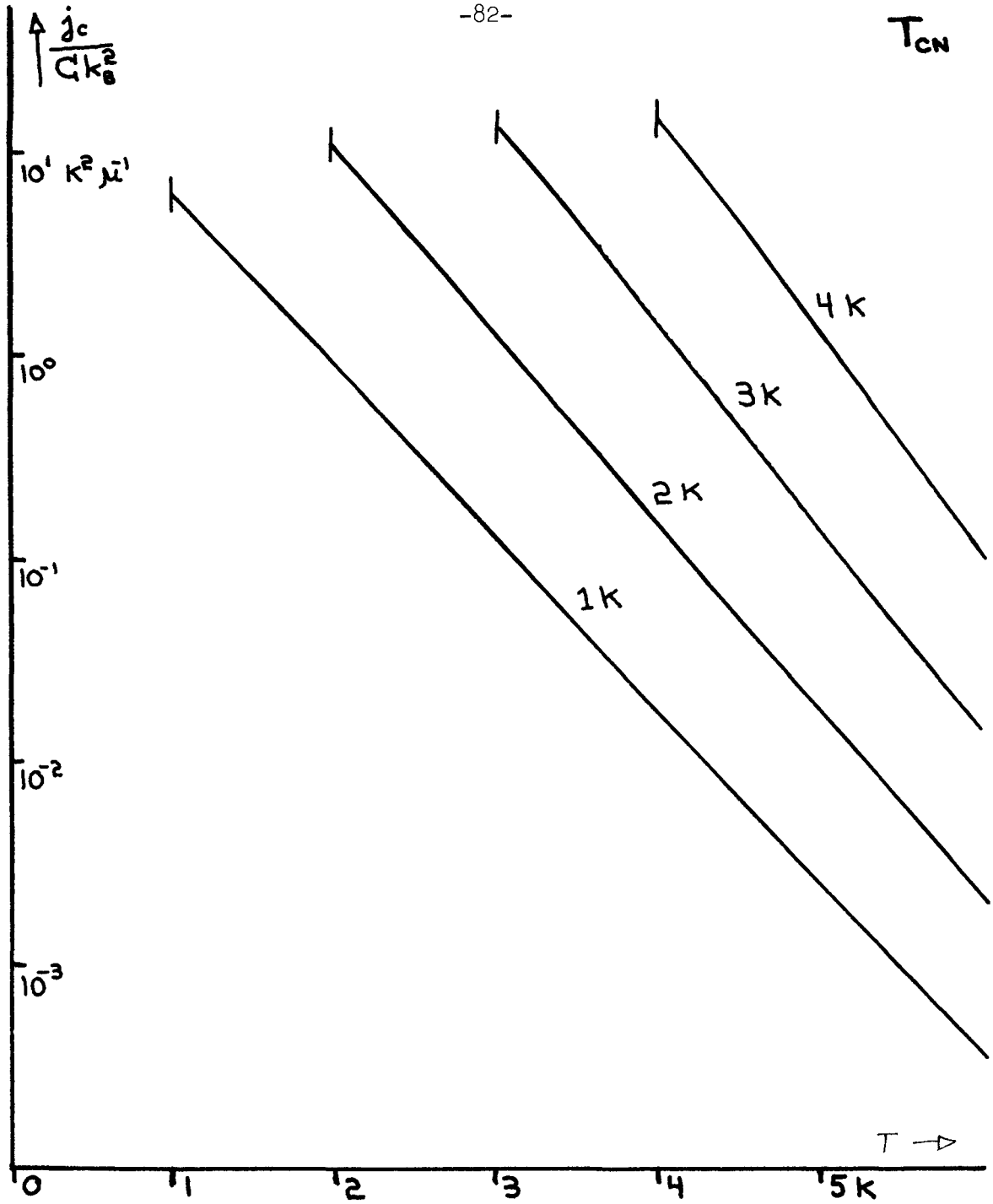


Fig. 35. The variation in the critical current density due to changes in the N material transition temperature T_{cN} (and in the N material pure bulk coherence length ξ_{cN} , which depends on T_{cN}^{-1}). The N region half-width was $.5 \mu$ for these curves.

while V_N/V_S was set equal to .6 (from the BCS result $NV^{-1} = \ln(2e^{\gamma} \hbar \omega_c / \pi k_B T_c)$ with $\hbar \omega_c$ taken as $1/3 k_B T_D$ [41] where T_D is the Debye temperature). The bulk coherence length of In was taken as $.44\mu$ [42]. The half-widths and electron mean free paths in the In were measured for each sandwich (Sections II.B and III.B); the transition temperature of the N material was taken as the knee temperature of the sandwiches (Section IV.B). Once the quantities above are fixed, the only remaining parameter available to adjust the fit of the theoretical and experimental curves is the constant C in Eq. (2). Variations in C multiply all the theoretical curves by the same amount, and thus shift the whole family of theoretical curves up or down as a unit on a plot of log critical current density versus temperature. Figure 36 shows the experimental curves of Fig. 25 and the family of theoretical curves corresponding to them; the theoretical curves have been adjusted vertically for an approximate best fit at the knees. The value of C resulting from this fit is $5 \times 10^{46} \text{ A J}^{-2} \text{ m}^{-1}$; considering the uncertainty of the fit, this estimate is good only to within a factor of 5. It is seen that the current density at the transition temperature varies from the theoretical prediction by (on the average) a factor of 5, and that the slope of the experimental curves also varies from the prediction. However, the slope variation (except in the case of the 8.3μ sandwich) is not as great as

[41] D. Zubarev, Soviet Physics Doklady 3, 570 (1960).

[42] E. Lynton, op. cit.; p. 63.

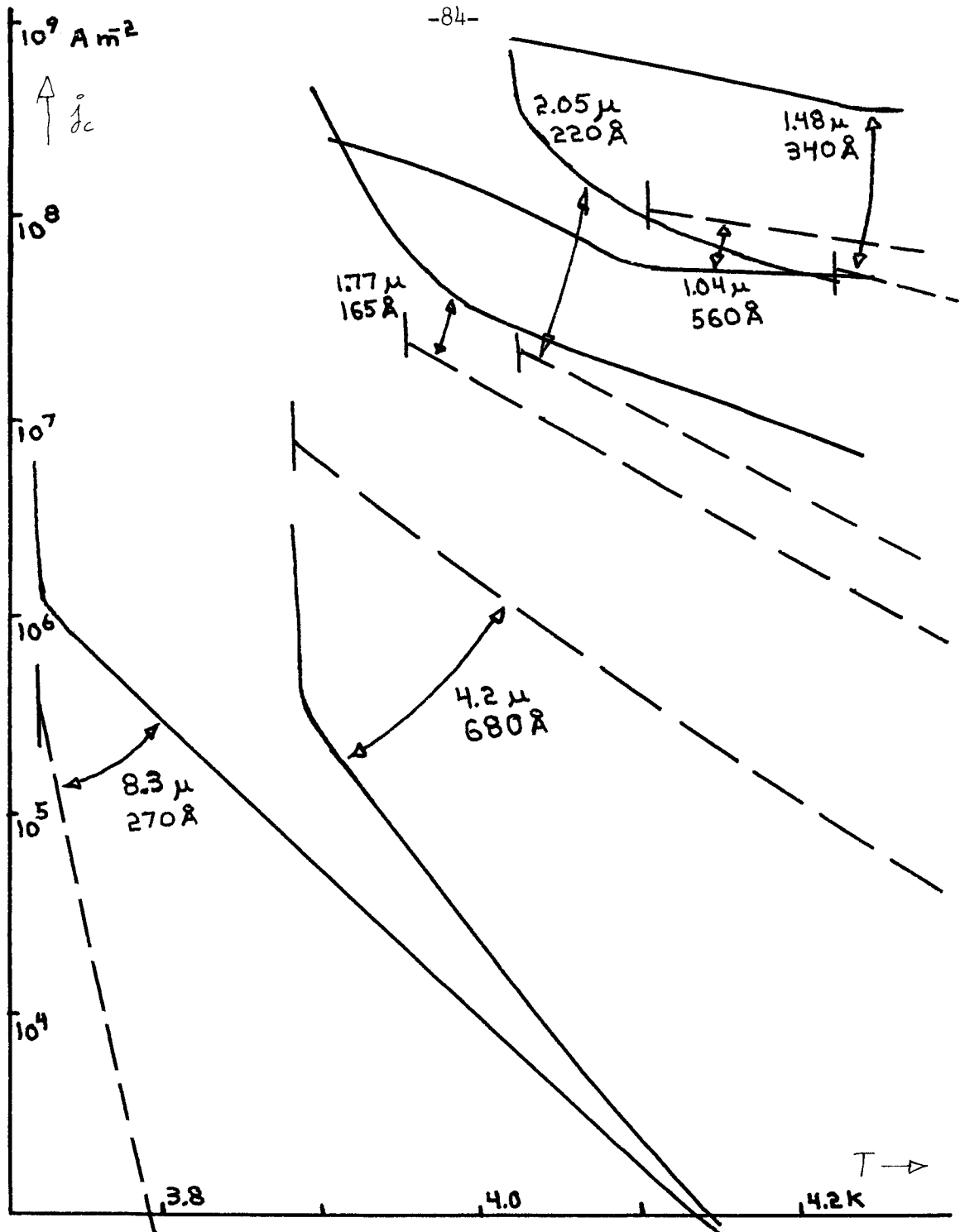


Fig. 36. Comparison of the self-field corrected experimental curves of Fig. 25 (solid lines) and the theoretical curves corresponding to each experimental curve (dotted lines). The theoretical curves have been adjusted vertically as a unit for a best fit at the sandwich transition temperatures.

the absolute value variation, and the slope fit is considered acceptable. Furthermore, and most importantly, the theoretical and experimental curves both show an essentially linear decrease of $\ln(j_c)$ with temperature for temperatures just above T_{cN} . The absolute value of the currents can be decreased by dirty or oxide-covered interfaces between the S and N regions even for room-temperature-deposited sandwiches [43], and more residual gases would be adsorbed on the interfaces of these cold-deposited sandwiches than on room-temperature-deposited sandwiches, so the variation of current absolute values is not too surprising; likewise uncertainties in W_N , ξ_{ON} , and λ_N can cause variations in the theoretically predicted slope of the $\ln(j_c)$ versus T curve. The linear decrease of $\ln(j_c)$ with T , however, is a prediction of the theory which is independent of such variations, and so the experimental observation of such a linear decrease is considered a corroboration of the theory.

The theoretical linear decrease of $\ln(j_c)$ with temperature depends both on the de Gennes-Werthamer theory of the temperature variation of the Ginzburg-Landau equation constants, and on the extension of r_B^2 to temperatures above T_{cN} which was made in Section V.B. The experimental observation of such a linear decrease is thus a verification both of the de Gennes-Werthamer theory and of the extension of r_B^2 . The presence of the term in r_B^2 is necessary because without it Eq. (8) remains linear at all temperatures and the $\ln(j_c)$ versus T

[43] J. Clarke, Proc. Roy. Soc. (London) A308, 447 (1969).

curve bends upward near T_{cN} (see Fig. 26); such upward bending is not observed experimentally. On the other hand, without the term in k^2 (whose temperature variation is given by the de Gennes-Werthamer theory) the temperature variation of $\ln(j_c)$ would be small (because the k^2/r_B^2 term has little temperature variation (see Fig. 18)), so the observed large temperature variation supports the de Gennes-Werthamer theory.

The theory predicts, and the experiments confirm, that there is no indication that the N region superconducting transition is about to occur, obtainable from the shape of the critical current density versus temperature. As the temperature is lowered, $\ln(j_c)$ increases linearly until the transition is reached, with no distinctive rise or fall to indicate the approach of intrinsic superconductivity in the N region. However, the absolute value of the current density can be used in the theory to predict T_{cN} from observations made above T_{cN} . As we have seen, the experimental results show large variations in the current from the theoretical expectations, making prediction uncertain. We conclude that greater confidence in the absolute current density is required before transition temperature predictions can be made from it.

D. Suggestions for Further Work

- 1) A number of materials should be used as the N material in SNS sandwich measurements.
- 2) The entire temperature range from T_{cN} to T_{cs} should be studied.
- 3) Materials with long mean free paths should be used as the N material. The theory does not apply in this case, but the

author expects that if the length $\sqrt{\xi_0 \ell}$ which appears in the definition of k is not allowed to rise above ξ_0 even for large electron mean free paths, the correct result will be obtained.

E. Summary

When a material in the superconducting state is in contact with a non-superconductor, superconductivity may "leak" from the superconductor into the non-superconductor. This leakage of superconductivity is called the proximity effect. The spatial distribution of superconductivity can be described by the Ginzburg-Landau equation, and so this equation is used to describe the distribution of the injected superconductivity in the non-superconductor. The de Gennes-Werthamer theory (valid in the "dirty limit" of short electron mean free paths) yields the temperature dependence of the terms in the Ginzburg-Landau equation.

The SNS sandwich method, in which the maximum lossless current which can be carried across a thin layer of non-superconductor between two superconductors is measured, is a good way of testing the predictions of the de Gennes-Werthamer theory. If the test is to be definitive, the non-superconductor should be a material which superconducts below some experimentally accessible transition temperature; it should be used at temperatures at and above this transition temperature. In this work, In (transition temperature 3.4K in bulk) was used. Lead was used as the superconductor in the sandwich, as it is a strong source of superconductivity in the temperature range used.

The sandwiches were vacuum deposited and stored at low tempera-

tures ($\sim 100\text{K}$) because In and Pb are mutually soluble; the low temperature preparation also produced the desired short electron mean free paths. The current flow in the sandwiches was made uniform by the presence of a superconducting ground plane, so that absolute values of critical current density could be derived from the critical current measurements.

The voltage resulting from current across the Pb-In-Pb sandwiches was in the nanovolt range; it was measured with a quantum interference voltmeter utilizing a Clarke SLUG. The abrupt appearance of voltage at the sandwich critical current made determination of this current accurate.

When the critical current was plotted versus temperature, the current was found to decrease strongly with increasing temperature below the transition temperature of the In, and to show a roughly exponential decrease with temperature above the transition temperature, due to proximity effect induced superconducting currents. When the log of the critical current density (corrected for Josephson self-field limiting) was plotted versus temperature, a fairly straight line was seen from the transition temperature of the In to 1.1 times this temperature.

The de Gennes-Werthamer theory was extended to the case of non-infinitesimal superconductivity by the addition of the temperature dependence of the non-linear term in the Ginzburg-Landau equation; the critical current density versus temperature was then calculated from the augmented theory. The theoretical curves of critical current density versus temperature showed the same linear decrease shown by the experimental curves above the transition temperature of the In,

although there was some variation in magnitude and slope (such variation can be caused by dirty interfaces and uncertainty in the material constants).

We conclude that the de Gennes-Werthamer theory (as extended) gives an accurate description of the temperature variation of the constants in the Ginzburg-Landau equation at and above the transition temperature of a material.

APPENDIX A. THE QUANTUM INTERFERENCE VOLTMETER

A. Introduction

Because the normal-state resistance of the SNS sandwiches measured in this work was very small, the voltage appearing across them due to the flow of currents above the critical current was also small. The sandwich voltages (which were in the nanovolt range) were therefore measured with a sensitive voltmeter of very low input impedance based on the phenomenon of quantum interference. The principle of this simple and reliable voltmeter was first described by Clarke [44].

B. Two-Junction Quantum Interference

A "weak link" is formed between two superconductors when there is a metallic bridge of small cross section between them, or when a thin insulating layer ($\sim 10 \text{ \AA}$) lies between them. Such a weak link will pass only a relatively small lossless or superconductive current; above this critical current the link reverts to non-superconductive behavior.

Consider two weak links on opposite sides of a closed ring of superconductor (Fig. 37). As long as the currents through the weak links are less than the weak link critical currents I_{c1} and I_{c2} , the superconductive state extends around the ring and tends to quantize the flux through the ring in units of the flux quantum $\phi_0 = 2.07 \times 10^{-15} \text{ Wb}$. To see why this is so, write the center-of-gravity part of the pair wave function into which the superconducting Cooper pairs are condensed as $D = re^{i\theta}$; the current density is then proportional to $\text{Im}[D^*(\nabla - i\frac{e^*}{\hbar}\underline{A})D]$, where \underline{A} is the vector potential and e^* is the charge of the electron pair (i.e., $2e$). The current density is thus proportional to $r^2(\nabla\theta - \frac{e^*}{\hbar}\underline{A})$.

[44] J. Clarke, *Phil. Mag.* 13(8th), 115 (1966).

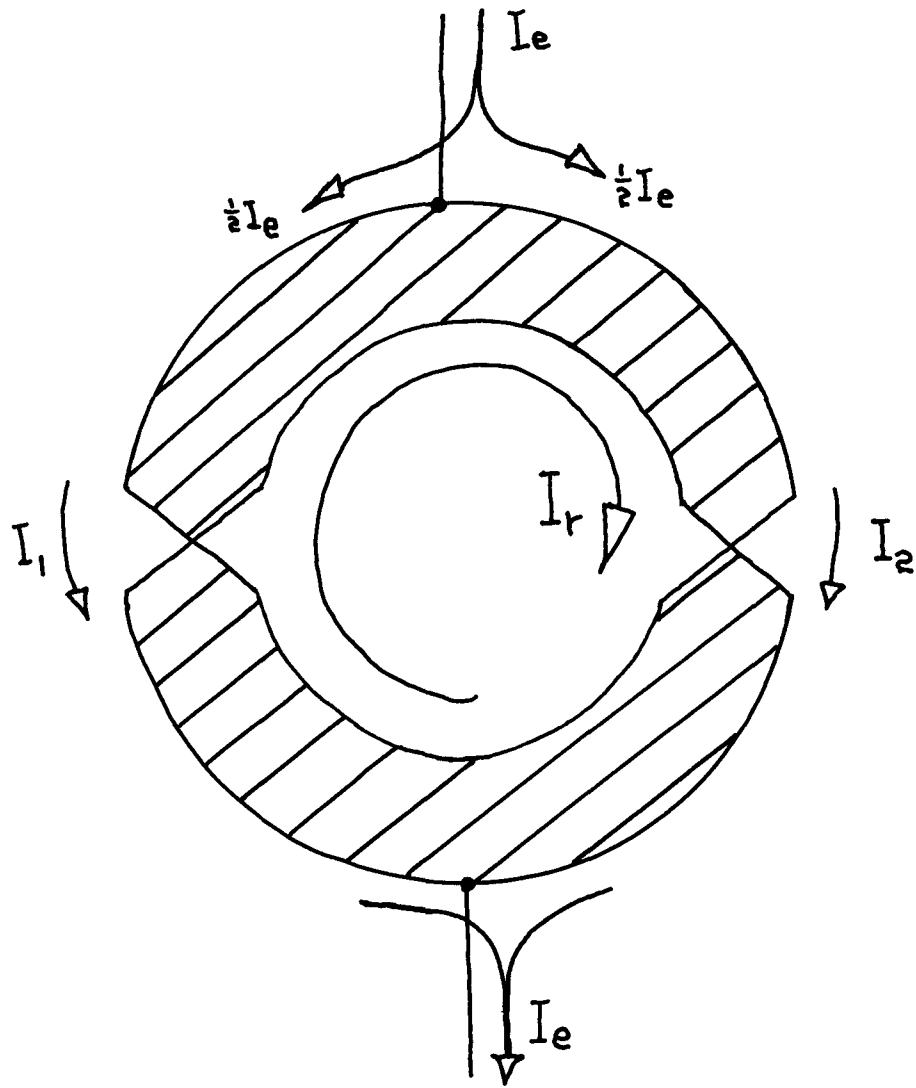


Fig. 37. A superconducting ring with two weak links, showing the weak link currents I_1 and I_2 . The weak link currents are found from the superposition of the circulating ring current I_r and the external current I_e (which splits evenly between the two weak links).

More than a few penetration depths inside the superconductor of the ring the current density is zero because the magnetic flux has been excluded, so $\nabla\theta = \frac{e^*}{\hbar}\underline{A}$. Integrating both sides of this equality around the hole in the ring, we have $\oint\nabla\theta\cdot d\underline{l} = \frac{e^*}{\hbar}\oint\underline{A}\cdot d\underline{l}$. The phase θ of the superconducting wave function must be single valued, so we must have $\oint\nabla\theta\cdot d\underline{l} = 2n\pi$, with n an integer. The field \underline{B} is given by $\underline{B}=\nabla\times\underline{A}$, so $\oint\underline{A}\cdot d\underline{l} = \oint\underline{B}\cdot d\underline{s} = \phi$, where ϕ is the flux **threading** the ring. We thus conclude that $\phi = \frac{\hbar}{e^*}n = \phi_0 n$, with the definition $\phi_0 = \frac{\hbar}{e^*} = \frac{\hbar}{2e} = 2.07 \times 10^{-15}$ Wb.

Let the inductance of the ring be L . The quantization of the flux through the ring in units of ϕ_0 then implies the quantization of the circulating current I_r in units of ϕ_0/L , if there is no external applied magnetic field. If there is an external field which causes a flux ϕ_e , then the total ring flux is $\phi_e + LI_r$ and the quantization condition becomes $n\phi_0 = \phi_e + LI_r$.

Suppose that an external current I_e is applied to the ring as shown in Fig. 37. The current through the first weak link is $I_1 = \frac{1}{2}I_e - I_r$, and that through the second weak link is $I_2 = \frac{1}{2}I_e + I_r$. We must not exceed the weak link critical currents, so we must have $|I_1| < I_{c1}$ and $|I_2| < I_{c2}$. These critical current limitations define a possible area of superconductive operation of the ring on the $I_e - I_r$ plane, as shown in Fig. 38. Because of the quantization condition $I_r = n\phi_0/L - \phi_e/L$, ring operation is further restricted to a series of lines parallel to the I_e axis and separated by ϕ_0/L ; these lines move up and down as the external flux is changed. (The operating point may jump from one line to another by passing a quantum of flux through one

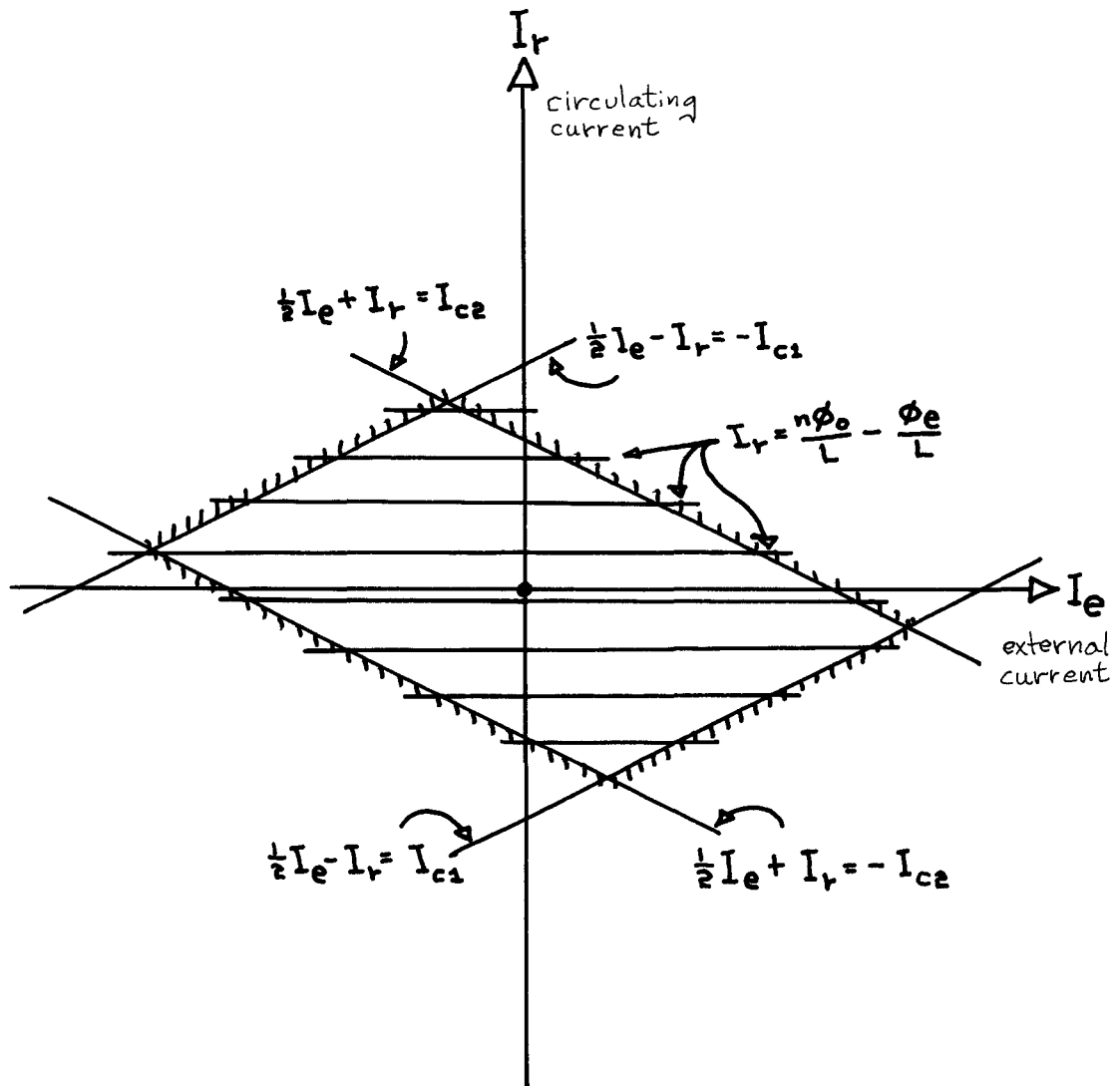


Fig. 38. Superconducting operating region of the ring of Fig. 37. The ring must operate on one of the horizontal lines because of flux quantization, and must remain within the parallelogram to avoid exceeding the critical current of either weak link.

of the weak links.)

What is the maximum external current which the ring will pass without becoming resistive? The maximum current depends on the external flux. When the external flux is such that one of the lines of quantization passes through the rightmost extension of the critical current parallelogram (Fig. 39a) the ring critical current I_m has its maximum value of $I_{c1} + I_{c2}$; when the external flux is changed by $\phi_0/2$ from the value leading to this maximum of I_m the critical current is decreased by ϕ_0/L , as we see from Fig. 39b. The result is that the ring critical current I_m depends on the external flux ϕ_e in the oscillatory manner shown in Fig. 40. A superconducting ring with two weak links thus acts as a sensitive fluxmeter; the high sensitivity is due to the small value of the flux quantum. The sensitivity to external fields can be made as large as desired by increasing the field-caused flux by an increase of the area of the ring, but unfortunately the unavoidable increase in the ring inductance due to the area increase decreases the size of the critical current oscillations and makes their detection more difficult.

C. The Principle of the Voltmeter

A superconducting ring with two weak links is sensitive to external flux. If the external flux is caused by the magnetic field of an external current, then the ring can be used as an ammeter to measure that current. Suppose the external circuit has self-inductance L_0 and mutual inductance to the ring M ; the current I in the external circuit will cause oscillations in the ring critical current of period $I_0 = \phi_0/M$. The external circuit can be superconducting, so the ammeter will have a pure

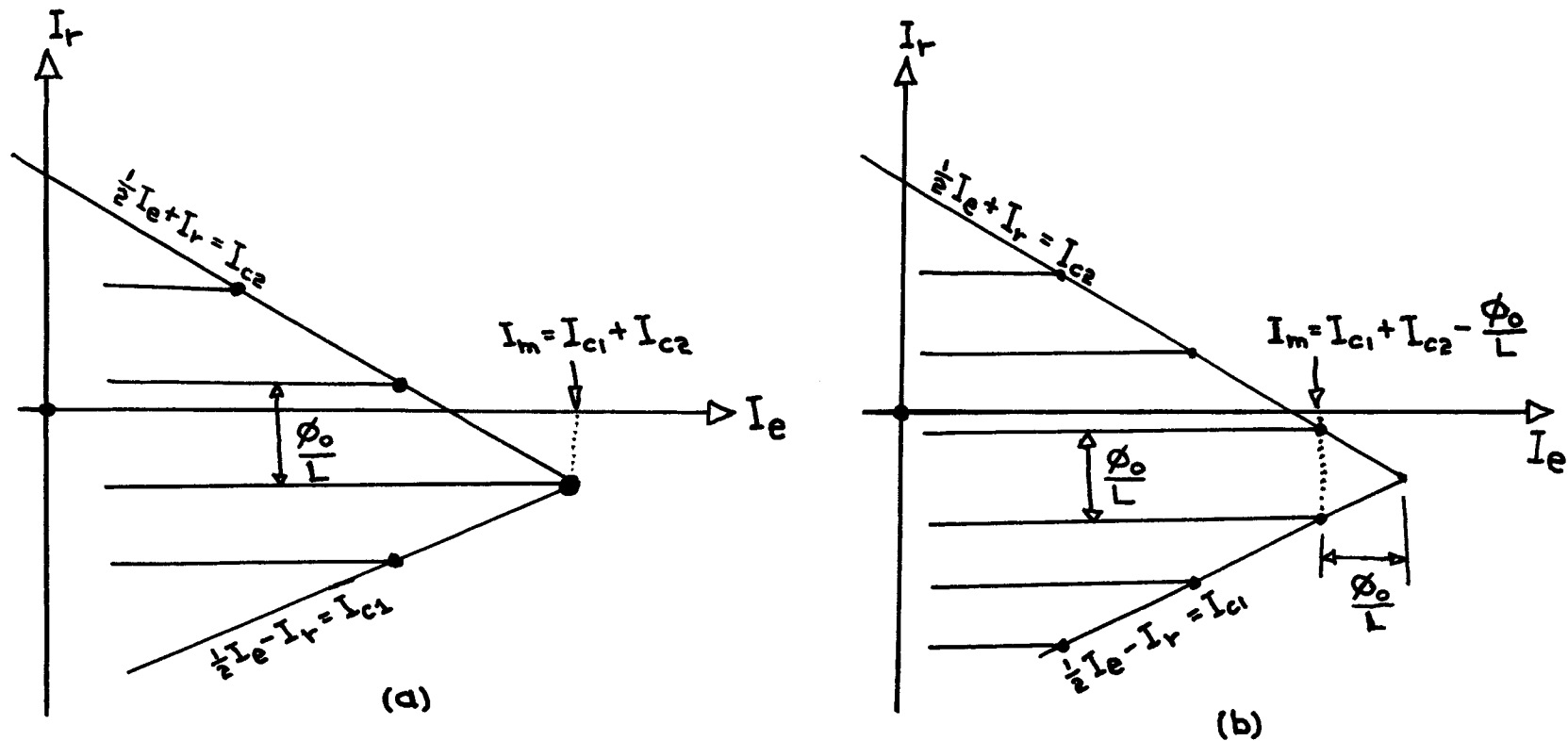


Fig. 39. The configuration of horizontal flux quantization lines shifts with respect to the critical current parallelogram due to changes in the external flux, thus changing the maximum superconducting external current. (a) One of the horizontal lines passes through the rightmost extension of the parallelogram; the maximum external current is $I_{c1} + I_{c2}$. (b) The external flux has changed by $\phi_0/2L$, reducing the maximum current by ϕ_0/L .

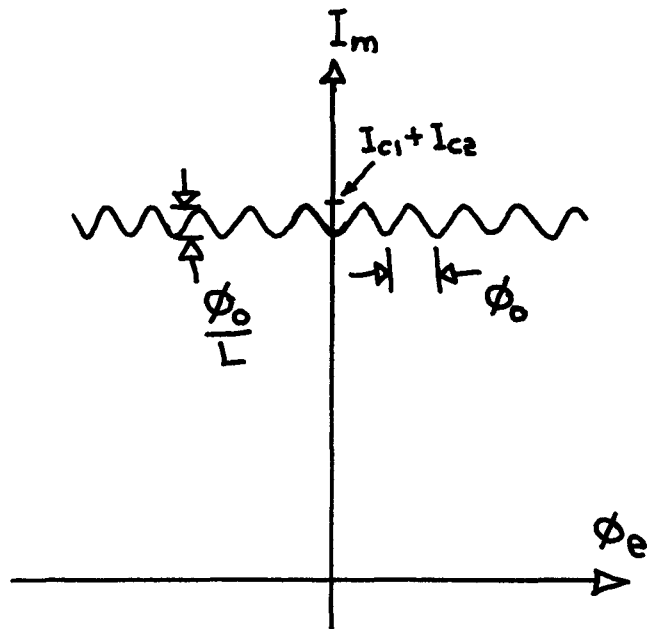


Fig. 40. The maximum external current I_m versus the external flux ϕ_e . The oscillations have period ϕ_0 and amplitude ϕ_0/L .

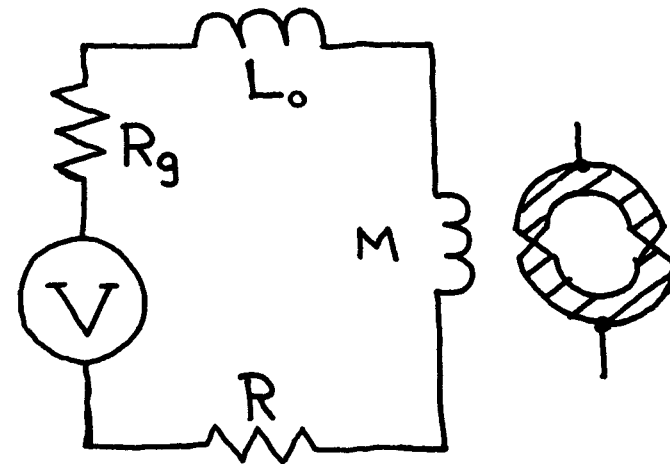


Fig. 41. The two-weak-link ring used as a voltmeter. The current in an external circuit couples flux into the ring via mutual inductance M , converting the flux response of Fig. 40 into a current response. Voltage is converted to current with the series resistor R .

reactive input impedance with zero resistance.

The ammeter described above can be converted to a voltmeter by the addition of a series resistor R (Fig. 41). The voltage necessary to produce one oscillation in the ring critical current will be $V_0 = I_0(R + R_g) = \phi_0(R + R_g)/M$, where R_g is the resistance of the source connected to the voltmeter. The time constant of the voltmeter is $\tau = (L_0 + M)/(R + R_g)$, under the pessimistic assumption that $I_r \ll I$, so we may write $V_0 = \phi_0(1 + L_0/M)/\tau$. If the external circuit is tightly coupled to the ring, so that $L_0 \ll M$, then a time constant of 1 second will yield a voltage of 2×10^{-15} v for one oscillation of the ring critical current. Even if the stray inductance is large, it is clearly possible to construct a voltmeter of great sensitivity. The current sensitivity of the meter cannot be increased to similarly low levels, because the necessary increase of M will decrease the amplitude of the critical current oscillations in the ring.

D. Fabrication of the Two-Junction Ring - the SLUG

A simple method of producing a multiple-junction quantum interference device suitable for use in a voltmeter was first described by Clark [45]. The device consists of a superconducting wire (typically Nb) surrounded by a small blob of Pb-Sn solder (such solder superconducts at liquid helium temperatures). The solder makes several weak link junctions to the wire; the flux through each of the resulting rings is quantized and modulates the critical current level. The resulting variation of critical current is often a complicated and apparently non-periodic function of the external flux, but is quite suitable as a

[45] J. Clarke, ibid.

voltmeter element. The external flux through the ring or rings is changed by sending a current through the superconducting wire itself, so the device (which is called a Superconducting Low-inductance Undulating Galvanometer, or SLUG) is a self-contained current detecting element.

The SLUGs used in this work were prepared in the standard manner [46-49]. About 10 cm of .3 mm diameter Nb wire had the Formvar insulation removed chemically (Fig. 42), and then was oxidized until dark in color by passing a dc current of ~ 3.5 A through it for several seconds in air. The oxide layer served as insulation between the Nb wire and the solder. A small scratch was then made in the oxide layer with a razor blade, so that the solder would make contact with the wire in only a small area. A small blob (from 3 to 6 mm in diameter) of ordinary 60-40 Sn-Pb solder was then melted with a soldering iron in a depression in a Teflon block, and a 10 cm length of #22 tinned Cu wire was laid through the blob. The recently scratched Nb wire was then also laid through the molten solder blob, and the solder was allowed to cool and solidify. During the solidification of the solder, the V-I characteristic between the Cu wire and the Nb wire was displayed on an oscilloscope. As the solder cooled, the resistance between the two fell from an initially large value to the range $.1\Omega - 10\Omega$. Resistance much larger or smaller than this range indicated an unsatisfactory SLUG (Clark has pointed out [50] that manual adjustment of the Nb wire during the cooling of the solder can be used to adjust the resistance of the SLUG junction). Superconducting connec-

[46] J. Clarke, *ibid.*

[47] R. DeBruynOuboter et.al., *Physica* 32, 1448 (1966)

[48] J. McWane et.al., *Rev. Sci. Inst.* 37, 1602 (1966)

[49] D. Zych, *Rev. Sci. Inst.* 39, 1058 (1968)

[50] J. Clarke, private communication

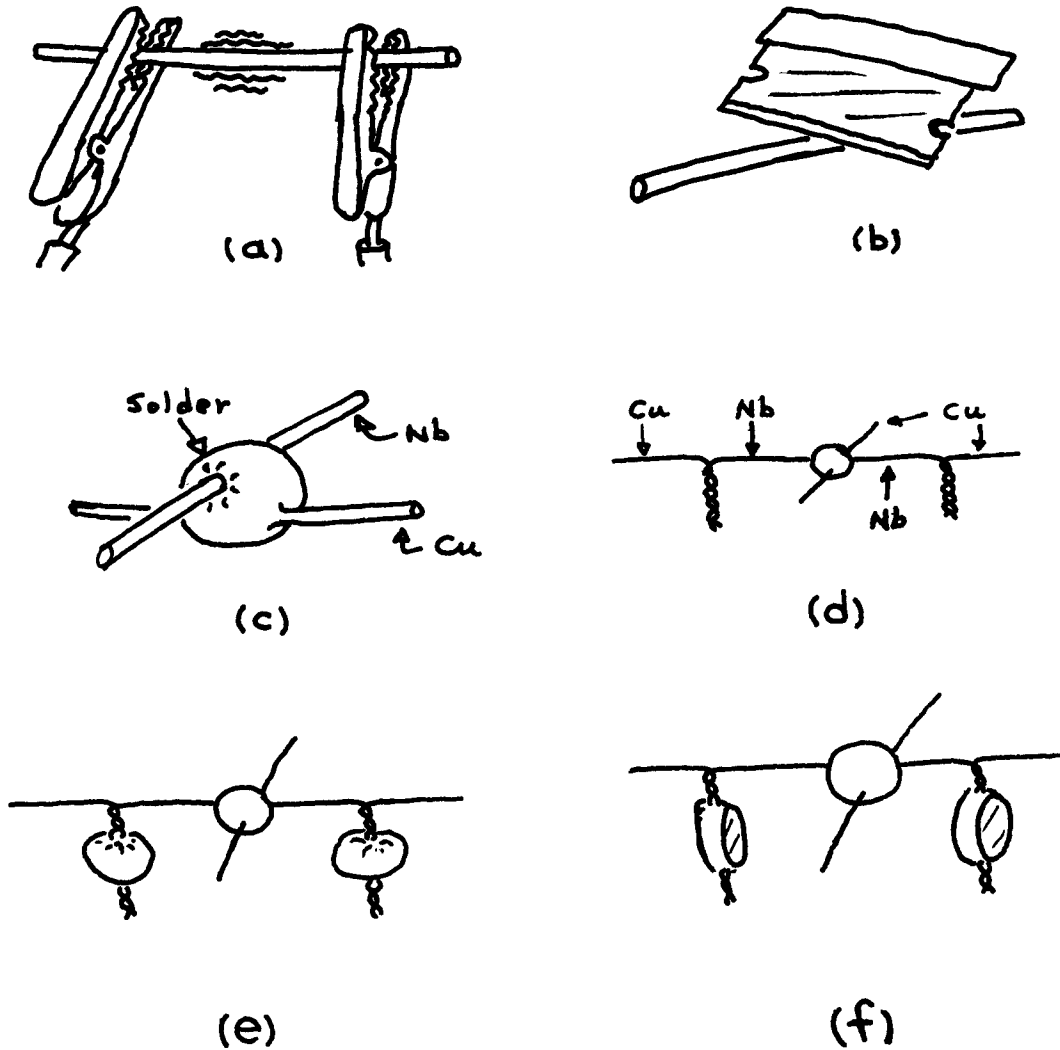


Fig. 42. Construction of a SLUG. (a) A 10 cm length of .3 mm Nb wire is electrically heated until oxide covers it. (b) A small scratch is made in the oxide layer. (c) The scratched area is immersed in a molten blob of solder on a tinned Cu wire. (d) Once the solder is solid, the ends of the Nb wire are twisted with tinned Cu wires. (e) The twisted pairs are plunged into molten solder blobs. (f) The solder is squeezed flat as soon as it solidifies.

tions were than made to the ends of the Nb wire by removing the Formvar insulation, twisting the Nb wire together with a tinned Cu wire, plunging the twisted pair into a blob of molten solder, allowing to solder to solidify, and compressing the solder (with a pair of pliers) by about 50% while it was still hot. Once prepared, the SLUGs were stored in liquid nitrogen to avoid any possible deterioration.

E. Characteristics of the SLUG

The SLUGs were checked for correct operation by attaching them to a four-terminal V-I characteristic tracer and placing them in liquid helium. Practically all SLUGs with resistance in the $.1\Omega - 10\Omega$ range displayed a V-I curve representative of weak-link superconductivity with critical current in the milliamperere range (Fig. 43). The presence of multiple-weak-link structure was then tested for by varying the current through the Nb wire. If such structure was present, the V-I curve near the critical current would be displaced and modified in shape as the wire current was varied. SLUGs with relatively large changes in the V-I characteristic were judged suitable for use as voltmeter elements; the larger the changes, the better the SLUG.

F. The SLUG Voltmeter

To utilize the unique properties of a SLUG, it is necessary to monitor the changes in its V-I characteristic due to current flow in the Nb wire. In the present work, this was accomplished by measuring the transfer resistance from the wire current to the multiple-weak-link structure voltage; this method was first described by Zych [51]. A small ac current at about 3kHz was superimposed on the steady dc current

[51] D. Zych, op. cit.

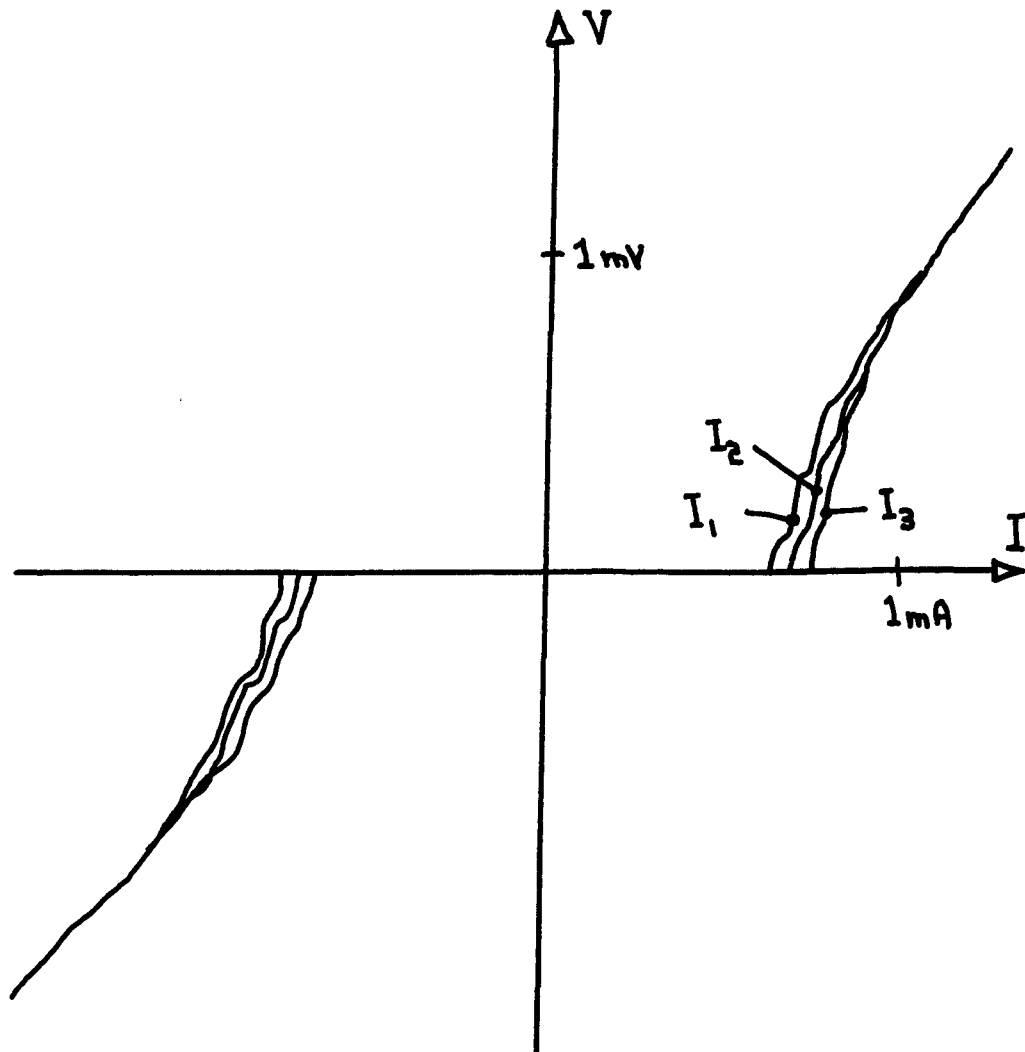


Fig. 43. The V-I curves of an active SLUG in liquid helium. Variation of the V-I curve with changes in the wire current (I_1 , I_2 , I_3) indicates the presence of flux-sensitive multiple weak link structure.

flowing through the Nb wire in the SLUG (Fig. 44), and the resulting ac SLUG junction voltage was amplified, synchronously detected, and passed through a low pass filter (usually of 10 Hz bandwidth). As the dc SLUG junction current is increased in such an arrangement, the transfer resistance remains small until the critical current of the SLUG multiple-weak-link junction structure is exceeded; a large peak is then seen in the transfer resistance (Fig. 45). The output of the SLUG is largest at the maximum of the peak, and so the junction current is maintained at the value corresponding to the peak (this value changes with temperature, and so the junction current must be readjusted when the temperature of the SLUG is changed).

Once the junction current of greatest sensitivity is found, the transresistance will be very sensitive to the dc current in the superconducting Nb wire. Figure 46 shows a representative plot of transresistance versus wire current. There are numerous regions of rapid change of transresistance with wire current; by biasing the wire in one of these regions, the SLUG can be made very sensitive to changes in the wire current.

The SLUG ammeter can be converted to a sensitive voltmeter by placing a small resistor in series with it. The resistors used in this work were made of .12 mm thick phosphor-bronze sheet; the sheet was cut into rectangles, and superconducting contacts were made to opposite edges of the rectangles with 60-40 Sn-Pb solder. Resistors of different resistances were made by varying the ratio of length to width of the rectangles. The resistance was placed in series with the Nb wire of the SLUG as shown in Fig. 47. An external current source was also

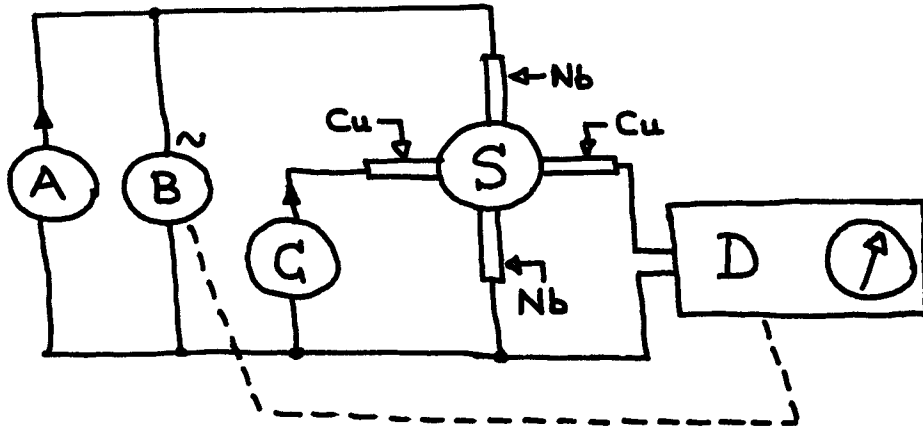


Fig. 44. Monitoring of the SLUG V-I changes to detect flux changes. The wire current from A is varied by a small ac current from B. The SLUG junction current from C biases the SLUG S in the region of maximum sensitivity. The small ac changes in the junction voltage are amplified, synchronously detected, low-pass filtered, and displayed by D (which is phase locked to B).

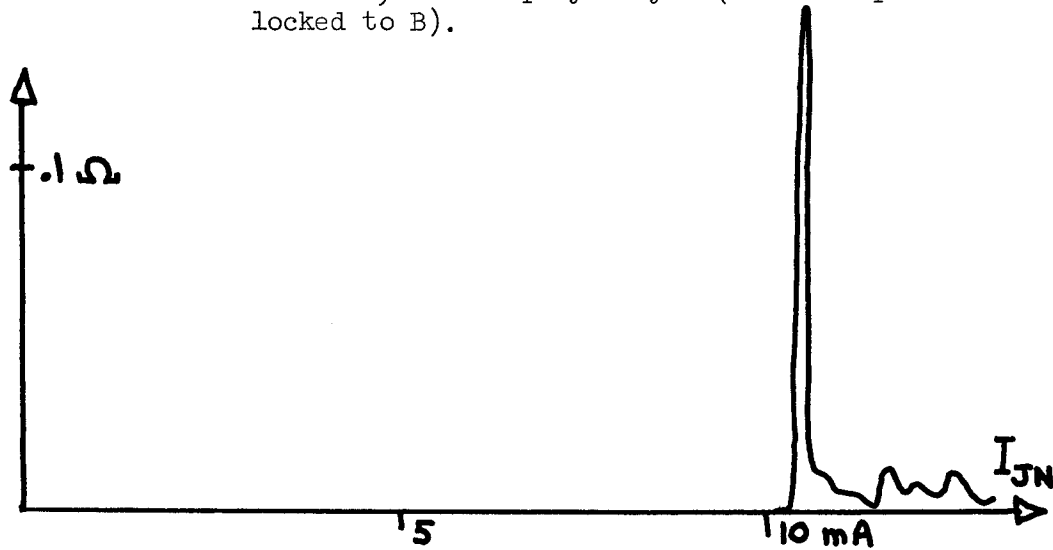


Fig. 45. SLUG transresistance from small modulating current to junction output voltage (see Fig. 44) versus SLUG junction current, showing the typical peak at the SLUG junction critical current.

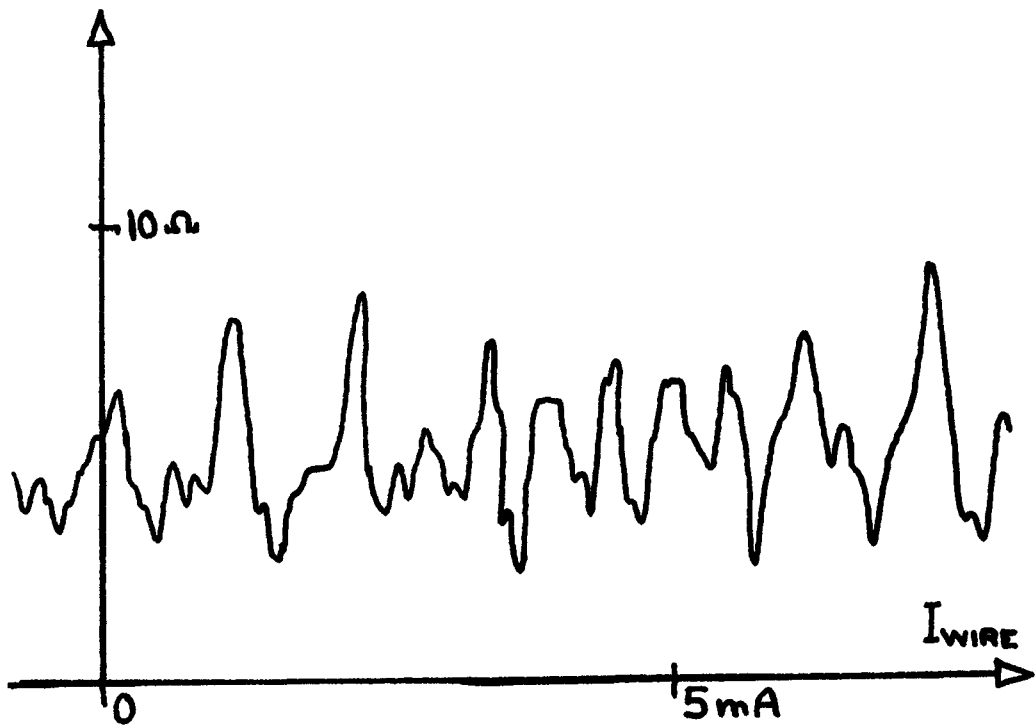


Fig. 46. SLUG transresistance versus Nb wire current for a typical SLUG. The complicated structure is due to the presence of more than two weak links. This is the fundamental transfer characteristic of the SLUG.

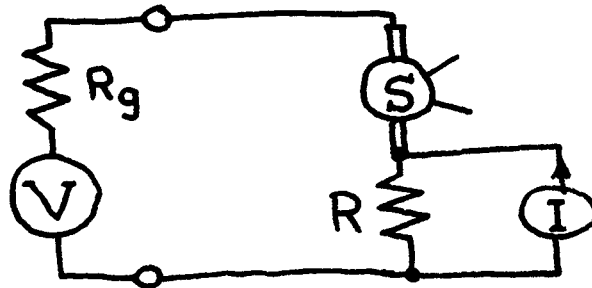


Fig. 47. The SLUG (a current-sensitive device - see Fig. 46) is converted to a voltmeter by the addition of a series resistor R . An external current I can be passed through the resistor to buck out the applied voltage V so the SLUG voltmeter can be used as a null detector.

placed across the resistor, so that the voltmeter could be used as a null detector by bucking out the input voltage with the voltage produced across the resistor by the external current source.

If the voltage calibration of the voltmeter is to be known, the resistance of the series resistor must be known. The resistors used in this work were in the micro-ohm range, so their values were difficult to measure. Their resistances were therefore found from their geometry and the resistivity of the phosphor-bronze used in their construction. The resistivity of the phosphor-bronze was found by measuring the resistance of a 14.5 cm by .15 cm strip. The helium-temperature resistance of the strip was $600 \mu\Omega$ with an uncertainty of 20% (due to noise and common-mode pickup during the measurement). The helium-temperature resistivity was thus $7.7 \times 10^{-8} \Omega\text{-cm}$ (the room temperature resistance was 15.5 m Ω , so the resistance ratio was ~ 25). The consistency of the resistance determinations was found by measuring the ratio of the resistor values; voltage was generated across a resistor by running an external current through it, and the voltage was connected across the SIUG voltmeter and nulled out by adjusting the external current through the voltmeter series resistor. The ratio of the external currents was then the same as the ratio of the resistors. The ratio as found in this manner differed from that calculated from the resistivity and geometry by as much as a factor of 1.8, so the actual resistance values are considered known only to a factor of two. This means that the absolute value of the voltage found by the voltmeter is also known only to within this factor of 2, although the relative values are known to the accuracy of the current determination (5%). Clarke has pointed out [52] that the

[52] J. Clarke, private communication

voltage sensitivity of the voltmeter can be found accurately by applying rf fields to an SNS sandwich and measuring the constant-voltage steps resulting from the inverse ac Josephson effect [53].

G. Use of the Voltmeter to Measure the Sandwich Characteristics

Figure 4 (on page 22) shows the connection of the sample, voltmeter, and various dc and ac current supplies. The Nb wire current and SLUG junction current connections are used to adjust the operating point of the SLUG for maximum sensitivity; when the voltmeter is used as a null detector, the current supply across the series resistor is used to balance out the input voltage due to current through the sample. The superconducting shield (a tinned sheet of thin brass) is used to prevent fields of the currents in the external leads from disturbing the SLUG or sandwich. All connections are made with superconducting tinned Cu wire.

In operation, the external currents are initially all set to zero. The ac wire current is adjusted to a p-p value small compared to the scale of Nb wire currents causing major variations in the transresistance (Fig. 46). The SLUG junction current is then increased until the transresistance is at the top of its initial large peak (Fig. 45); the synchronous detector phase is adjusted for maximum output. The Nb wire current is then adjusted until the variation of transresistance with current is large. The voltmeter is now ready for use.

The critical current of the sandwich is found by applying a voltage proportional to the sandwich current to one axis of a chart recorder, and applying the filtered output of the synchronous detector to the

[53] S. Shapiro, Phys. Rev. Letters 11, 80 (1963)

other axis. Resistive behavior of the sandwich produces a voltage proportional to the sandwich current as input to the voltmeter; the SLUG output voltage versus sandwich current display then traces out the oscillatory curve of transresistance versus Nb wire current of the SLUG (see Fig. 5 on page 23). When the sandwich has a non-zero critical current, no voltage appears until the critical current is exceeded and the SLUG output is constant in the current range below the critical current (Fig. 5). The sandwich critical current was usually large compared to the current necessary to cause an oscillation of the voltmeter output, so the voltmeter input current was usually a small fraction of the current supplied to the sample. The critical current is thus found as the current at which oscillatory behavior abruptly begins.

The entire V-I curve of the sandwich can be traced out by applying a voltage proportional to the sandwich current to one axis of the chart recorder, and applying a voltage proportional to the external current applied to the series resistor in the SLUG voltmeter to the other axis. The sandwich current is then increased from zero, and the series resistor current is adjusted to maintain the output of the SLUG constant. The current **through** the series resistor thus always produces a voltage equal to the sandwich voltage, so the series resistor current is proportional to the sandwich voltage. The V-I curve of the sandwich is then traced out, as shown in Fig. 9 (page 31).

APPENDIX B. EXACT CALCULATION OF THE CRITICAL CURRENT DENSITY

A. Introductory Discussion

The results of Eq. (24) are exact solutions of the Ginzburg-Landau equation in the presence of current, within the assumptions of one-dimensional variations and the absence of magnetic effects ($\underline{A} = 0$). If we find the constants of the Ginzburg-Landau equation from the de Gennes-Werthamer theory, then the maximum current density for which the solutions of Eq. (24) can be matched to the boundary conditions of Eq. (28) at sample half-width W_N is the exact critical current density of the sample in the de Gennes-Werthamer theory.

Determination of the exact critical current density j_c then proceeds in a straightforward manner. First, a particular level of current density j is chosen. We then attempt simultaneous solution of Eq. (24) and Eq. (28). If solution is possible, j was less than j_c and the next current level attempted is larger; if no solution is possible, j was larger than j_c and the next current level attempted is smaller. Two current densities which bracket j_c can be found by continued attempts; the critical current can then be found to any required accuracy by subdividing the interval in which j_c lies.

B. Simultaneous Solution of Eq. (24) and Eq. (28)

Given W_N and a current density j , it is difficult to solve Eq. (24) and Eq. (28) simultaneously for the two unknowns r_N and r_0 . A simultaneous solution was therefore searched for by varying r_N to see if the two equations were simultaneously satisfied for any r_N . First, Eq. (28) was used to find r_0 from the chosen r_N (by interval halving, which was faster than exact solution of the cubic). Second, the width W

corresponding to r_N and r_o was found from Eq. (24) by solving for x to get

$$1) \quad j \leq \frac{C\alpha r_o}{2\sqrt{2}r_m} (r_o^2 + 2r_m^2)$$

$$W = \frac{r_m}{\alpha} \sqrt{\frac{2}{r_o^2 - \gamma_2}} F \left(\cos^{-1} \sqrt{\frac{r_o^2 - \gamma_1}{r_N^2 - \gamma_1}} \mid \frac{\gamma_1 - \gamma_2}{r_o^2 - \gamma_2} \right)$$

$$2) \quad j \geq \frac{C\alpha r_o}{2\sqrt{2}r_m} (r_o^2 + 2r_m^2)$$

$$W = \frac{r_m}{\alpha} \frac{1}{\sqrt{2\zeta}} F \left(\cos^{-1} \left(\frac{2\zeta}{r_N^2 - r_o^2 + \zeta} - 1 \right) \mid \frac{1}{2} - \frac{3r_o^2 + 2r_m^2}{4\zeta} \right)$$

where γ_1 , γ_2 , and ζ are defined in Eq. (24), and $F(\vartheta|m)$ is the incomplete elliptic integral of the first kind [54]. (When ϑ becomes greater than $\pi/2$ in the second of the forms above, it is convenient to use the relation $F(\pi - \vartheta|m) = 2K(m) - F(\vartheta|m)$ [55], where $K(m)$ is the complete elliptic integral of the first kind.) If the width found in this manner is equal to W_N , then Eq. (24) and Eq. (28) are simultaneously satisfied. Figure 48 shows a plot of W versus r_N for a sample with the parameters given on page 67 at the transition temperature T_{cN} ; we see that the width is much less than W_N for most values of r_N , and exceeds W_N only for a small range of r_N . Figure 49 shows the width spike of Fig. 48 on an expanded r_N scale, and shows the effect of different current densities j . The two current densities shown are above and below

[54] M. Abramowitz and I. Stegun, op. cit.; p. 589

[55] ibid.; p. 592

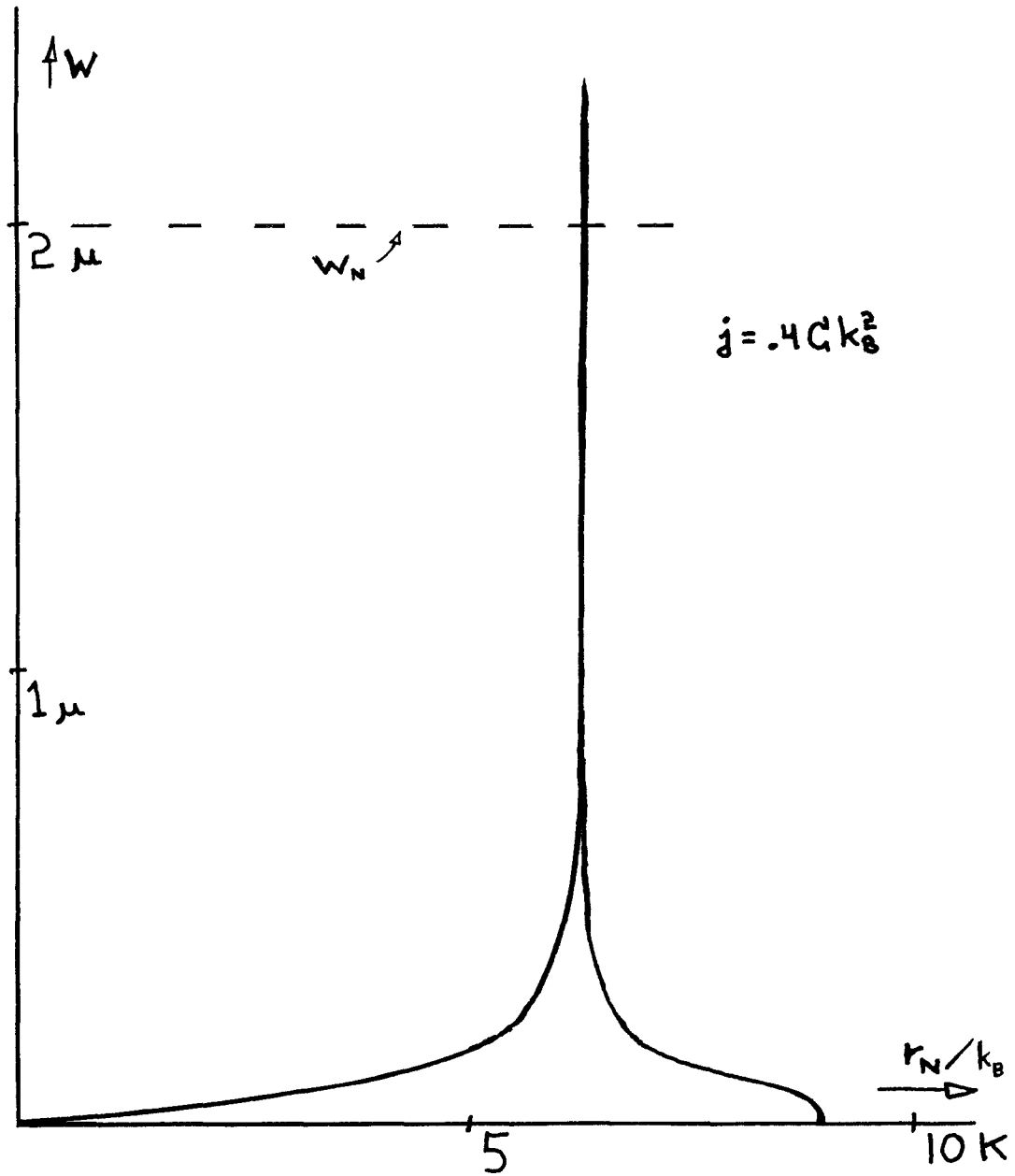


Fig. 48. The solution half-width W versus the SN interface value of the energy gap amplitude r_N for the basic parameters of p. 67 (at T_{cN}), showing the narrow spike at the maximum width.

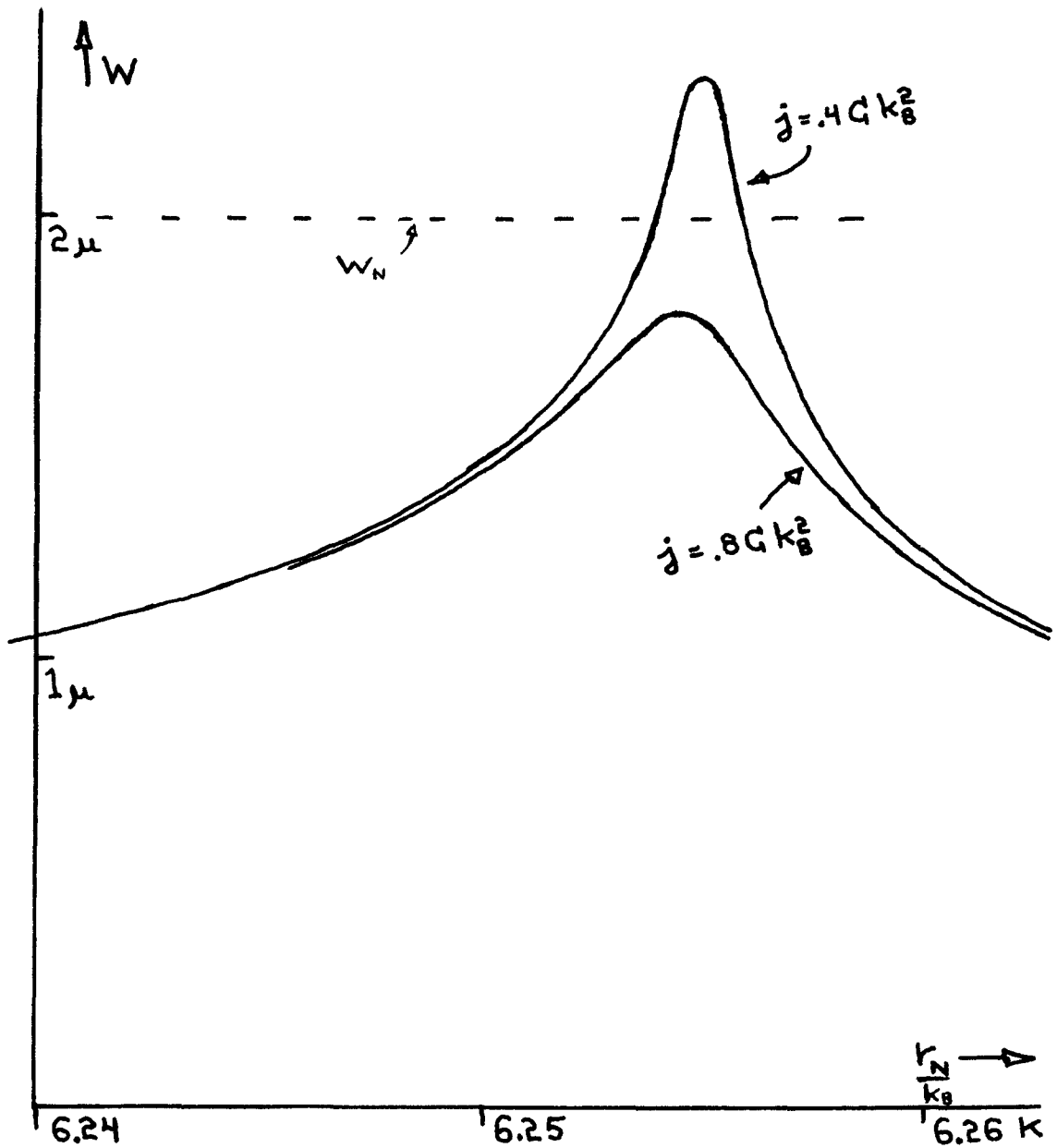


Fig. 49. The spike region of Fig. 48 expanded to show details near the maximum width. The smaller current density is less than j_c , and so two solutions are possible for it; the larger current density is greater than j_c , and no solution is possible because the maximum width corresponding to this current density is less than W_N .

the critical current density; when $j < j_c$ there are two values of r_N which give the correct width W_N , and when $j > j_c$ the solution width never reaches W_N and no solution of width W_N exists.

In this work, all that was desired was information as to whether j was above or below the critical current density j_c . A search was therefore instituted for the maximum value of the half-width W corresponding to the given value of j ; if the maximum was less than W_N then $j > j_c$. To find the maximum W , the possible range of r_N was divided into quarters (the minimum value of r_N is zero, and the maximum value is $r_{\frac{N}{B} \frac{N}{S} \frac{N}{S}}$) and W was evaluated at 1/4, 1/2, and 3/4 of the maximum r_N . The largest of the resulting W values was found, and W was evaluated for values of r_N on either side of the r_N which had led to the largest W ; the new values of r_N were situated halfway between the old r_N values. The maximum value of W was again found, and new values evaluated for r_N values situated halfway between the previous values, and so on. This interval halving procedure converges to the maximum of the width. If the value of W ever exceeded W_N during the interval halving, the search for the maximum W was terminated and j was known to be less than j_c . If the value of W never exceeded W_N , the search was terminated when the changes in r_N approached the limit of resolution of the computer used (one part in 10^7), and j was known to be greater than j_c .

C. The Search for the Critical Current Density

The search for a solution of Eq. (24) and Eq. (28) described above was used to determine if a given current density j was less than or greater than the critical current density j_c . The determination of j_c then proceeded as follows. First, an initial value of j was chosen.

The method of the previous section was used to determine whether this j was above or below j_c . If it was above j_c , then the next value of j used was half the first value; if it was below j_c , then the next value of j used was twice the first value. The relation to j_c was again determined, and the current density again halved or doubled. This process was continued until the critical current density was passed. Once j_c had been passed two values of j were available, one above and one below j_c . The next value of j tested was halfway between these values; once more two values of j were available above and below j_c , but the interval between them had been halved. This interval halving procedure was continued until the critical current density was known to a specified tolerance (usually 1%).

D. Improvements to the Method of Search

The search procedures described above could be speeded up if more rapid methods than interval halving were used. For example, the maximum half-width W could be searched for by the golden section method, or by a Fibonacci search. The critical current could be searched for by regula falsi or other more efficient root-finding methods if a quantity proportional to the deviation from the critical current were available; this quantity could be the difference between W_N and the maximum value of W found for the chosen current density.